

University of Nevada, Reno

Laboratory Chemical Characterization of Fresh and Aged Bioaerosols

A dissertation submitted in partial fulfillment of the
requirements for the degree of Doctor of Philosophy in
Atmospheric Science

by

Palina Bahdanovich

Vera Samburova, Ph.D. / Dissertation Advisor

May 2025

© 2025

Palina Bahdanovich

All Rights Reserved



THE GRADUATE SCHOOL

We recommend that the dissertation
prepared under our supervision by

entitled

be accepted in partial fulfillment of the
requirements for the degree of

Advisor

Committee Member

Committee Member

Committee Member

Committee Member

Graduate School Representative

Markus Kemmelmeier, Ph.D., Dean
Graduate School

Abstract

Bioaerosols are biological aerosol particles in the atmosphere, such as pollen, fungi, algae, and bacteria, with sizes ranging from a few nanometers to hundreds of micrometers. The importance of bioaerosols has been growing due to climate change, however, their chemistry and atmospheric fate are still largely unexplored. The contribution of bioaerosols and their organic compounds to the atmospheric organic carbon load, and their role in cloud physics and atmospheric processes should be studied further. To address this knowledge gap, this dissertation investigates the chemical composition of water-soluble extracts of various types of bioaerosols and the effects of laboratory aging, such as exposure to simulated solar radiation and OH radicals. The bioaerosols chosen for chemical characterization were lodgepole pine pollen, rabbitbrush pollen, western gall rust fungi, hay Bacillus bacteria, *Pedobacter* bacteria, and *Spirulina* alga. Using various analytical techniques, such as gas chromatography – mass spectrometry (GC-MS), ultra-high performance liquid chromatography – mass spectrometry (UPLC-MS), ultraviolet-visible-near-infrared spectrophotometry (UV-Vis-NIR), proton nuclear magnetic resonance spectroscopy ($^1\text{H-NMR}$), and Fourier-transform infrared spectroscopy (FTIR), organic species (saccharides, amino acids, and fatty acids) and functional groups of these bioaerosols were determined. Chemical analysis showed that the saccharide glucose was common between all analyzed bioaerosol extracts, and the major contribution of organic species in pollen was from saccharides. Laboratory aging was performed on lodgepole pine pollen and *Spirulina* alga using the Suntest CPS solar simulator. These bioaerosols were exposed to (1) simulated solar radiation, ranging from 300 to 800 nanometers, and (2) OH radicals formed by hydrogen peroxide through photolysis. Functional groups were

compared before and after aging using $^1\text{H-NMR}$ and FTIR spectroscopy to uncover the chemical transformation and changes in polarity of the bioaerosols. FTIR results showed an overall increase of polar functional groups in the two bioaerosols after aging with simulated solar radiation. Though $^1\text{H-NMR}$ showed no significant changes after simulated solar aging, the functional group distribution transformed dramatically after exposure to OH radicals. In summary, this research was instrumental in understanding the contribution of various organic compounds to bioaerosol chemistry and the transformation of bioaerosols after exposure to atmospheric aging.

“Never give up on a dream just because of the time it will take to accomplish it.

The time will pass anyway.” – attributed to Earl Nightingale

There are countless people who have helped, supported, and mentored me throughout my Ph.D. journey. I would like to thank my mom and the rest of my family for wholeheartedly supporting and encouraging me through one of the most stressful and trying times of my life. I am grateful to have such loving and selfless people in my life. I would like to acknowledge my advisor and mentor, Dr. Vera Samburova, for guiding me through this journey and being an incredible role model as a female scientist and teacher. I would like to extend my gratitude to Dr. Kevin Axelrod, who mentored me through the first half of my Ph.D. and is one of the most encouraging and patient people I know. Thank you to my friends for their support, love, adventurous spirit, and for always keeping me grounded. I would like to acknowledge Dr. Andrey Khlystov, who is the PI of this project, for allowing me to be a part of this project and providing valuable advice and feedback. I would also like to acknowledge Dr. Hans Moosmüller for his guidance and his unique insight on academia and life. Thank you to my Ph.D. committee for challenging me and providing helpful feedback on my research. Finally, thank you to the University of Nevada, Reno, the Desert Research Institute, and the National Science Foundation for their sources of funding that allowed me to conduct my research and contribute to the field of bioaerosol chemistry.

Table of Contents

Chapter 1	1
Introduction	1
1.1. Current State of Knowledge	4
1.2. Goals and Objectives of the Present Research	6
Chapter 2	9
Optimized Spectrophotometry Method for Starch Quantification	9
2.1. Abstract	10
2.2. Introduction	10
2.3. Experimental Section	13
2.3.1. Chemicals and Reagents	13
2.3.2. Instrumentation	14
2.3.3. Starch Preparation	15
2.3.4. Bioaerosol Preparation	19
2.4. Results and Discussion	20
2.4.1. Calibration and MDL	22
2.4.2. Bioaerosol and Saccharide Analysis	23
2.5. Conclusion	28
2.6. Acknowledgments	29
2.7. Chapter 2 Appendix	29
Chapter 3	33
Characterization of Organic Species and Functional Groups in Pollen, Fungi, Algae, and Bacteria Bioaerosols	33
3.1. Abstract	34
3.2. Introduction	35
3.3. Experimental Section	39
3.3.1. Standards and materials	39
3.3.2. Bioaerosol species	40
3.3.3. ¹ H-NMR analysis	42
3.3.4. GC-MS analysis	46
3.3.5. UV-Vis-NIR starch analysis	47
3.3.6. UPLC-MS analysis	48
3.4. Results and Discussion	50
3.4.1. ¹ H-NMR analysis	50
3.3.2. Saccharide Analysis	55
3.4.3. Amino acid analysis	59
3.4.4. Fatty acid analysis	62
3.4.5. Correlation analysis	64
3.5. Conclusion	65

3.6. Acknowledgements	68
3.7. Chapter 3 Appendix	69
Chapter 4	75
Effects of Simulated Atmospheric Aging on Bioaerosol Chemistry	75
4.1. Abstract	75
4.2. Introduction	76
4.3. Experimental Section	80
4.3.1. Bioaerosol species	80
4.3.2. ¹ H-NMR analysis	80
4.3.3. FTIR analysis	83
4.3.4. Laboratory aging	86
4.4. Results and Discussion	88
4.4.1. FTIR results	89
4.4.2. ¹ H-NMR results	93
4.5. Conclusion	102
4.6. Chapter 4 Appendix	104
Chapter 5	108
Summary, Conclusions, and Future Recommendations	108
Products	112
Peer-reviewed Publications	112
Presentations/Conference Proceedings	112
Proposals	112
References	115

List of Tables

Table 1. Bioaerosols used for sample preparation of starch content quantification. ____	19
Table 2. Bioaerosols species selected for the present study. _____	42
Table 3. Segments of chemical shifts assigned for ¹ H-NMR functional group analysis in bioaerosol extracts _____	46
Table 4. Functional group and proton placement in ¹ H-NMR spectra. _____	82
Table 5. Wavenumber ranges of common functional groups found in FTIR spectra. ____	85
Table 6. Samples that were extracted and analyzed for this study. _____	88
Table 7. Polar/non-polar functional group ratios. _____	92

List of Figures

Figure 1. Optimized procedure of starch preparation for amylose-iodine complex spectrophotometry analysis. _____	16
Figure 2. Absorption spectrum of calibration level 4 (50 $\mu\text{g/mL}$) at pH 6 and iodine reagent (I ₂ /KI) concentration of 0.2% _____	22
Figure 3. Concentration of starch per milligram of dry weight of selected bioaerosols. _____	25
Figure 4. Absorbance spectra of selected saccharides. _____	26
Figure 5. Deterioration of starch solution after four weeks and four months. _____	28
Figure 6. Pie chart percent distribution of functional groups in select bioaerosol extracts analyzed with ¹ H-NMR spectroscopy. _____	55
Figure 7. Saccharide and starch concentration of selected bioaerosols. _____	59
Figure 8. Amino acid concentration of selected bioaerosols (primary axis). _____	62
Figure 9. Fatty acid concentration of selected bioaerosols. _____	64
Figure 10. Fresh and aged lodgepole pine pollen extract FTIR spectra. _____	90
Figure 11. Fresh and aged <i>Spirulina</i> alga extract FTIR spectra. _____	91
Figure 12. Functional group percent distribution of a) lodgepole pine pollen and b) <i>Spirulina</i> alga extracts after aging. _____	94
Figure 13. Functional group percent difference of a) lodgepole pine pollen and b) <i>Spirulina</i> alga extracts after aging. _____	96
Figure 14. Functional group percent difference of a) saccharide and b) amino acid. _____	98
Figure 15. Possible oxidation pathway for OH radical reaction with proline. _____	100
Figure 16. Diagram of a part of a peptide backbone containing leucine and tyrosine amino acids. _____	101
Figure 17. Example of a triglyceride, containing three fatty acids. _____	102

Chapter 1

Introduction

Bioaerosols (commonly referred to as primary biological aerosol particles, or PBAPs) are atmospheric particles of biological origin (Fröhlich-Nowoisky et al., 2016). Some examples of bioaerosols include pollen grains, fungal spores, bacteria, viruses, algae, and their dispersal units and fragments (Després et al., 2012; Mainelis, 2020; Möhler et al., 2007). These particles are emitted by various sources, such as vegetation (Faske et al., 2021), soil (Bjerketorp et al., 2021), water (Vo et al., 2015), and humans and animals (Xie et al., 2021). In size, bioaerosols range from ~ 0.5 to ~ 100 μm , but some (i.e., pollen) can be larger (e.g., ~ 200 μm (Pope, 2010)) than most anthropogenic aerosols (Fröhlich-Nowoisky et al., 2016). Global emissions of bioaerosols are estimated to be near 1000 Tg per year (including cellular fragments), with pollen emissions at 84 Tg/year, fungi at 186 Tg/year, and bacteria at 28.1 Tg/year (Després et al., 2012). Bioaerosol emissions represent a large fraction (up to 25% (Jaenicke, 2005)) of total global atmospheric aerosol mass, and they may also contribute to atmospheric organic carbon (Bauer et al., 2002). Thorough research of bioaerosols is crucial due to their severe impacts to human health, i.e., seasonal allergies due to pollen (Sénéchal et al., 2015), which affects around 24.4 million people in the U.S. (Center for Health Statistics, 2018). Fungi (Magnussen and Parsi, 2013) and algae (Gartner et al., 2021; May et al., 2018a) species can emit various toxins, some of which can be cancerous or deadly. For example, *Aspergillus* fungi species produce aflatoxin (a

carcinogen), which targets the liver (Magnussen and Parsi, 2013), and can become airborne through handling contaminated foods (Burg et al., 1981). Moreover, *Sargassum* algae blooms that wash ashore release gasses as they decompose, which can cause respiratory issues and even fatality in humans (Fidai et al., 2020). Recently, it has been found that a warming climate is enhancing the concentration (+21%) and duration (+20 days) of pollen seasons (Anderegg et al., 2021; D'Amato et al., 2020; Zhang and Steiner, 2022) and amplifying neurotoxin-emitting harmful algal blooms (May et al., 2018a). Although bioaerosols are estimated to be quite abundant in the atmosphere and affect human health, little is known about their chemistry, contribution to the total atmospheric carbon, and atmospheric transformation during transport.

Atmospheric transport is made possible by their aerodynamic size and structure (Romano, 2023), and some can even be transported intercontinentally (Tesson et al., 2016; Warren and St. Clair, 2021). They can be dispersed by wind and other mechanisms and thus play a role in atmospheric chemical and physical processes. Bioaerosols are typically found in the troposphere, however, microorganisms (bacteria, fungi, and algae species) have been found at the stratospheric level, where they are exposed to harsh atmospheric conditions such as ultra-violet (UV) radiation, very low temperatures, and desiccation (DasSarma and DasSarma, 2018; Smith et al., 2011). Bioaerosols can directly affect cloud physics and climate by acting as cloud condensation nuclei (CCN) (Sun and Ariya, 2006) and ice nuclei (IN) (Huffman et al., 2013). Pollen (Pope, 2010), bacteria, and fungi (Bauer et al., 2002) are known to be efficient IN and CCN. Recently, sub-pollen particles have gained a lot of attention for their role in cloud formation (Burkart et al., 2021). Bioaerosols may undergo physical and chemical transformations during their transport in the

atmosphere, especially from their interaction with atmospheric oxidants (i.e., OH radicals, ozone) and UV radiation (Xie et al., 2021). As they change their properties, they can affect various atmospheric processes (Pan et al., 2021a). For example, a bioaerosol's hygroscopicity may change upon exposure to high-concentration ozone or another oxidant, which could improve its chances for IN. A deeper understanding of how bioaerosols transform in the atmosphere is needed to better identify their effect on atmospheric physical and chemical processes.

Bioaerosols are composed of common organic compounds, such as saccharides (Axelrod et al., 2021; Pacini et al., 2006), starch (Bahdanovich et al., 2022; Mampage et al., 2022), amino acids (Chalbot et al., 2013; Kuznetsova et al., 2005), fatty acids, lipids (Kumar et al., 2014), and proteins (Estillore et al., 2016). Various analytical techniques can be applied for the determination of their chemical composition, such as gas chromatography – mass spectrometry (GC-MS), ultra-high performance liquid chromatography – mass spectrometry (UPLC-MS), ultraviolet-visible-near-infrared spectrophotometry (UV-Vis), proton nuclear magnetic resonance spectroscopy ($^1\text{H-NMR}$), and Fourier-transform infrared spectroscopy (FTIR). Individual organic compounds (saccharides, starch, amino acids, and fatty acids) and various functional groups are analyzed using these techniques in this dissertation. The physical and chemical transformations of bioaerosols after exposure to oxidants and photolysis (natural sunlight and OH radicals) are determined as well, using FTIR and $^1\text{H-NMR}$ techniques.

1.1. Current State of Knowledge

The chemical composition of bioaerosols has not been thoroughly studied (Chalbot et al., 2013; Fröhlich-Nowoisky et al., 2016), and thus remains of important scientific interest. **As far as we are aware, no comprehensive chemical study of bioaerosols has been conducted or published.** Comprehensive analyses of various bioaerosol properties have only been compiled in reviews (Després et al., 2012; Pan et al., 2021a; Xie et al., 2021). A highly-cited, thorough review of bioaerosols (Fröhlich-Nowoisky et al., 2016) states:

“... to gain a better understanding of the abundance, sources, transport, and transformation of bioaerosols, it is crucial to determine their **chemical**, genetic, and taxonomic composition as well as their concentration, seasonal variation, vitality, regional diversity, and evolution. Sophisticated techniques in the field of **instrumental trace analysis (e.g., mass spectrometry)** and microbiology, especially DNA sequencing technologies, need to be further developed and applied.”

An area of interest that concern bioaerosols is the study of bioaerosol roles in cloud formation. Bacteria bioaerosols have been studied for their IN properties (Delort et al., 2010; Sun and Ariya, 2006), as well as pollen and sub-pollen particles (Gute et al., 2020; Pope, 2010), and some fungi species (Kunert et al., 2019). The oxidation and polarity changes of certain bioaerosols, such as sub-pollen particles, have been found to affect IN activity after exposure to atmospheric aging (sunlight and OH radicals) (Gute et al., 2020). Although minimal research has been published on the comprehensive chemical

composition of bioaerosols using $^1\text{H-NMR}$, individual compounds of a few specific species have been thoroughly studied using NMR and other techniques, for various purposes. For example, certain algae species (such as *Spirulina platensis*) have been meticulously studied for their biofuel, nutritional, and pharmaceutical potentials (Hannon et al., 2010; Samburova et al., 2013b; Sarpal et al., 2016; Vo et al., 2015). However, generally only a few compounds (i.e., starch, fatty acids, lipids) are of interest for these purposes. Amino acid profiles continue to be studied in various species of algae, but these studies fail to provide a comprehensive analysis of the chemical composition of algae (Andreeva et al., 2021; Siahbalaei et al., 2021).

Another example is western gall rust, which is a tree fungus native to North America (Old et al., 1986). It has only been studied for forest management purposes (Hoffman and Hagle, 2011; Old et al., 1986; Ramsfield et al., 2007), and as far as we know, there are virtually no studies of its' chemical composition. This is surprising, because the spores exist in a powder-like form and are easily dispersible by wind (Old, 1981). Bee pollen has been rigorously studied for its pharmacological and nutritional properties, although it slightly varies from tree pollen in composition (De-Melo and de Almeida-Muradian, 2017; Komosinska-Vassev et al., 2015; Mărgăoan and Bobis, 2010). Studies of anthropogenic aerosol chemical compounds (Chalbot and Kavouras, 2019; Duarte and Duarte, 2015; Suzuki et al., 2001) using $^1\text{H-NMR}$ spectroscopy have been conducted, as well as NMR analysis of various specific compounds of pollen (Chalbot et al., 2013; Hlersa et al., 1999; Otify et al., 2019), algae (Sarpal et al., 2016), and bacteria (Saleh Al-Rubaye et al., 2018). **However, there is poor characterization of these individual $^1\text{H-NMR}$ spectra for the purpose of bioaerosol chemistry research.** In addition, virtually none of

the mentioned studies use the deuterated solvent DMSO-d₆ for bioaerosol analysis with ¹H-NMR. Using a different solvent such as DMSO-d₆ may allow us to see more diverse functional groups.

Although bioaerosols are gaining attention in the scientific community and increasing in concentration with the rapidly changing climate (Anderegg et al., 2021; Ariano et al., 2010; D'Amato et al., 2020, 2013; May et al., 2018a), the Intergovernmental Panel on Climate Change's (IPCC) most recent report ("IPCC Sixth Assessment Report," 2023) fails to mention bioaerosols. The most recent mention of bioaerosols from the IPCC is found in the "Climate Change and Land" special report (published August 2019), where they are stated to be an "important component of carbonaceous aerosols" (Jia et al., 2019). Furthermore, bioaerosols are only briefly mentioned in IPCC's 5th assessment report, where they are reported as being good IN, and one of the main constituents of overall atmospheric aerosols (Boucher et al., 2013). **Therefore, this dissertation is dedicated to expanding the knowledge of the chemical composition (individual compounds and functional groups) and the chemical transformation of bioaerosols in the atmosphere upon exposure to sunlight and oxidants.**

1.2. Goals and Objectives of the Present Research

As was mentioned above, very little is known about the chemical composition and aging of atmospheric bioaerosols. Thus, the purpose of this study is to fill this gap and provide a comprehensive analytical study on their chemical composition, as well as their transformation upon exposure to simulated atmospheric conditions (i.e., oxidants,

photolysis). This research will assist in creating bioaerosol markers that can be used in analysis of ambient filters.

The following research questions will be answered:

1. What is the organic chemical composition of bioaerosols?
2. What are the major chemical functional groups of the most common bioaerosols (e.g., algae, pollen, fungi, bacteria)?
3. How do bioaerosols change chemically upon exposure to atmospheric oxidants and photolysis (i.e., exposure to OH radicals, ultra-violet radiation, and simulated solar radiation)?
4. How do the polarity and functional groups of bioaerosols change after aging, which can be important for IN and CCN?

To answer these research questions, we selected several bioaerosols (pollen (lodgepole pine and rabbitbrush), fungi (western gall rust), bacteria (*Pedobacter* and hay *Bacillus*), and algae (*Spirulina*)) and characterized their individual organic species and chemical functional groups with different analytical techniques: GC-MS, UPLC-MS, UV-Vis-NIR spectrophotometry, ¹H-NMR spectroscopy, and FTIR spectroscopy.

The tasks conducted in the present research are described in the following Chapters. In Chapter 2, the starch content of four bioaerosol species (pollen, fungi, algae, and bacteria) was determined using UV-Vis-NIR spectrophotometry. To do so, an existing colorimetry method was optimized for quantitative analysis of starch content in low-concentration samples. This task is imperative for differentiating between mono/di-saccharides (simple sugars) and polysaccharides (starch) in ¹H-NMR spectra. Chapter 3 is

dedicated to the characterization of the chemical composition and functional groups of organic compounds within bioaerosols using $^1\text{H-NMR}$ spectroscopy. The obtained results are compared with quantitative analyses of individual bioaerosol organic species (saccharides, amino acids, and fatty acids). These quantitative analyses are performed using GC-MS and UPLC-MS. Starch content (Chapter 2) is also compared with $^1\text{H-NMR}$ spectra of bioaerosol extracts. Chapter 4 focuses on the changes in polarity and functional groups of bioaerosols (lodgepole pine pollen and *Spirulina* algae) after exposure to (1) simulated solar radiation and (2) OH radicals formed from hydrogen peroxide through photolysis. The results of the present study will provide a comprehensive characterization of bioaerosol chemical organic components and their transformation upon atmospheric aging. **The results of this research will help to assess, predict, and model the chemical behavior of bioaerosols and their organic species in the atmosphere.**

Chapter 2

Adapted from:

Optimized Spectrophotometry Method for Starch Quantification

Palina Bahdanovich^{1,2}, Kevin Axelrod^{1,2}, Andrey Khlystov¹, and Vera Samburova^{1,*}

¹Division of Atmospheric Sciences, Desert Research Institute, Reno, NV 89512, USA

²Department of Physics, College of Science, University of Nevada, Reno, Reno, NV
89557, USA

*Correspondence: vera.samburova@dri.edu

Published in MDPI's *Analytica*, October 26, 2022

DOI: 10.3390/analytica3040027

2.1. Abstract

Starch is a polysaccharide that is abundantly found in nature and is generally used as an energy source and energy storage in many biological and environmental processes. Naturally, starch tends to be in miniscule amounts, creating a necessity for quantitative analysis of starch in low-concentration samples. Existing studies that are based on the spectrophotometric detection of starch using the colorful amylose–iodine complex lack a detailed description of the analytical procedure and important parameters. In the present study, this spectrophotometry method was optimized, tested, and applied to studying starch content of atmospheric bioaerosols such as pollen, fungi, bacteria, and algae, whose chemical composition is not well known. Different experimental parameters, including pH, iodine solution concentrations, and starch solution stability, were tested, and method detection limit (MDL) and limit of quantification (LOQ) were determined at 590 nm. It was found that the highest spectrophotometry signal for the same starch concentration occurs at pH 6.0, with an iodine reagent concentration of 0.2%. The MDL was determined to be 0.22 $\mu\text{g/mL}$, with an LOQ of 0.79 $\mu\text{g/mL}$. This optimized method was successfully tested on bioaerosols and can be used to determine starch content in low-concentration samples. Starch content in bioaerosols ranged from 0.45 ± 0.05 (in bacteria) to 4.3 ± 0.06 $\mu\text{g/mg}$ (in fungi).

Keywords: starch; polysaccharide; spectrophotometry; pH; amylose–iodine complex

2.2. Introduction

Starch is a polysaccharide that is used as an energy source for humans and can be found in different amounts in plants, bacteria, algae, and other microorganisms (Buléon et

al., 1998; Lafont-Mendoza et al., 2018; Yong et al., 2019). It is an abundant source of energy (Bashir and Aggarwal, 2019) and one of the most important and plentiful polysaccharides commercially (Lafont-Mendoza et al., 2018). Its structure consists of amylose and amylopectin, both of which are polymer glucose chains (McCready and Hassid, 1943; Subroto et al., 2020), and their ratio varies depending on the type of starch (Bates et al., 1943; Egharevba, 2019). Major sources of starch are grains (such as corn), tubers (i.e., potatoes), roots, and fruit (Han and BeMiller, 2007; Takeda et al., 1989). It has been studied in many disciplines and used in different applications, such as agriculture, food science, biofuels, and medicine (Nakayoshi et al., 2015; Subroto et al., 2020; Sulistyarti et al., 2015; Yong et al., 2019). There is also a large interest in using starch as a biodegradable and renewable polymer (Pokhrel, 2015). Quantifying its content is essential to chemical composition studies and assists in differentiating between mono-/disaccharides and polysaccharides in samples.

Available research studies on starch have been mainly focused on the food industry and modification of starch components (Bashir and Aggarwal, 2019; Desai et al., 2018; Han and BeMiller, 2007; Nakayoshi et al., 2015; Subroto et al., 2020). There are several studies that describe starch quantification methods for commercial purposes (i.e., biofuel), which mainly focus on cost and conversion of starch to ethanol (Krajang et al., 2021; Yong et al., 2019). One known method on quantitative analysis of starch is based on the formation of the colorful amylose-iodine complex which can be detected with ultraviolet-visible-near-infrared (UV-Vis-NIR) spectrophotometry. Only a limited number of studies, which are based on the method published in 1943, describe this analytical method of starch quantification (Boonpo and Kungwankunakorn, 2017; Desai et al., 2018; McCready and

Hassid, 1943). Starch and amylose-iodine complex optimization using a spectrophotometry method has also been used in medical research (Sulistiyarti et al., 2015). However, some important analytical parameters have not been investigated, such as optimized method detection limit (MDL) and limit of quantification (LOQ), and pH and iodine concentration dependence, which are important, particularly when quantitative analysis of low-level starch samples is required. One example of these samples are bioaerosols such as pollen, bacteria, fungi, and microalgae.

Bioaerosols are small ($\sim 0.5 - \sim 100 \mu\text{m}$ (Fröhlich-Nowoisky et al., 2016)) airborne biological particles and can be very abundant in the atmosphere (Fröhlich-Nowoisky et al., 2016; Zhang and Steiner, 2022). For example, global emissions of fungal spores can be as high as 190 teragrams (Tg) annually (Tg/a), while pollen emissions can range from 47 to 84 Tg/a (Després et al., 2012). Bioaerosols can become airborne by different mechanisms and can affect biological and atmospheric processes (Fröhlich-Nowoisky et al., 2016). They have become an important research topic in recent years, as anthropogenic climate change is causing an increase in pollen season duration and pollen concentrations in air (Anderegg et al., 2021; Ariano et al., 2010; D'Amato et al., 2020). In addition, an increase in harmful algal blooms is causing an amplification of biological toxins being introduced into the atmosphere (May et al., 2018a). Major components of bioaerosols are proteins, carbohydrates, amino acids, fatty acids, and lipids (Axelrod et al., 2021; Estillore et al., 2016; Kumar et al., 2014). A recent study reported significant chemical constituents of pollen species to be amino acids and saccharides (Axelrod et al., 2021). Some functional groups have also been studied in pollen (Chalbot et al., 2013) and microalgae (Kumar et

al., 2014). In addition, sub-pollen particles ($\sim 0.60 - \sim 2.5 \mu\text{m}$ (Hughes et al., 2020)) have been found to be mainly composed of starch (Burkart et al., 2021; Mampage et al., 2022). However, the chemical composition (including starch reserves), transformation and atmospheric behavior of these bioaerosol particles are still largely unknown (Fröhlich-Nowoisky et al., 2016), which creates a necessity to quantify low level starch concentrations.

The goal of this study is to optimize the absorption spectrophotometry method for quantitative analysis of low concentration starch samples, including bioaerosols. For this purpose, we adopted the McCready et al. (1943) and Boonpo et al. (2017) method, examined it, and optimized the method further for analysis of samples with low starch content. We used the Perkin Elmer Lambda 1050 UV-Vis-NIR spectrophotometer. pH dependence and iodine reagent concentration for amylose determination were optimized in this study. In addition, we determined the MDL, LOQ, and linearity of the calibration for low concentration ranges of starch for this colorimetry method.

2.3. Experimental Section

2.3.1. Chemicals and Reagents

Powdered soluble potato starch ($\geq 95\%$ purity) was purchased from Sigma-Aldrich Inc. (St. Louis, MO, USA). Ethyl alcohol (class 1b) and sodium hydroxide (NaOH) solutions (1 N) were obtained from Fisher Scientific (Fair Lawn, NJ, USA). Hydrochloric acid solution (1 N), d-(+)-glucose (99%), and sucrose (99.5%) were purchased from Sigma-Aldrich, Inc. pH test strips were acquired from JNW Direct (Amazon, Inc.). Reagents (potassium iodide and iodine) and NaOH pellets were purchased from Ward's Science

(Rochester, NY, USA). Ultra-high purity water ($\geq 18 \text{ M}\Omega \text{ cm}^{-1}$) was dispensed by the Elga Veolia PURELAB Chorus 1 (Woodridge, IL, USA) water purification system. Bioaerosols were acquired in different ways. Microalgae (*Spirulina*) was purchased from Amazon, Inc. in freeze-dried powder form, and bacteria (hay Bacillus) was cultured (Desert Research Institute, NV, USA), then freeze-dried prior to extraction. Fungi (western gall rust) and pollen (lodgepole pine) were collected locally (see Table 1) through surface deposition. Bioaerosol specifications are listed in Table 1.

2.3.2. Instrumentation

The Perkin Elmer Lambda 1050 UV-Vis-NIR Spectrophotometer (Waltham, MA, USA) was used for this study, with the wavelength range set to 250-800 nm. Photomultiplier tube (PMT) slits were fixed at 2.00 nm, with a PMT detector response of 0.20 seconds. The ordinate mode was set at absorbance (A), and the data interval at 1.00 nm. For bioaerosol sample preparation, Foxx Life Sciences EZFlow Syringe Filters with hydrophilic polytetrafluoroethylene (PTFE) membrane (Salem, NH, USA) were used, with a pore size of 0.45 μm and diameter of 0.25 mm. 3.5 mL UV quartz spectrophotometer cuvettes (with PTFE covers and a light path of 10 mm) were purchased from FireflySci, Inc. (Northport, NY, USA). Reagents and samples were weighed using a Cahn C-33 microbalance (Cerritos, CA, USA). Bioaerosol bacteria samples were freeze-dried at -40°C for 24 hours prior to extraction using a Thermo Micro Modulyo 115 freeze dryer system (Asheville, NC, USA).

2.3.3. Amylose Iodine Reagent Preparation

The 0.2% iodine reagent (I₂/KI) was prepared by adding 20 mg iodine (I₂) and 200 mg potassium iodide (KI), then adjusted to 10 mL with water. Similarly, the 0.1% iodine reagent was prepared by adding 10 mg of I₂ and 100 mg KI, and the 0.02% iodine reagent was prepared by adding 2 mg I₂ and 20 mg KI, then adjusted to 10 mL with ultra-high purity water. The iodine reagent solution was red-brown in color.

2.3.3. Starch Preparation

The optimized procedure on preparation of starch/iodine reagent solution is presented in Figure 1. To prepare the starch stock solution, one gram of starch was heated at 105 °C for 24 hours, following the temperature optimization of Noranizan et al. (2010). Afterwards, the starch was kept in a desiccator with NaOH pellets until ready for use. 10 mg of desiccated starch was hydrated with 0.1 mL 95% ethanol and 1 mL NaOH solution (1 N) in a 10 mL volumetric flask. It is well-described that in the presence of heat and NaOH, starch molecules swell and are physically modified, which encourages amylose to seep out due to its linear structure (Roberts and Cameron, 2022; Sun et al., 2014). This reaction is what allows detection of starch by measuring the colorful amylose-iodine complex in the visible range of the spectrum with the UV-Vis-NIR spectrophotometer (Baldwin et al., 1944). Although amylopectin is a significant portion of starch (Egharevba, 2019), it has been long known and well described in previous studies (Baldwin et al., 1944; McGrance et al., 1998) that the amylopectin-iodine absorbs at much shorter wave lengths than amylose-iodine complex, which makes amylose a perfect compound for quantitative analysis of starch. Moreover, amylopectin is not as easily extracted due to its highly branched structure (Hermansson and Svegmarm, 1996), and thus the transmission/absorption of the iodine solution is affected more by amylose than

amylopectin (Baldwin et al., 1944). The prepared starch mixture was refrigerated for 24 hours at 4°C. Next, the volume was then adjusted to 10 mL with ultra-pure water at the same temperature and refrigerated again for 16-18 hours. The final concentration of the starch stock was 1000 µg/mL. Also, a “blank” sample with zero starch was prepared with 0.1 mL ethanol and 1 mL NaOH, then adjusted to 10 mL with water (following the same time frame).

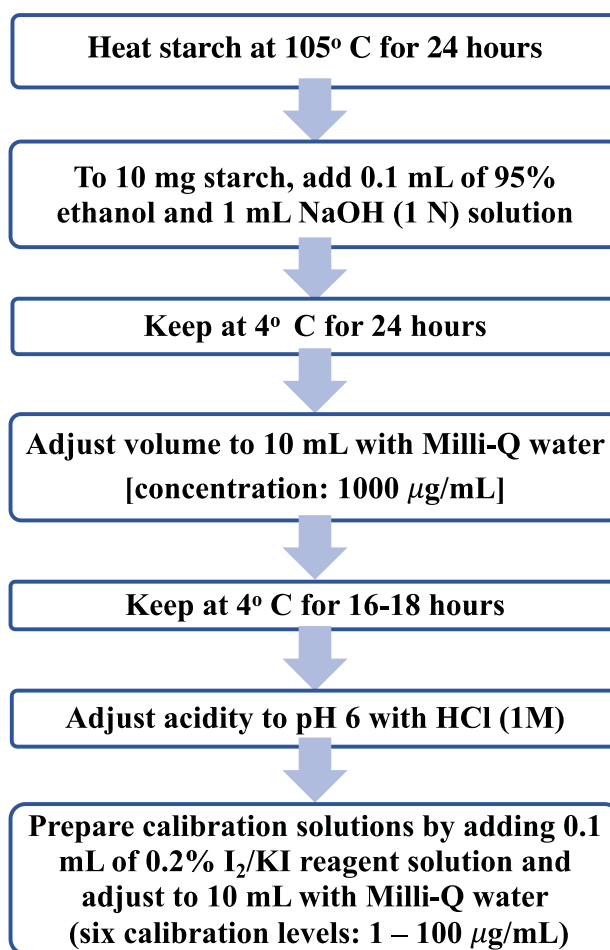


Figure 1. Optimized procedure of starch preparation for amylose-iodine complex spectrophotometry analysis, adapted from Boonpo and Kungwankunakorn, 2017.

5 mL of the prepared starch stock solution was brought to pH 6 by adding 500 μ L of HCl (1 M). This final solution was used for calibration using calibration levels of 1, 10, 25, 50, 75, and 100 μ g/mL (see Table A2.1). To prepare the calibration standards (concentration range: 1 – 100 (μ g/mL)), 0.01, 0.1, 0.25, 0.5, 0.75, and 1.0 mL of stock solution (1000 μ g/mL) was added to six separate volumetric flasks. Then, 0.1 mL of iodine reagent solution was added to each calibration level. With the addition of the iodine reagent, each level forms a different color. Boonpo et al., (2017) varied the iodine solution amount added to each sample, however, we decided to keep the iodine solution amount consistent and vary the starch stock quantity instead. The calibration for this study was run in triplicates to determine the error of the sample preparation and/or the instrument, as well as for statistical purposes.

Due to the lack of studies on amylose-iodine complex absorbance due to pH dependence, starch solutions with varied pH levels (pH 2, 4, and 6) were prepared and analyzed to determine the optimized pH level. In addition, iodine reagent concentrations of 0.02, 0.1, and 0.2% were studied to determine which optimizes the absorbance. Although the iodine reagent concentrations were varied, the amount of the iodine solution added remained the same for every sample (0.1 mL). For these experimental conditions, calibration levels of 1 and 50 μ g/mL were used and ran in duplicates. A monosaccharide (glucose) and disaccharide (sucrose) were also analyzed for starch content at a concentration of 50 μ g/mL, to ensure that the amylose-iodine complex does not form in simple saccharide solutions. These were prepared following the method described for starch, excluding the heat applied in the first step. The stability of the reagents was

determined by testing an aliquot of six-week-old and 16-week-old starch at 50 $\mu\text{g}/\text{mL}$ (0.5 mL stock) and adding freshly prepared iodine reagent solution (0.1 mL). The liquid starch stock solution was stored at 4°C.

The MDL and LOQ were determined following procedures adopted from the Analytical Detection Limit Guidance manual (Ripp, 1996). Ten samples were prepared for MDL analysis, following the blueprint presented in Figure 1. All ten samples were used in calculation for the MDL, with 9 degrees of freedom and a t-value of 2.821 at the 99% confidence level. The samples were prepared according to the optimized pH (pH=6) and amylose iodine reagent concentration (0.2%). The MDL was calculated by taking the standard deviation of the 10 trials and multiplying by the t-value of 2.821. To obtain an accurate MDL, two of three major requirements should pass. The spike level should be less than $\text{MDL} \times 10$, and greater than the MDL itself (Ripp, 1996). The last requirement states that the signal-to-noise ratio (S/N) should be between 2.5 and 10. S/N is calculated by dividing the mean by the standard deviation. LOQ was calculated by multiplying the standard deviation of the MDL by 10 (Ripp, 1996).

To estimate the uncertainty associated with the instrument (spectrophotometer) performance, two calibration standards (level 1 and level 4) and one sample (lodgepole pine pollen, see Table 1) were run as three replicate spectrophotometer measurements of each solution and estimated by calculation mean and standard deviation values. It must be noted that these values were not used in reporting starch concentrations in bioaerosol samples below. The standard deviations used in presenting starch measurements and shown in Figure 3 were calculated based on three replicates of bioaerosol samples prepared

separately following the described procedure (Figure 1) from the same collected sample (lodgepole pine pollen, Table 1).

2.3.4. Bioaerosol Preparation

Several bioaerosols such as pollen, fungi, bacteria, and microalgae were chosen for starch content quantification (see Table 1). Microalgae and bacteria were both freeze-dried prior to the extraction. Bioaerosols were prepared following the same blueprint as starch (see Figure 1), along with centrifuging and syringe filtering (Foxy Life Sciences, 0.45 μm pore size) prior to pH adjustment. One set of bioaerosol samples was prepared without the heating step (Figure 1). Another set of samples was prepared using the additional step in which bioaerosol samples were preheated at 105 °C for 24 hours (Figure 1). This was done to check if the pre-heating step helps release amylose in the starch from the tested bioaerosols.

Table 1. Bioaerosols used for sample preparation of starch content quantification.

Bioaerosol type	Common name	Botanical name	Origin
Pollen	Lodgepole pine	<i>Pinus contorta</i>	Collected in North Lake Tahoe, NV, USA (39°18'03'' N 119°55'22'' W) on 7/05/2020
Fungi	Western gall rust	<i>Endocronartium harknessii</i>	Collected in Mt. Shasta, CA, USA on 5/31/2021
Bacteria	Hay Bacillus	<i>Bacillus subtilis</i>	Cultured in the Molecular Microbial Ecology and Genomics Lab at the Desert Research Institute, NV, USA
Microalgae	Spirulina	<i>Arthrospira platensis</i>	Purchased commercially from Amazon, Inc.

2.4. Results and Discussion

2.4.1. Dependence of pH and Iodine Reagent Concentration

The purpose of this study is to optimize the spectrophotometry method (Boonpo and Kungwankunakorn, 2017) for starch content quantification in low concentration samples. For this task, first the experimental parameters such as pH and iodine reagent concentration were tested. Figure 2 shows the dependence of pH and iodine reagent concentration on the absorption values of 50 $\mu\text{g/mL}$ starch solution. We found that the addition of 0.1 mL of 0.2% iodine solution concentration to the starch solution (final volume 10 mL) shows maximum absorption peak in the visible range at 590 nm, which was observed and confirmed in a previous study (McGrance et al., 1998). The UV-Vis-NIR spectrum of 50 $\mu\text{g/mL}$ calibration level is presented in Figure 2. The maximum absorption was observed at the wavelength of 590 nm, and it is marked by a dashed grey line (Figure 2). In the previous studies, the absorption maximum of the amylose-iodine complex was reported at slightly longer wavelengths: 610 nm [13] and 615 nm [10]. This could be caused by differences in instrument calibrations, purity of the standards, or variation of pH levels. This could also be due to differences in starch types (Brust et al., 2020).

The absorption spectra acquired for the amylose-iodine complex standard solution prepared at different pH levels (pH 2, 4, and 6) is presented in Figure 2 Panel *a*, while Panel *b* shows the absorption spectra for standard starch solutions prepared with different percent of iodine reagent (0.02%, 0.1%, 0.2%). 0.1 mL of iodine reagent was added to the standard starch solutions, with a final volume of 10 mL. We found that the highest amylose-iodine complex absorption values were at pH 6.0, using an iodine reagent concentration of 0.2%

(the final iodine concentration after addition to the starch solution is 0.002%). We did not see the formation of amylose-iodine complex at neutral and basic pH; therefore, we did not test solutions at pH 7 and higher (pH >7). It has been found that optimization of the absorption at 590 nm depends more on iodine reagent concentration than pH, as the absorption at the chosen pH values ranges from 0.52 to 0.56 A and at the tested iodine concentration the absorption ranges from 0.13 to 0.56 A. Although pH 2, 4, and 6 all provide linear calibrations, absorption values are 0.04 A higher in a solution of pH 6, providing a better sensitivity of absorption. Sulistyarti et al. (Sulistyarti et al., 2015) study found that pH 5 was optimal for iodine quantification with the spectrophotometry method (Sulistyarti et al., 2015), while Boonpo et al. (2017) (Boonpo and Kungwankunakorn, 2017) did not specify what pH of starch solution was used. In addition, 0.2% iodine solution was found to be optimal in Boonpo et al. study (Boonpo and Kungwankunakorn, 2017). However, in their study, they found that larger amounts of iodine solution/higher concentration (4 mL) show maximum absorbance near 596-599 nm. In our study, we found that a small amount (0.1 mL) of iodine with 0.002% in the final starch solution shows the maximum absorption at 590 nm; both studies obtained the same final iodine concentration of 0.002% in the starch solution. Our results are comparable with Boonpo et al. study (Boonpo and Kungwankunakorn, 2017) since their method was adopted for this experiment, and both studies used the same iodine solution concentration of 0.2% (and therefore resulted in the same concentration of iodine in the final starch solution of 0.002%). Higher iodine reagent concentration values (>0.2%) were not tested in this study since low starch content samples were analyzed. However, higher concentrations of iodine reagent solution can be considered if testing for higher concentrations of starch. The 0.2%

iodine solution was selected to be added to starch standards and bioaerosol samples to make the concentration of iodine 0.002% in the 10 mL final volume of starch sample.

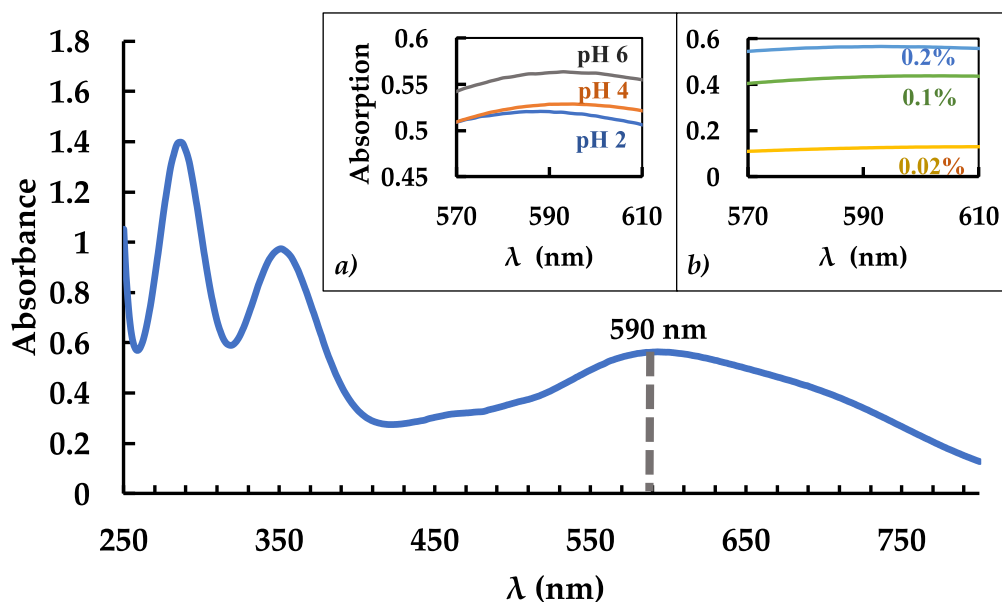


Figure 2. Absorption spectrum of calibration level 4 (50 µg/mL) at pH 6 and iodine reagent (I₂/KI) concentration of 0.2% (which was added to the starch sample (final volume 10 mL)) with a wavelength range 250-800 nm. The peak absorption is noted at 590 nm. 2a) shows pH dependence of starch, with 3 pH levels noted near the peak of 590 nm (50 µg/mL). Panel b shows the iodine reagent concentration added to the starch solution, with 3 concentration levels near the peak of 590 nm (50 µg/mL). Full spectra figures at different pH and iodine reagent concentrations are provided in the appendix (Figures A2.3 and A2.4).

2.4.1. Calibration and MDL

The calibration curve was plotted based on six calibration levels and it was linear between 1-100 µg/mL ($y = 0.0106x - 0.002$), with an R^2 value average of 0.9989 ± 0.0015 . The R^2 value was calculated as an average of five separately prepared and run starch calibrations. The highest calibration level for this experiment was at a concentration of 100 µg/mL, since the trendline begins to plateau for concentrations higher than 100 µg/mL. The calibration curve and spectra can be found in the appendix (Figures A2.1 and A2.2).

The MDL for this study was found to be 0.22 $\mu\text{g/mL}$, which is lower than the spike level of 0.25 $\mu\text{g/mL}$. MDL $\times 10$ is greater than the spike of 0.25 $\mu\text{g/mL}$. The signal-to-noise ratio is 9.9. According to the MDL Guide (Ripp, 1996), our MDL passes major required criteria. The MDL standard deviation is 0.079, from which the LOQ was found to be 0.79 $\mu\text{g/mL}$. To our knowledge, there have not been any MDL or LOQ reported for starch quantification using the spectrophotometry technique. The analytical uncertainty was calculated based on three consecutive spectrophotometry measurements of the lowest calibration level (calibration level 1, concentration 1 $\mu\text{g/mL}$) for the instrument used in this study and is 1.1%. For calibration level 4 (concentration 50 $\mu\text{g/mL}$), the instrument analytical uncertainty is 0.07%. Analytical uncertainty for bioaerosol sample preparation in this study is 0.3%.

2.4.2. Bioaerosol and Saccharide Analysis

To prove this method can be used for starch quantification of low-concentration samples, several bioaerosols were selected (Table 1) and analyzed for starch content at 590 nm. 50 mg of each bioaerosol was prepared for the quantitative analysis of starch following the procedure described in Section 2.3.3. Figure 3 shows starch content in bioaerosols in μg of starch per mg of dry weight of each individual bioaerosol. Microalgae, bacteria, and pollen have <1 μg of starch per mg of dry weight (microalgae: 0.69 ± 0.02 $\mu\text{g/mg}$, heated microalgae: 0.64 ± 0.05 $\mu\text{g/mg}$, bacteria: 0.45 ± 0.03 $\mu\text{g/mg}$, heated bacteria: 0.45 ± 0.05 $\mu\text{g/mg}$, pollen: 0.52 ± 0.03 $\mu\text{g/mg}$, heated pollen: 0.94 ± 0.06 $\mu\text{g/mg}$), whereas both fresh and heated fungi samples have >1 μg . Fresh fungi has 3.5 ± 0.03 μg of starch per mg dry weight, and heated fungi has 4.3 ± 0.06 $\mu\text{g/mg}$ (see Table A2.2 in the appendix). Although

the starch content is lower in microalgae, bacteria, and pollen; the concentration values are 33-127% higher the LOQ (0.79 $\mu\text{g}/\text{mL}$).

An unpaired (independent) t-test (Ross and Willson, 2017) was used for statistical analysis of starch content in bioaerosols. Pre-heating of microalgae and bacteria bioaerosol samples (Figure 3) does not show a statistically significant difference in starch content, being 6.4% for microalgae ($P=0.23$) and 0.3% for bacteria ($P=0.97$), as it clearly does for fungi (19% difference, $P < 0.0001$) and pollen (45% difference, $P=0.0004$) (Figure 3). The higher concentration of starch for pre-heated fungi and pollen samples than for those without heating step, could be explained by the release of amylose during the heating process (Figure 1), while the microalgae and bacteria samples were initially freeze-dried that caused the starch release. Across all bioaerosols, the concentration values are 1.4-11.6 times higher than the MDL (0.22 $\mu\text{g}/\text{mL}$), allowing us to have 99% confidence in the starch quantification method. This method may need to be adjusted for other types of bioaerosol particles (e.g., small fragments), especially those that may require additional preparation and starch isolation steps. This method can be applied for further research regarding the chemistry of starch in bioaerosols in the atmosphere.

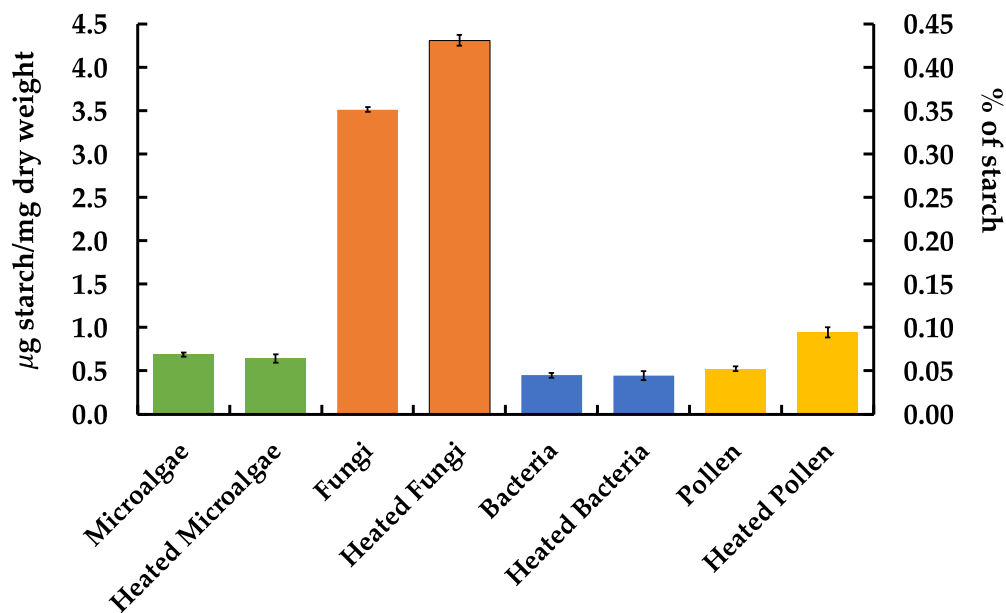


Figure 3. Concentration of starch per milligram of dry weight of selected bioaerosols on the primary axis, with standard deviations. Standard deviations were calculated based on three separate replicates prepared from the same pre-heated pollen stock sample. Percentage of starch of dry weight is found on the secondary axis.

Since saccharides have been also found to be present in bioaerosols, we examined if a mono- and di-saccharide may contribute to background noise during the spectrophotometric quantitative analysis of starch using the amylose-iodine complex approach. A recent study found that some pollen species can contain high concentrations (ranging from 4 to 24% of the dry mass) of saccharides and the most abundant saccharides were found to be glucose and sucrose (Axelrod et al., 2021; Pacini et al., 2006). Thus, glucose and sucrose were selected for the method assessment. When the iodine reagent was added to both saccharide solutions, no color change was observed as it would for starch-containing samples or starch standard solution. Figure 4 shows the absorption spectra for standard starch, glucose, and sucrose prepared at 50 $\mu\text{g/mL}$ concentration. Neither

monosaccharide (fructose) or disaccharide (sucrose) gives a strong signal at 590 nm (green and yellow curves), whereas the starch standard does (blue curve). The saccharide spectra are quite similar in absorption and concentration, showing virtually no difference between mono- and di- saccharides as it pertains to absorbance spectrophotometry. Both glucose and sucrose standard solutions (concentration 50 $\mu\text{g}/\text{mL}$) give a similar background signal at 590 nm that corresponds to 0.30 $\mu\text{g}/\text{mL}$. This is 8.2% above the MDL (0.22 $\mu\text{g}/\text{mL}$) and 48% below the LOQ level (0.79 $\mu\text{g}/\text{mL}$) (whereas bioaerosols are 33-840% higher than the LOQ), indicating that mono- and di-saccharides may add some background noise when analyzing for amylose-iodine complex in starch samples.

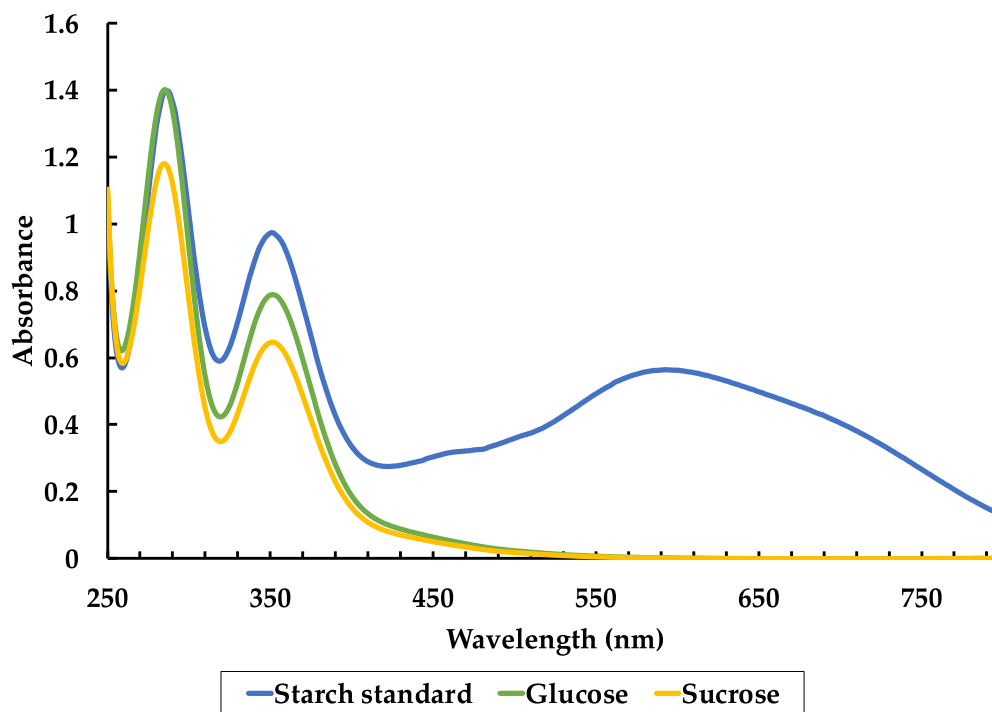


Figure 4. Absorbance spectra of selected saccharides with starch standard for reference using a wavelength range 250-800 nm. Each sample was run using a concentration of 50 $\mu\text{g}/\text{mL}$.

The stability of the stock starch solution was studied over a 16-week period. Figure 5 shows starch decomposition in the stock solution with NaOH, ethanol, and water using percentage of decay on the y-axis over time (in weeks) on the x-axis. After 6 weeks, the starch content decreased from 100% to 84.7% (which is a decomposition of 15.3%). After 16 weeks (about 4 months), the starch content further degraded to 40.9% (a decomposition of 59.1% from the original, fresh stock solution). Standard deviation percentage for starch decay is 0.32%, based on three replicates of fresh starch solution (starch content at 100%), which is almost negligible and thus was not added to the figure. This degradation is likely due to the decay of the starch molecule chains in the presence of high NaOH concentration, which is caused by the oxidation of the hydroxyl groups in the starch (Boonpo and Kungwankunakorn, 2017; Qin et al., 2019). It must be noted that cooling of the starch solution (at 4°C) after the dry heating process may strengthen the amylose-amylopectin and amylose-amylose chains (Gou et al., 2019), which may account for the decrease in absorption values of starch over time. Because of the decomposition, it is recommended to prepare new starch stock for every study and use within a couple of days' time.

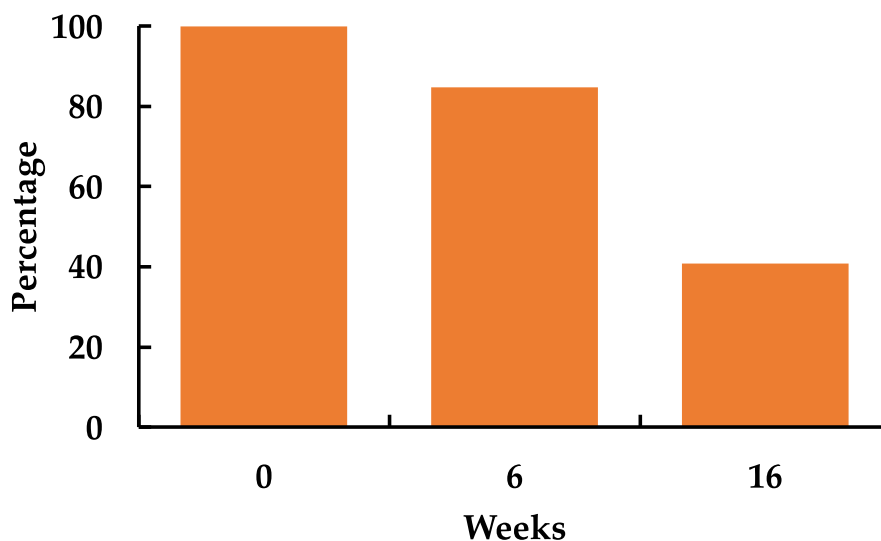


Figure 5. Deterioration of starch solution after four weeks and four months. Each sample was run at 50 $\mu\text{g}/\text{mL}$ in the wavelength range 250-800 nm.

2.5. Conclusion

In the present study the spectrophotometry method for quantitative analysis of starch/iodine complex in low concentration starch samples, such as bioaerosols, was tested and optimized. The MDL for starch in low concentration samples using the Perkin Elmer Lambda 1050 UV/Vis spectrophotometer is 0.22 $\mu\text{g}/\text{mL}$, and the LOQ is 0.79 $\mu\text{g}/\text{mL}$. The linearity of the starch calibration is 0.9989. This method was successfully tested on bioaerosols (pollen, fungi, bacteria, and algae) and it is suitable for analysis of starch in low concentrations. Naturally, there are some limitations to this study. Due to the plateauing of linearity past 100 $\mu\text{g}/\text{mL}$, and the fact that this study was conducted to optimize low-level starch concentrations, we did not test concentrations higher than 100 $\mu\text{g}/\text{mL}$. The plateauing could be due to high concentrations of starch overwhelming the spectrophotometer, as the color of higher concentration samples was near black. We did

not check if other compounds would add to or interfere with the signal of amylose-iodine complex. However, since amylose and amylopectin are composed of polymer glucose chains, we believe that testing glucose for interferences within the UV-Vis-NIR spectrum was sufficient. In addition, amylose content naturally varies from source to source (22-29% (McGrance et al., 1998)), which may affect starch quantification for different bioaerosols. We chose only pH 2, 4, and 6 for the optimization of this method, as one study found that pH 5 was optimal for iodine determination (Sulistiyarti et al., 2015). This study furthers our understanding and knowledge of starch content in bioaerosols, and this method can be used for fields other than bioaerosols, such as agriculture and medicine.

2.6. Acknowledgments

The authors would like to thank Dr. Hans Moosmüller (Desert Research Institute, NV, USA) for generously providing the equipment necessary for this study. The authors would also like to thank Dr. Allison Murray (Desert Research Institute, NV, USA) for the donation of cultured bacteria for our bioaerosol sample study.

2.7. Chapter 2 Appendix

Table A2.1. Calibration levels used for calibration curve of starch content.

Calibration level	Calibration concentration ($\mu\text{g/mL}$)	Volume added (mL)	Dilution from stock solution (1000 $\mu\text{g/mL}$)
1	1	0.01	1000x
2	10	0.1	100x
3	25	0.25	40x
4	50	0.5	20x
5	75	0.75	13.3x
6	100	1.0	10x

Table A2.2. Concentration of starch in bioaerosols (μg starch/mg dry weight) at 590 nm.

Bioaerosol type	Fresh concentration (μg starch/mg dry weight)	Heated concentration (μg starch/mg dry weight)
Pollen (<i>Pinus Contorta</i>)	0.52 ± 0.03	0.94 ± 0.06
Fungi (<i>Endocronartium Harknessii</i>)	3.51 ± 0.03	4.31 ± 0.06
Bacteria (<i>Bacillus subtilis</i>)	0.45 ± 0.03	0.45 ± 0.05
Microalgae (<i>Arthrospira Platensis</i>)	0.69 ± 0.02	0.64 ± 0.05

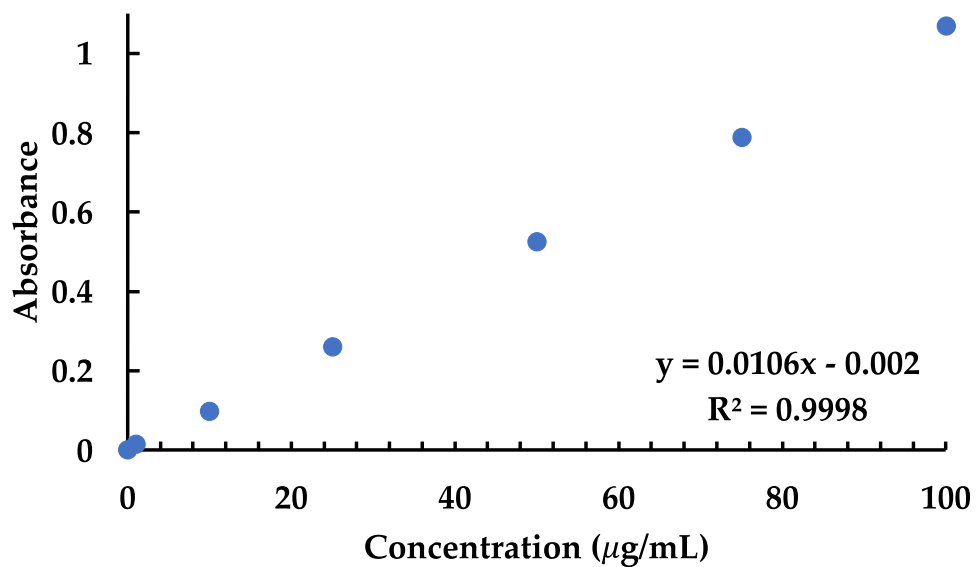


Figure A2.1. Calibration curve at 0.2% iodine reagent concentration (see table A2.1 for concentrations of calibration levels).

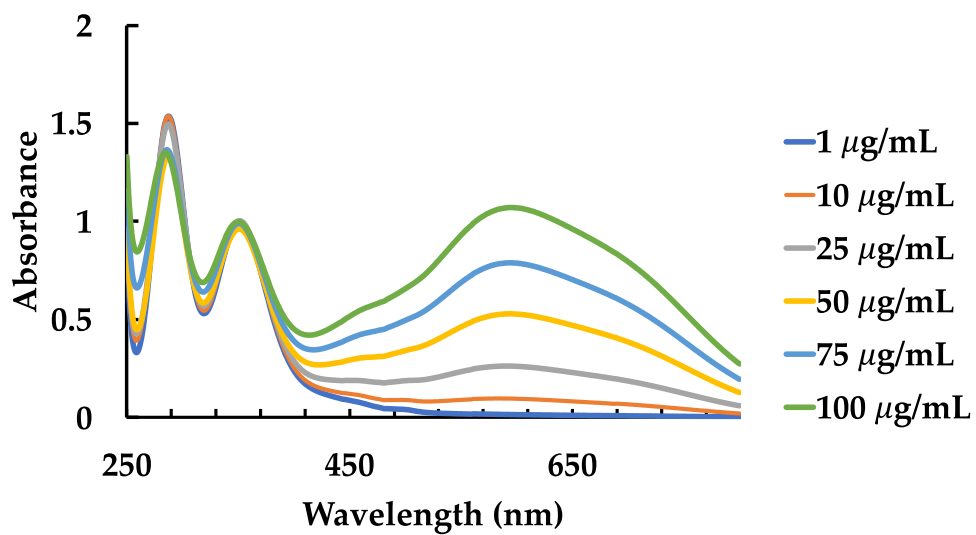


Figure A2.2. Spectra of calibration levels at 0.2% iodine reagent concentration.

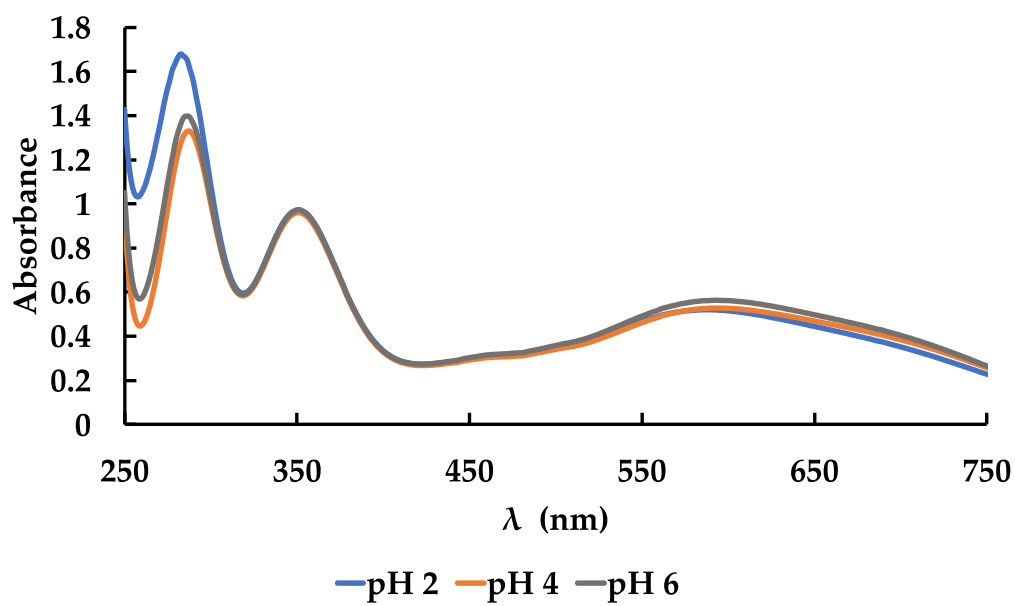


Figure A2.3. Full spectrum of calibration level 4 (50 $\mu\text{g/mL}$) at pH 2, 4, and 6.

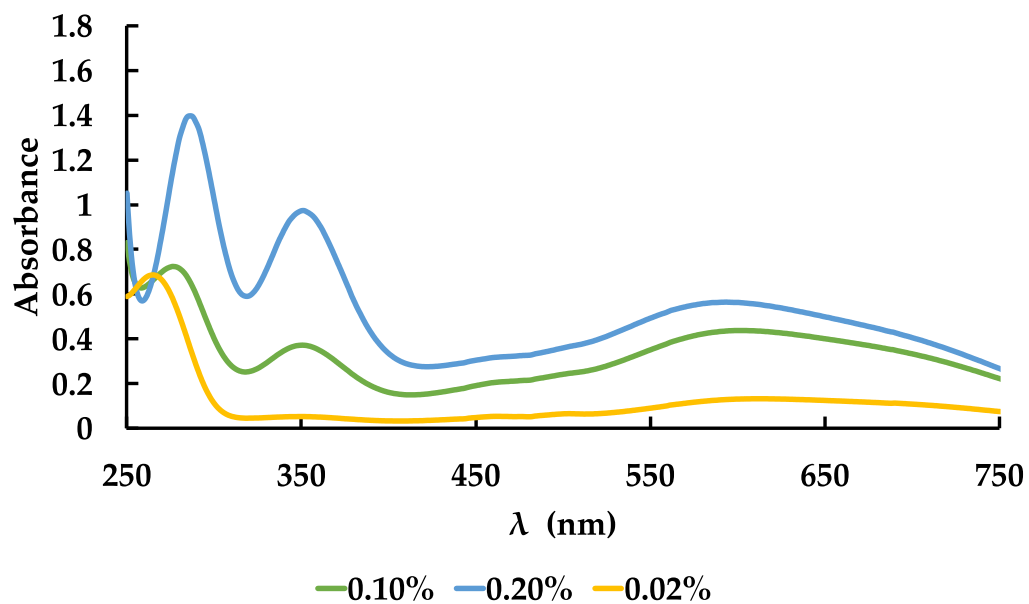


Figure A2.4. Full spectrum of calibration level 4 (50 µg/mL) at iodine reagent concentration 0.02, 0.1, and 0.2%.

Chapter 3

Adapted from:

Characterization of Organic Species and Functional Groups in Pollen, Fungi, Algae, and Bacteria Bioaerosols

Palina Bahdanovich^{1,2}, Kevin Axelrod^{1,2}, Andrey Khlystov^{1,2}, and Vera Samburova^{1,2,*}

¹Division of Atmospheric Sciences, Desert Research Institute, Reno, NV 89512, USA

²Department of Physics, College of Science, University of Nevada, Reno, Reno, NV
89557, USA

*Correspondence: vera.samburova@dri.edu

Published in RSC's *Environmental Science: Atmospheres*, August 13, 2024

DOI: 10.1039/D4EA00083H

3.1. Abstract

Though the importance of bioaerosols is increasing with the changing climate, very little is known about the chemistry of bioaerosols, their atmospheric fate, and chemical composition. This paper is focused on the characterization of chemical functional groups of four atmospherically relevant bioaerosols: pollen (lodgepole pine and rabbitbrush), fungi (western gall rust), bacteria (*Pedobacter* and hay *Bacillus*), and algae (*Spirulina*). For this purpose, the proton nuclear magnetic resonance spectroscopy ($^1\text{H-NMR}$) technique was used on water-soluble extracts of the selected bioaerosols, while quantitative analysis of individual organic species (saccharides, amino acids, and fatty acids) was performed using gas chromatography mass spectrometry (GC-MS), ultra-high performance liquid chromatography (UPLC-MS), and ultraviolet-visible-near-infrared spectrophotometry (UV-Vis-NIR). The obtained $^1\text{H-NMR}$ results revealed major contributions from aliphatic protons in hay *Bacillus* (50.2%) and *Pedobacter* (57.0%) bacteria, western gall rust fungus (39.7%), *Spirulina* alga (73.8%), and rabbitbrush pollen (31.3%). Protons from saccharides were dominant in lodgepole pine pollen (27.6%). The quantitative analysis shows that the saccharide glucose is common among the analyzed bioaerosols, as well as proline, leucine, isoleucine, alanine, and phenylalanine amino acids, and palmitic, oleic, linoleic, linolenic, and stearic fatty acids (except in hay *Bacillus* bacteria). Concentrations of analyzed saccharides ranged between $2.01 \mu\text{g mg}^{-1}$ of dry mass (in hay *Bacillus* bacteria) and $183.54 \mu\text{g mg}^{-1}$ (in lodgepole pine pollen), followed by amino acids (from $2.57 \mu\text{g mg}^{-1}$ in western gall rust fungus to $21.38 \mu\text{g mg}^{-1}$ in hay *Bacillus* bacteria), and fatty acids (from $0.05 \mu\text{g mg}^{-1}$ in hay *Bacillus* bacteria to $25.82 \mu\text{g mg}^{-1}$ in lodgepole pine pollen). Comparison of

$^1\text{H-NMR}$ and quantitative analyses showed a good correlation ($R^2 = 0.608$) between the saccharide segment of $^1\text{H-NMR}$ bioaerosol spectra and individual saccharide analysis.

Key words: $^1\text{H-NMR}$, mass spectrometry, chemical composition, saccharides, fatty acids, bioaerosols, functional groups

3.2. Introduction

Bioaerosols are particles, such as pollen, fungi, bacteria, microalgae, and their dispersal units and fragments, emitted into the atmosphere from biological sources (Bowers et al., 2011; Fröhlich-Nowoisky et al., 2016; Mainelis, 2020). These particles range from tens of nanometers to a few hundred micrometers in diameter (Kim et al., 2018; Lazaridis, 2019; Samburova et al., 2013a). Bioaerosols can represent a significant portion of the atmospheric aerosol load (Després et al., 2012; Huffman et al., 2013; Schumacher et al., 2013) being emitted into the atmosphere in thousands of tera-grams (Tg) per year, with concentrations fluctuating based on region and season (Després et al., 2012; Jaenicke, 2005). Recent estimates of bioaerosol contribution to atmospheric particulate matter (PM) indicate that bioaerosols can account for 16.5% of $\text{PM}_{2.5}$ and 16.3% of PM_{10} (Hyde and Mahalov, 2020). Due to their aerodynamic size and structure, bioaerosols can be transferred by wind and other mechanisms, and thus may play a role in atmospheric chemical and physical processes. Although the atmospheric abundance of bioaerosols is roughly 30% in urban and rural environments (Fröhlich-Nowoisky et al., 2016), several studies have found that some bioaerosols, such as pollen, bacteria, and fungi, can be effective cloud condensation nuclei (CCN) and ice nucleating particles (INP) (Burkart et al., 2021; Haga et al., 2014; Lazaridis, 2019; Möhler et al., 2007; Pope, 2010; Schiffer et

al., 2018; Sun and Ariya, 2006). For example, Bauer et al., (2003) analyzed cloud water and atmospheric aerosol samples in the Austrian mountains and determined that the main identified species (*A. agilis* and *S. echinoides*) were CCN active. Huffman et al., (2013) performed DNA analysis of bioaerosol samples collected in the central Rocky Mountains (Colorado, USA) and showed that some bacteria and fungi can play a significant role in the precipitation formation, especially during rain events, which can trigger a large emission of bioaerosols from the forest. Another study highlighted the importance of fungal spores in cloud formation processes on local and regional scales (Haga et al., 2014). Further, a recent field study by Cornwell and colleagues determined that the major source of INPs between -12 and -20 °C were bioaerosols (Cornwell et al., 2023). Microorganisms (i.e., bacteria, fungi, and algae) have been found as high as the stratosphere, where they endure extreme atmospheric conditions, such as short wavelength radiation, desiccation, and very low temperatures (DasSarma and DasSarma, 2018). Airborne biological particles can also be transported long distances, even intercontinentally (Smith et al., 2011; Tesson et al., 2016; Warren and St. Clair, 2021).

Like other atmospheric aerosols, bioaerosols significantly affect human health (Kampa and Castanas, 2008; Sénéchal et al., 2015), including respiratory irritation due to allergens (D'Amato et al., 2013; Taylor et al., 2007), exposure to bacteria, pathogens, and possible inhalation of neurotoxins (Mayer et al., 2007). Recent studies have reported that a changing climate fuels algal blooms (May et al., 2018b) and increases concentrations of pollen (Anderegg et al., 2021). The amplified harmful algal blooms can emit toxins via lake spray aerosol (May et al., 2018b), which can negatively impact humans and the environment (Carmichael and Boyer, 2016). In addition to airborne toxin emission, some

algae species can produce allergic reactions like that of pollen, such as respiratory issues and reactions on the skin (Gartner et al., 2021). Dramatic changes in pollen concentrations and longer pollen seasons negatively impact public health (Anderegg et al., 2021). According to the Center for Disease Control and Prevention, 24.4 million people suffer from seasonal pollen allergies in the U.S. (Center for Health Statistics, 2018). These concerns and lack of studies on contribution of bioaerosols to the atmospheric processes create an urgency to study bioaerosols, especially their chemical composition and atmospheric fate.

In the present study, several bioaerosols were selected considering their relevance, abundance in the atmosphere, and availability: lodgepole pine and rabbitbrush pollens (*Pinus contorta* and *Ericameria nauseosa*), western gall rust fungus (*Endocronartium harknessii*), *Pedobacter* and hay Bacillus bacteria (*Pedobacter sp.* and *Bacillus subtilis*), and *Spirulina* alga (*Arthrospira platensis*). Lodgepole pine and rabbitbrush are two dominant producers of pollen in western North America (Chileen et al., 2020; Faske et al., 2021). Pine pollen species have been detected in air samples in the Arctic (transported from other locations to the pine-free area of the Arctic), which confirms their presence in the atmosphere (Jędryczka et al., 2023). Western gall rust is a fungus that affects hard pine trees in western and northern North America (Old et al., 1986; Powell and Hiratsuka, 1973). This fungus produces galls on pine trees, which contain orange spores (Hoffman and Hagle, 2011) that can easily be dispersed through the atmosphere (Ramsfield et al., 2007). Although there is limited literature available regarding western gall rust, airborne fungal spore counts can range from 1,000 to 50,000 spores per cubic meter of air (Després et al., 2012; Hughes et al., 2022), which highlights their contribution to the atmospheric

aerosol load. *Pedobacter sp.* and hay *Bacillus* are commonly found in soil (Bjerketorp et al., 2021; Hashem et al., 2019; Tan et al., 2020), and several *Bacillus* species have been identified in thousands of PM_{2.5} aerosol samples across the U.S. (Merrill et al., 2006). *Spirulina* is an incredibly adaptable alga that can thrive in extreme conditions and is commonly found in soil, freshwater, and saltwater, among other aquatic habitats (Vo et al., 2015). To our knowledge, there have been no studies conducted on airborne *Spirulina* alga, however, algae and other microorganisms (i.e., bacteria and fungi) can become airborne by aerosolization (Delort et al., 2010; Sahu and Tangutur, 2015), and even survive stratospheric conditions (DasSarma and DasSarma, 2018).

To characterize chemical functional groups of water-soluble bioaerosol extracts, the proton nuclear magnetic resonance (¹H-NMR) spectroscopy technique was selected for the present study. ¹H-NMR has been widely used for analysis of atmospheric organic aerosols, especially those of anthropogenic origin (Duarte and Duarte, 2015). While research surrounding analysis of airborne pollen particles and water-soluble aerosols by means of ¹H-NMR has been published (Chalbot et al., 2013; Duarte and Duarte, 2015; Horník et al., 2020; Suzuki et al., 2001), limited research was conducted on the chemistry of other types of biological aerosols. Several studies on the chemical composition of bioaerosols reported that bioaerosols generally contain common organic compounds like saccharides, amino acids (Axelrod et al., 2021; Chalbot et al., 2013; Kuznetsova et al., 2005), carbohydrates (Bahdanovich et al., 2022; Elbert et al., 2007), proteins (Estillore et al., 2016), fatty acids, and lipids (Kumar et al., 2014). Saccharides such as glucose and sucrose can comprise anywhere from 4.0 to 29% (total dry weight) in pollen (Axelrod et al., 2021; Pacini et al., 2006), while amino acid content ranges from 0.29 to 15% (total dry

weight) (Axelrod et al., 2021). Recent studies found that sub pollen particles ($\sim 0.60 - \sim 2.5 \mu\text{m}$) (Hughes et al., 2020) are largely composed of starch (Burkart et al., 2021; Mampage et al., 2022). In our recent study we found that the starch content in bioaerosols can range from 0.045 (in hay *Bacillus* bacteria) to 0.43% (in western gall rust fungus) (total dry weight) (Bahdanovich et al., 2022). However, there is still a large knowledge gap on the chemical composition and the atmospheric transformation of these bioaerosols and their fragments (Chalbot et al., 2013; Fröhlich-Nowoisky et al., 2016; Gute et al., 2020). Therefore, the goal of the present study is to characterize the chemical composition and functional groups of organic compounds in the aqueous extracts of the selected bioaerosols. For this purpose, the bioaerosols were lysed to represent the fragmentation that can occur in the atmosphere (Fröhlich-Nowoisky et al., 2016; Lindsley et al., 2017). $^1\text{H-NMR}$ spectroscopy results were compared with the data obtained using quantitative analyses such as gas chromatography-mass spectrometry (GC-MS) and ultra-high performance liquid chromatography-mass spectrometry (UPLC-MS). The starch content of the selected bioaerosols was assessed with ultraviolet-visible-infrared (UV-Vis-NIR) spectroscopy (Bahdanovich et al., 2022; Boonpo and Kungwankunakorn, 2017).

3.3. Experimental Section

3.3.1. Standards and materials

Deuterated dimethyl sulfoxide (DMSO-d_6) (99.9%) and deuterium oxide (D_2O) (99.96%) were used as solvents in this study and were purchased from Cambridge Isotope Laboratories, Inc. (Andover, MA, USA). Standards were purchased from Sigma-Aldrich, Co. (St. Louis, MO, USA) and can be found in Table A3.1 of the appendix. Sodium

hydroxide (NaOH) pellets were purchased from Ward's Science (Rochester, NY, USA). Ultra-high purity water ($\geq 18 \text{ M}\Omega \text{ cm}^{-1}$) used in this study was dispensed by Elga Veolia PURELAB Chorus 1 water purification system (Woodridge, IL, USA). For GC-MS sample derivatization, N,O-bis(trimethylsilyl)trifluoroacetamide (BSTFA) with 1% trimethylchlorosilane (TMCS) (Thermo Fisher Scientific, Waltham, MA, USA) and pyridine (Sigma-Aldrich) were used. Eluents such as toluene, acetonitrile (ACN), and HPLC-grade water were purchased from Thermo Fisher Scientific. Saccharide standards were purchased from Sigma-Aldrich, Cambridge Isotope Laboratories, Inc., and Accustandard (New Haven, CT, USA).

UPLC-MS eluents include HPLC-grade ACN (Fisher Scientific) and ultra-high purity water. Formic acid (Fisher Scientific, Fair Lawn, NJ, USA) and ammonium formate (Sigma-Aldrich) were used as additives in the eluent for amino acid analysis. Amino acid and fatty acid standards were purchased from Sigma-Aldrich and Toronto Research Chemicals (North York, ON, Canada). A collection of calibration standards for saccharide, amino acid, and fatty acid analysis can be found in the appendix (Table A3.2). Soluble potato starch ($\geq 95\%$ purity) was purchased from Sigma-Aldrich. Class 1b ethyl alcohol (Fisher Scientific), 1 N sodium hydroxide solution (Fisher Scientific), and 1M hydrochloric acid (HCl) (Sigma-Aldrich) were used for starch and fatty acid preparation. Potassium iodide and iodine were obtained from Ward's Science.

3.3.2. Bioaerosol species

Bioaerosols were either purchased or collected in the field (see Table 2). Samples consist of 15 mg (dry weight) of each bioaerosol for $^1\text{H-NMR}$ analysis (samples weighed

using the Cahn C-33 microbalance, Cerritos, CA, USA). For GC- and UPLC-MS analysis, bioaerosol samples were weighed at 3 mg each. *Arthrospira platensis* (commonly known as *Spirulina*) was commercially purchased from Amazon.com, Inc. (Seattle, WA, USA) in freeze-dried form. *Endocronartium harknessii* (commonly known as western gall rust) was collected by deposition in Mount Shasta, CA, USA. *Ericameria nauseosa* (rubber-rabbit brush) and *Pinus contorta* (lodgepole pine) pollen were collected by deposition in various areas near Reno, NV, USA (see Table 2 for specific locations). Lodgepole pine pollen was collected throughout a period of three years (July 2020; June 2021; May 2022). *Pedobacter sp.* and *Bacillus subtilis* were cultured at the Molecular Microbial Ecology Genomics Laboratory, Desert Research Institute, Reno, NV USA. Freshly cultured bacteria samples were lyophilized (freeze-fried) at -40 °C for 24 hours using the Thermo Micro Modulyo 115 freeze dryer system (Asheville, NC, USA). Bioaerosols are referred to using their common name throughout this study.

Table 2. Bioaerosols species selected for the present study.

Bioaerosol	Common name	Botanical name	Origin
Pollen	Lodgepole pine	<i>Pinus contorta</i>	Collected July-5-2020 in North Lake Tahoe, NV, USA (2020 season)
			Collected June-22-2021 at the Mt. Rose Summit, NV, USA (2021 season)
			Collected May-23-2022 in Reno, NV, USA (2022 season)
Fungus	Rabbitbrush	<i>Ericameria nauseosa</i>	Collected October-8-2019 in Reno, NV, USA
	Western gall rust	<i>Endocronartium harknessii</i>	Collected May-31-2021 in Mt. Shasta, CA, USA
Bacteria	Hay Bacillus;	<i>Bacillus subtilis</i> ;	Cultured in the Molecular Microbial Ecology and Genomics Lab at the Desert Research Institute, NV, USA and freeze-dried on February-13-2022
	<i>Pedobacter</i>	<i>Pedobacter sp.</i>	
Microalgae	<i>Spirulina</i>	<i>Arthrospira platensis</i>	Commercially purchased from Amazon, Inc.

3.3.3. ¹H-NMR analysis

¹H-NMR analysis was performed using the Agilent Technologies, Inc. 500 MHz PremiumCompact+ NMR (Santa Clara, CA, USA) at 25° C, using VnmrJ software (“VnmrJ 4.0 (Revision A),” 2013). The spectra were acquired in the range of 0.0 – 14.0 ppm. For ¹H-NMR characterization of functional groups of the selected bioaerosols (Table 2) and for assigning chemical shifts, standards were prepared, and ¹H-NMR spectra acquired for the compounds of the following chemical classes: fatty acids, amino acids, triacylglycerols (TAG), saccharides, sugar alcohols, starch, polycyclic aromatic

hydrocarbons (PAH's), oxygenated PAH's, aldehydes, aliphatic alcohols, and aromatic alcohols (see Table A3.1 for specific compounds). Dry standards were desiccated with NaOH pellets (to reduce water signal in $^1\text{H-NMR}$ spectra) prior to addition of 0.75 mL DMSO- d_6 or D_2O . Standards were dissolved in DMSO- d_6 or D_2O (see Table A3.1) directly for each trial and sonicated for five minutes at 30 °C. Standard solutions were then transferred to 5 mm high-throughput 8" standard series NMR tubes (Norell, Morganton, NC, USA and Wilmad LabGlass, Vineland, NJ, USA). Three replicates of saccharides and fatty acids were prepared separately to determine consistency of sample preparation. Standards were run for 64 scans to assign chemical shifts and major functional groups for analysis of the bioaerosol sample spectra (Table 3).

Bioaerosol samples (see Table 2) were hydrated with ultra-high purity water (Elga Veolia PURELAB Chorus) for a concentration of 10 mg mL^{-1} . Samples were thoroughly lysed (Bertin Instruments Precellys 2 mL Lysing Kit, Rockville, MD, USA) for one minute, in intervals of 20 seconds at 20,000 revolutions per minute (RPM) using the Bertin Instruments Minilys Personal Homogenizer (Rockville, MD, USA) to encourage compound extraction from bioaerosol cells and fragmentation of the bioaerosols. The vials containing the homogenized mixtures were put on ice for one minute between each 20 second interval. Then, the samples were centrifuged for two minutes at 10,000 RPM to separate the supernatant from the pellet that did not dissolve in the solution. The supernatant was filtered through a 0.45 μm pore size syringe filter (hydrophilic polytetrafluoroethylene (PTFE) membrane, 25 mm diameter, Foxx Life Sciences (EZFlow, Salem, NH, USA) and Thermo Fisher Scientific Inc. (Titan 3) (Rockwood, TN, USA)). To prepare the samples for $^1\text{H-NMR}$ analysis, the supernatant was evaporated using ultra-high

purity nitrogen gas (Pierce Reacti-Vap Evaporating Unit Model 18780, Rockford, IL, USA) and fully dried in a vacuum oven (Precision Scientific Inc, Chicago, IL, USA) overnight at room temperature (20 – 22 °C). Once the sample was dry, 0.75 mL of DMSO- d_6 was added to all vials. DMSO- d_6 was chosen as the solvent for our samples due to its common use as a solvent in $^1\text{H-NMR}$ spectroscopy and ability to display OH functional groups in the spectra (Jones and Fleming, 2014). To promote dissolution of the samples in DMSO- d_6 , each mixture was sonicated for five minutes at 30 °C. Three analytical replicates of lodgepole pine pollen (2022 season), western gall rust fungus, and *Spirulina* alga samples were prepared separately to ensure sample preparation consistency. Each bioaerosol sample (in DMSO- d_6) was run for 256 scans.

0.75 mL of pure DMSO- d_6 and D_2O were analyzed to determine the reference peaks of the solvents. Standard and analyte $^1\text{H-NMR}$ spectra were analyzed using MestReNova software (“MestReNova 14.2,” 2020). The chemical shift range for this study was set to 0 to 14 parts per million (ppm). Each spectrum was phased and referenced at DMSO- d_6 (2.50 ppm; for bioaerosol samples) and D_2O (4.79 ppm; for several standards) solvent peaks. To determine the quality of the shims, the Tetramethylsilane (TMS) peak (internal standard used in $^1\text{H-NMR}$) (Tiers, 1958) width (at 0.0 ppm) of each spectrum was under 1 Hz at half height of the peak. The baseline was corrected at the 3rd polynomial order. The H_2O peak, which was present in all DMSO- d_6 samples and standards, was suppressed at 3.32 ppm, using the convolution method and a selectivity parameter of 64. This suppressed area was not integrated. DMSO- d_6 is hygroscopic (R. Ellson et al., 2005), thus water peaks are present when DMSO- d_6 is used as a solvent in $^1\text{H-NMR}$, despite desiccation of the samples. For the D_2O standard spectra, the solvent (D_2O) peak was cut from 4.75 to 4.85 ppm.

Spectra were integrated based on chemical shift ranges found in previous $^1\text{H-NMR}$ studies (Chalbot et al., 2013; Duarte and Duarte, 2015; Jones and Fleming, 2014; Pretsch et al., 2009; Starkey, n.d.) and by analysis of standard compounds in the present study (Table 3, Table A3.1). However, some of the studies' segments are incomplete or broad, thus for the present research, selected standards (Table A3.1) were analyzed, and $^1\text{H-NMR}$ segments were determined (see Figure A3.1). Chemical shift ranges were set for the following chemical groups: C-H (aliphatic groups, such as -CH, -CH₂, -CH₃) at 0.5 – 2.0 ppm (Jones and Fleming, 2014), α -carbon (such as O=CH_{1,2}, CH-COO:, and α to amine H) and amines (NH and NH₂) at 2.0 – 2.7 ppm (Jones and Fleming, 2014; Starkey, n.d.), protons in saccharides at 2.7 – 3.7 ppm, H-C-O (oxygenated aliphatics, alcohol CH and OH, and saccharide H) at 3.7 – 4.1 ppm (Duarte and Duarte, 2015), -OH (carbonyls and -OH found in saccharide, glycerol, alcohol, and TAG molecules) at 4.1 – 5.7 ppm (Chalbot et al., 2013), OH in saccharides at 6.0 – 6.6 ppm, Ar-H (aromatics) and amides (CONH and CONH₂) at 6.6 – 8.3 ppm (Jones and Fleming, 2014; Pretsch et al., 2009; Starkey, n.d.), and Ar-OH, -CHO, -COOH (oxygenated aromatics, aldehydes, and carboxylic acids) at 9.0 – 14.0 ppm (Pretsch et al., 2009) (see Table 3). Oxygenated aromatic and carboxylic acid segments were not used for analysis in this chapter, as bioaerosol spectra has weak signals in these regions. A total of seven segments were assigned and used, where the majority of bioaerosol signals reside. After subtraction of the solvent peaks, absolute integration values were summed from 0.5 – 8.3 ppm, with the first segment (aliphatic at 0.5 – 2.0 ppm) normalized to one (1). Each chemical shift range was divided by the total and recalculated as a percentage for percent distribution of functional groups (see the

Results Section). An NMR Solvent Data Chart (Cambridge Isotope Laboratories Inc., n.d.) was used to determine locations of solvent peaks (see Table A3.3).

Table 3. Segments of chemical shifts assigned for ¹H-NMR functional group analysis in bioaerosol extracts (0-14 ppm) based on analyzed standards (Table A3.1) and existing literature (Chalbot et al., 2013; Duarte and Duarte, 2015; Jones and Fleming, 2014; Pretsch et al., 2009; Starkey, n.d.). Segment 8 was not used for analysis due to weak signal in this segment.

Segment	1	2	3	4	5	6	7	8
Spectral Shift (ppm)	0.5 – 2.0	2.0 – 2.7	2.7 – 3.7	– 3.7 – 4.1	4.1 – 5.7	6.0 – 6.6	6.6 – 8.3	9.0–14
	Aliphatic CH	α-carbon O=CH _{1,2}	H in sugar ring	Alcohol CH	All OH in saccharide ring except -O-CH(OH)-	OH in saccharide ring -O-CH(OH)-	Aromatic-H ^A	Ar-OH ^A
	Aliphatic CH ₂	α-carbon CH-COO:	CH-OH in sugar alcohol	Alcohol OH	Glycerol OH		CONH, CONH ₂ ^A	COOH ^A
	Aliphatic CH ₃	α to amine H	C-H in sug-CH ₂ -OH	H in saccharide ring	CH=CH ₂			C(O)H ^A
		NH, NH ₂		α-carbon CH ₂ -C-NH ₂ ^A	Alcohol OH			
					OH in TAG			

^A Weak signal

3.3.4. GC-MS analysis

Selected bioaerosols (excluding *Pedobacter* bacteria due to lack of specimen, rabbit brush and 2020 season lodgepole pine pollen (saccharide content determined by Axelrod et al., (2021)) (see Table 2) were prepared and extracted following the same blueprint as those for ¹H-NMR (lysing, centrifuge, and syringe filtering). For GC-MS saccharide

analysis, the additional step of chemical derivatization via silylation (Schummer et al., 2009) after filtration was conducted. Samples were prepared at a concentration of 3 mg mL⁻¹, lysed, centrifuged, filtered with 0.45 µm pore size syringe filters, and placed into deactivated vials (Waters Co., Milford, MA, USA). Lodgepole pine pollen (2022) was prepared in three replicates (3 mg mL⁻¹) for preparation error and statistical purposes. For derivatization, 20 µL of internal standard (glucose-d₇) was added to 50 µL of filtered bioaerosol sample solution (total 70 µL volume prior to evaporation), then evaporated to dryness with nitrogen gas. Then, 50 µL of ACN was added to the evaporated samples following sonication (no heat) for 10 minutes. 50 µL of 99.8% pyridine and 150 µL BSTFA (with 1% TMCS) were added, and the samples were heated for 2 hours at 65 °C. After heating, 50 µL of toluene was added to the samples. The Varian CP-3800 gas chromatograph coupled with the Varian 4000 Ion Trap Mass Spectrometer were used for GC-MS analysis. A 30-meter DB-5MS 5% phenylmethylsilicone fused silica capillary column was used for the chromatograph (Agilent Technologies, Santa Clara, CA, USA), at a temperature of 320 °C. This saccharide analysis used five calibration points, with a range of 5 ng µL⁻¹ – 100 ng µL⁻¹, and an R² range of 0.969 – 0.998. Detailed GC-MS methodology for saccharide analysis can be found in Axelrod et al., (2021), and analyzed standards can be found in the appendix (Table A3.2).

3.3.5. UV-Vis-NIR starch analysis

The starch UV-Vis-NIR quantitative method was described in Chapter 2. Briefly, bioaerosols were heated for 24 hours at 105°C. 0.1 mL of 95% ethanol and 1 mL NaOH (1 N) solution were added to 10 mg of bioaerosol dry weight. The mixture was kept at 4°C for 24 hours. Then, the volume of the mixture was adjusted to 10 mL with ultra-high purity

water for a concentration of $1000 \mu\text{g mL}^{-1}$ and kept at 4°C for 16-18 hours. The acidity of the solution was adjusted to pH 6 with 1M HCl. An iodine reagent (0.2% concentration) was prepared to detect starch in bioaerosol samples by combining 20 mg iodine and 200 mg potassium iodide, then adjusting to 10 mL with ultra-high purity water. 0.1 mL of this reagent solution was added to each bioaerosol sample. The Perkin Elmer Lambda 1050 UV-Vis-NIR Spectrophotometer (Waltham, MA, USA) was used for starch analysis, with 3.5 mL UV quartz cuvettes (FireflySci, Inc., Northport, NY, USA). This method used six calibration levels ($1\text{-}100 \text{ ng } \mu\text{L}^{-1}$), and the R^2 of the calibration was 0.999. The starch MDL was $0.22 \text{ ng } \mu\text{L}^{-1}$.

3.3.6. UPLC-MS analysis

Bioaerosol samples were prepared at 3 mg mL^{-1} (for both amino acid and fatty acid analysis), using ultra-high purity water. Sample preparation followed the same blueprint as for $^1\text{H-NMR}$ (Section 3.3.3). After lysing, centrifuging, and filtration with $0.45 \mu\text{m}$ pore size syringe filters, the samples were run on a Waters Acquity UPLC tandem the Waters MicroMass Quattro Micro API MS system (Waters Co., Milford, MA, USA). The column installed in the UPLC was the Waters Acquity UPLC BEH Amide $1.7 \mu\text{m}$ $2.1 \times 150 \text{ mm}$ (Waters, Co.). Column temperature was set at 35°C , with an injection volume of $5 \mu\text{L}$, and a flow of 0.4 mL min^{-1} . The samples were run at room temperature. This method used positive ionization, a desolvation temperature of 300°C , and a desolvation flow of 350 L hr^{-1} . Eluents used for this purpose were water and ACN, with additives ammonium formate and formic acid. The capillary voltage was set to 3.00 kV , and the cone voltage varied from 20 to 60 V . The total run time was 18 minutes, and the quantification mode was single ion recording (SIR). Six calibration levels in the range of $0.5 - 50 \text{ ng } \mu\text{L}^{-1}$ were used, resulting

in an R^2 value range of 0.972 – 0.999. Method detection limit (MDL) values of amino acids range from 0.009 to 0.26 ng μL^{-1} . Detailed UPLC-MS methodology for amino acid analysis can be found in Axelrod et al., (2021) and analyzed standards can be found in the appendix (Table A3.2).

Existing literature shows that pollen (Manning, 2001; Muth et al., 2018) and algae (Maltsev and Maltseva, 2021; Samburova et al., 2013b) species share common fatty acids: myristic (C14:0), palmitic (C16:0), stearic (C18:0), oleic (C18:1), linoleic (C18:2), and linolenic (C18:3) acids. There is a lack of information on fatty acids present in the fungus selected for this study (western gall rust). These seven fatty acids were chosen as standards for this analysis (Table A3.2), with nonadecanoic acid (C19:0) as the internal standard. Saponification, or alkaline hydrolysis, is a well described and efficient method for the extraction of fatty acids from lipids in biological samples (Burja et al., 2007; Liu, 1994; Salimon et al., 2011). Bioaerosols were prepared as described above (Section 3.3.3), and after drying with nitrogen gas, were saponified with ethanolic NaOH (0.1 M NaOH in ethanol). 1 mL of the ethanolic NaOH was added to vials containing the dried bioaerosols and sonicated at 60 °C for 1 hour. Afterward, the samples were dried with nitrogen gas and resuspended in equal parts ACN and water (850 μL total), then neutralized from pH 12 to pH 7 with 12 μL of 1M HCl.

A previously optimized method for UPLC-MS quantification of fatty acids was adapted, but modified, for our analysis (Samburova et al., 2013b). Fatty acids of bioaerosols were analyzed using the Waters Aquity Class I UPLC (Waters, Co.) in tandem with the Waters Xevo TQ-S MS (Waters, Co.). A reverse phase Waters BEH-C18 2.1 mm

× 50 mm column (Waters, Co.) was used for this purpose, set to 40 °C. The MS method used negative ionization with a desolvation temperature of 500 °C and a desolvation flow of 700 L Hr⁻¹. The cone voltage was set at 35 V, and the capillary voltage at 2.00 kV. The LC used an injection volume of 10 μL, a flow of 0.3 mL min⁻¹. and the sample temperature was set to 20 °C. The inlet method used ACN (A) and water (B) as eluents, with the elution method as follows: 30% A 70% B initially, 75% A 25% B over 10 minutes, then 100% A 0% B over 12 minutes, and 30% A 70% B over eight minutes. The total run time was 30 minutes, and data was quantified using SIR quantification mode. Six calibration points (0.05 – 5 ng μL⁻¹) were used and resulted in an R² range of 0.965 – 0.997. The MDL range for fatty acids is 0.003 – 0.10 ng μL⁻¹. The uncertainty of sample preparation was determined by using three replicates of bioaerosol samples prepared separately, from which standard deviations were calculated. The water-soluble fraction of bioaerosol extracts ranged from 9.8% to 22.3%.

3.4. Results and Discussion

3.4.1. ¹H-NMR analysis

Figure 6 shows the percent distribution of bioaerosol functional groups' protons detected with ¹H-NMR for hay *Bacillus* and *Pedobacter* bacteria species, western gall rust fungus, *Spirulina* alga, 2020 (July), 2021 (June) and 2022 (May) lodgepole pine pollen, and rabbitbrush pollen. Overall, results from bioaerosol ¹H-NMR analysis show aliphatic protons (segment 1), protons in saccharides (segment 3), and various OH (segment 5) as the major segments (aliphatic protons – up to 73.8% in *Spirulina*, saccharide protons – up to 36.1% in 2022 lodgepole pine pollen, various -OH – up to 27.2% in rabbitbrush pollen).

The percent distribution varies for each type of bioaerosol, as well as between the different bacteria and pollen species.

¹H-NMR analysis of bacteria functional groups (Figure 6 a, b.) shows the largest contribution (50.2% in hay *Bacillus*, 57.0% in *Pedobacter*) from the aliphatic proton (segment 1; Figure 6 a, b). This may be due to the presence of fatty acids, which have long aliphatic chains in their molecules (Jones and Fleming, 2014). The bacteria species also show a proton signal (12.4% in hay *Bacillus*, 10.5% in *Pedobacter*) that represents α -carbon (segment 2) of fatty acids or amino acids. To assess the presence of saccharides in our bioaerosol aqueous extracts, we selected segment 3 since it is mainly responsible for protons in saccharide molecules (see Table 3). Hay *Bacillus* (34.5%) has nearly twice as much of the saccharide proton signal (segment 3) as *Pedobacter* (17.0%). The largest difference in total proton signal among the two bacteria samples was observed for segment 5, which is responsible for OH (in saccharides, glycerol, alcohol, and triglycerides) and CH=CH₂ functional groups (see Table 3). This indicates that the chemical contribution of organic compounds with these functional groups varies between the analyzed bacteria species. The signals of aromatic and amide protons (segment 7) were found to be low in bacteria (1.1% in hay *Bacillus*, 3.4% in *Pedobacter*) relative to other assigned segments. To our knowledge, the functional groups of hay *Bacillus* and *Pedobacter* species in aqueous extracts have not been studied in detail, except for some of their products. However, several studies (Reichhardt and Cegelski, 2014; Romaniuk and Cegelski, 2015) used solid-state ¹³C and ¹⁵N CPMAS NMR and reported specific signals for amine, aliphatic, α -carbon, and saccharide functional groups in *S. aureus* and *E. coli* bacteria,

which were also observed in our study. Further, one study which evaluated biosurfactant production from *Bacillus subtilis* found aliphatic, α -carbon, and amide signals in their ^1H -NMR analysis of the biosurfactant (Pemmaraju et al., 2012), while another study by Mohapatra et al. (2017) determined the polyhydroxybutyrate produced by the same bacterium contained aliphatic, carbonyl, and $\text{HC}=\text{CH}$ signals when analyzed by ^{13}C NMR. ^1H -NMR analysis of a biopolymer of *Pedobacter sp.* in DMSO-d_6 by Beltrani et al. (2015) showed signals belonging to aliphatic protons and sugars, which were also identified in our analysis.

The western gall rust fungus has a high contribution from aliphatic protons (39.7%) and an α -carbon proton contribution of 9.7% (Figure 6c). Approximately a quarter of protons signals were from saccharides (24.6%), while 25.1% of the total signal of the fungus extract were from OH and $\text{CH}=\text{CH}_2$ functional groups. Western gall rust is unique in its proton percent distribution and does not follow the pattern of any of the other bioaerosols (see Figure 6). To our knowledge, western gall rust has not been studied for its chemical composition.

Distribution of proton chemical shifts in *Spirulina* shows the largest contribution from aliphatic protons (73.8%), followed by α -carbon protons (15.9%), and saccharide proton signals (7.1%) (Figure 6d). OH and $\text{CH}=\text{CH}_2$ protons contributed only 0.7%, while aromatic and amide proton signals were only 0.4%. Functional groups and chemical composition of *Spirulina* have been previously studied from biofuel and nutrition perspectives, though different methods were used (Kavisri et al., 2021; Kumar et al., 2014; Rajasekar et al., 2019; Sarpal et al., 2016). For example, Sarpal et al. (2016) conducted a

study on biodiesel potential of various types of algae, including *Spirulina*. Although their study was focused on fatty acid and lipid extraction, the *Spirulina* $^1\text{H-NMR}$ spectrum shows strong aliphatic signals, as well as α -carbon, saccharide protons, and OH and $\text{CH}=\text{CH}_2$. Additionally, a study by Rajasekar et al. (2019), which examined the composition of sulfated polysaccharide isolated from *Spirulina*, showed similar peaks to Sarpal et al. (2016) study. Kumar et al. (2014) developed a method that produces a stable extract of *Spirulina* alga for oil extraction using solid-state ^{13}C CPMAS NMR, which reveals signals for carbohydrates, and carboxyl and amide carbons. Our results are comparable to the existing studies, although completely different extraction methods and techniques were used, overall, similar functional groups are present (aliphatic, α -carbon, saccharides/carbohydrates, OH and $\text{CH}=\text{CH}_2$, and amides).

$^1\text{H-NMR}$ analysis of three lodgepole pine pollen extracts (2020, 2021, 2022 – Figure 6e, f, g) reveals the presence of strong aliphatic proton signals (24.7 – 27.6%) as well as α -carbon protons (7.4 – 8.9%). Unlike the bacteria, fungus, and alga analysis, for lodgepole pine pollen, saccharide protons have the largest contribution (35.7 – 36.1%). The third largest segment is attributed to the -OH and $\text{CH}=\text{CH}_2$ functional groups (23.4 – 25.7%). Proton distribution varies slightly (between 0.02 and 2.9%) between the 2020, 2021, and 2022 lodgepole pine pollen samples, collected in the same area. These small differences are also reflected in the quantitative analysis of individual saccharides (discussed below in Section 3.3.2). Comparable to the other bioaerosols (bacteria, fungus, and alga), the amide proton signal in lodgepole pine pollen is weak, at 0.8 – 0.9%.

In the case of rabbitbrush pollen (Figure 6h), we see a similar pattern of the distribution of the proton chemical shift segments as in lodgepole pine pollen, however, there is some variation. For example, the aliphatic proton signal in rabbitbrush is 31.3%, while the α -carbon signal is 0.9% larger than in lodgepole pine pollen. Protons from saccharides contribute to 27.4%, which is 8.5% less than lodgepole pine. Like lodgepole pine pollen, rabbitbrush contains a weak amide proton signal (0.7%), but a high signal from -OH and CH=CH₂ functional groups (27.2%). Several studies on ¹H-NMR analysis of aqueous pollen extracts (resuspended in deuterated solvents) found fatty and amino acid proton signals in the aliphatic region, and sucrose (and other saccharides) in the saccharide proton regions of the spectra (Chalbot and Kavouras, 2019; Otify et al., 2019). The results from these studies are in good agreement with our findings, as we have high aliphatic and saccharide proton signals in our pollen samples. For characterization of the specific compounds that may be responsible for the protons analyzed with ¹H-NMR (i.e., aliphatic, α -carbon, H and OH in saccharides), we conducted analysis of individual compounds: starch, saccharides, amino acids, and fatty acids.

Based on our segment assignment (see Table 3), we use segment 5 as a representative segment for polar functional groups (OH groups found in glycerol, alcohol, and triglyceride molecules). Analysis of the polar segment among all analyzed species, shows that the most polar bioaerosols are both pollen species and western gall rust (lodgepole pine 2020 – 23.4%; lodgepole pine 2021 – 25.7%; lodgepole pine 2022 – 24.6%; rabbitbrush – 27.2%; western gall rust – 25.1%) in comparison with *Spirulina* and *Pedobacter*, which are only about 0% and 11.8% polar, respectively. These polar

functional groups are not detected in the hay *Bacillus* spectra, most likely due to a limited amount extracted from hay *Bacillus*. These differences in polarity may significantly affect the solubility of these bioaerosols in water in the atmosphere. For instance, we know from existing literature that pollen grains rupture in the presence of water (Mampage et al., 2022).

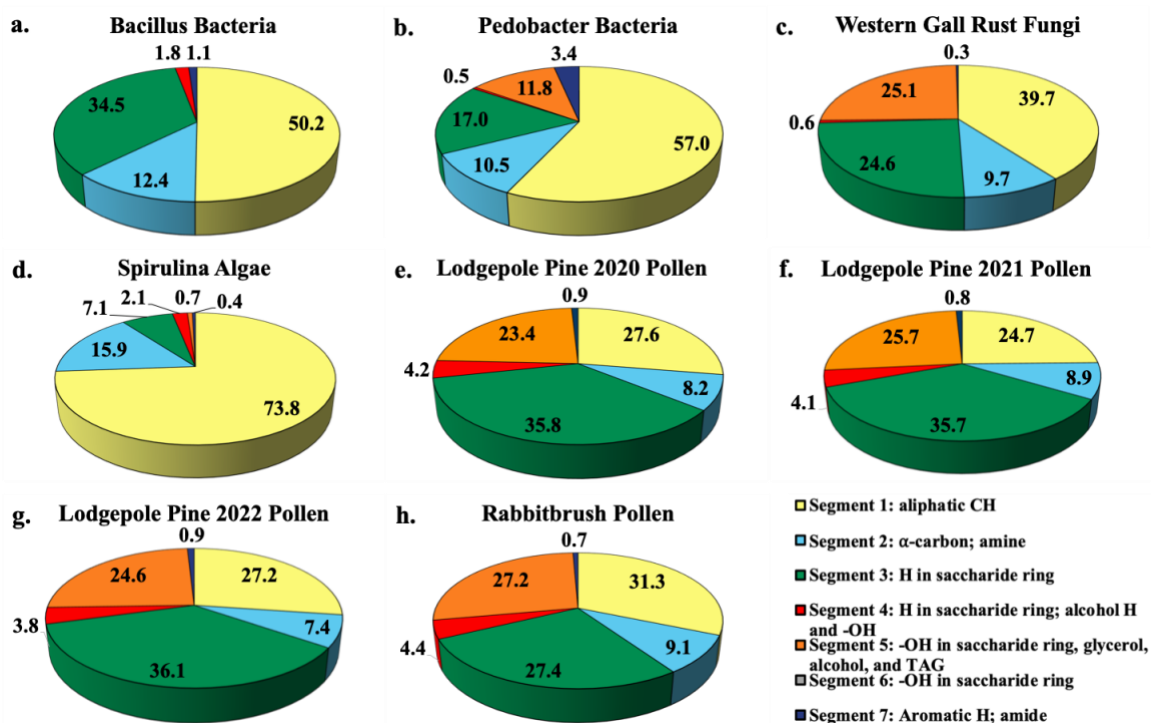


Figure 6. Pie chart percent distribution of functional groups in select bioaerosol extracts (water extracts resuspended in DMSO- d_6), analyzed with 1H -NMR spectroscopy. Each pie slice corresponds to chemical shift segments 1 through 7 (see legend). Details on each segment can be found in Table 3.

3.3.2. Saccharide Analysis

The distribution of saccharides in the tested bioaerosols (analyzed with GC-MS) is presented in Figure 7, in $\mu g\ mg^{-1}$ of dry bioaerosol mass. The two analyzed pollen species (lodgepole pine and rabbitbrush) were found to have the highest total saccharide

concentrations (95.3 – 183.5 $\mu\text{g mg}^{-1}$ in lodgepole pine samples; 87.2 $\mu\text{g mg}^{-1}$ in rabbitbrush). The secondary y-axis represents the percentage of total analyzed saccharides per milligram of dry bioaerosol mass. The most common saccharide in all analyzed bioaerosols was glucose (from 5.8% of the total analyzed saccharides in hay *Bacillus* bacteria to 49.8% in rabbitbrush pollen). Sucrose was also present in all samples (from 3.6% in *Spirulina* alga to 87.2% in 2022 lodgepole pine pollen), except for rabbitbrush pollen.

Analysis of saccharides in hay *Bacillus* (Figure 7) reveals only sucrose (71.9%) and glucose (5.8%), which is most likely due to low concentrations of analyzed species in the water extract. Western gall rust shows a mix of saccharides, with the most abundant ones being β -D-fructose (26.9%) and glucose (15.9%). Other saccharides in western gall rust were found in low concentrations (α - and β -D-arabinose (1.2% and 0.9%, respectively), β -D-xylose (1.5%), α -L-mannose/ α -D-fructose (8.7%), D-galactose (5.4%), β -L-mannose (10.0%), and sucrose (7.3%)). Our results show that β -D-fructose (50.0%) is the most dominant saccharide in *Spirulina*, followed by glucose (33.3%) and sucrose (3.6%). Our results are in good agreement with Brown (1991) study, where glucose was also one of the major saccharides found in 16 various microalgae species, though *Spirulina* was not analyzed. Another study that did analyze *Spirulina* for saccharide content, also determined that glucose contributed to ~54% of total saccharides, followed by rhamnose at ~22% (Madhavi et al., 1987). Meanwhile, Chaiklahan et al. (2013) study showed rhamnose as the major contributor (~54%) to overall saccharide concentrations in *Spirulina*, followed by glucose (~14%). Fructose was not analyzed in either study.

Lodgepole pine pollen shows particularly high concentrations of sucrose (79.4 to 87.2%), followed by glucose (6.7 to 12.8%) and β -D-fructose (4.0 to 7.0%). Low levels were observed for galactose (1.4 to 3.3%), β -L-mannose (0.2 to 0.3%), and β -D-arabinose (0.04 to 0.1%). Lodgepole pine pollen saccharide concentrations vary from May (2022) to June (2021) and July (2020); with May (2022) having the highest overall saccharide concentration (183.54 $\mu\text{g mg}^{-1}$ total analyzed saccharides), as well as the highest sucrose value (87.2% of the total analyzed saccharides). Overall, July 2020 lodgepole pine has 6.7% less saccharides than in June 2021, and June 2021 lodgepole pine pollen has 2.1% less than that of May 2022. The variation of saccharide content in lodgepole pine pollen may be explained by the collection of the pollen at different times of the season, in different years. Previous studies showed that saccharide concentrations vary seasonally in pollen, and the highest saccharide concentration is typically found earlier in the pollen season (Fu et al., 2012). Furthermore, Fu et al. (2012) also found that sucrose had the highest contribution earlier in the pollen season. This justifies the differences of lodgepole pine pollen samples (July 2020, June 2021, May 2022) in our results, as the May 2022 sample was collected earlier in the season and contains more saccharides overall and has a higher sucrose concentration than the other samples.

The dominant saccharides in rabbitbrush pollen were glucose (49.8%) and β -D-fructose (48.4%), followed by galactose, α -D-arabinose, and β -D-arabinose (< 1.0%). α -D-xylose, α -lactose, and trehalose were also analyzed in the selected bioaerosol samples; however, their concentrations were below the detection limit. Common saccharides found in various pollen species in Axelrod et al. (2021) study were β -D-fructose and glucose,

which were also found in the pollen samples selected for this study. Fu et al. (2012) reported sucrose as the dominant saccharide among all tested pollen samples, however, in our study, only lodgepole pine pollen had sucrose as the major saccharide. As such, sucrose may not be a suitable tracer for airborne pollen analysis (e.g., source apportionment), as Fu et al. concluded. Starch content analyzed with UV-Vis-NIR spectrophotometry (Chapter 2) is presented together with saccharides, in Figure 7, to show a total distribution of mono- (i.e., glucose, etc.), di- (i.e., sucrose), and poly- (i.e., starch) saccharides in the chosen bioaerosols. The results showed that starch contributes to 22.3% of total analyzed saccharides in hay *Bacillus*, 22.2% in western gall rust, 13.1% in *Spirulina*, and 1.0% 2020 lodgepole pine.

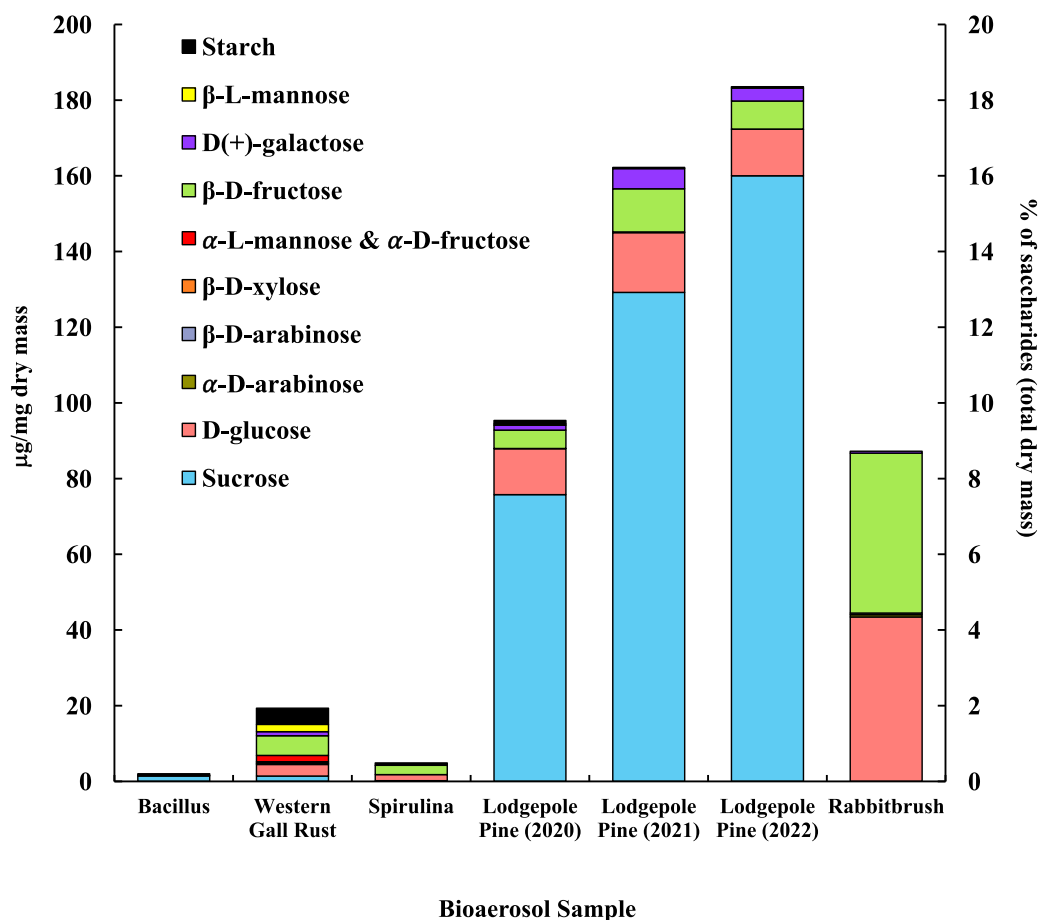


Figure 7. Saccharide and starch concentration (in $\mu\text{g mg}^{-1}$ dry mass) of selected bioaerosols. The secondary axis shows the percentage of saccharides per milligram of dry mass. Standard deviations range from $0.004 \mu\text{g mg}^{-1}$ in galactose (rabbitbrush) to $12.92 \mu\text{g mg}^{-1}$ in sucrose (lodgepole pine 2021) (see Table A3.4 for details). α -L-mannose and α -D-fructose are presented together due to their co-elution during gas chromatography separation.

3.4.3. Amino acid analysis

Figure 8 shows the distribution of analyzed amino acids (analyzed with UPLC-MS) in selected bioaerosols (Table 2). The concentration and composition of amino acids among bioaerosols vary significantly. We found that proline, leucine, isoleucine, alanine, and phenylalanine are the only common amino acids between all the tested bioaerosols, among 20 amino acids. Hay Bacillus bacteria ($21.4 \mu\text{g mg}^{-1}$) and rabbitbrush pollen ($18.1 \mu\text{g mg}^{-1}$)

¹) show the highest concentrations of total analyzed amino acids overall. Hay *Bacillus*, *Pedobacter*, and *Spirulina* show the highest values of glutamic acid (64.5%, 14.8%, and 49.1% of total analyzed amino acids, respectively), while both pollen species are rich in proline (lodgepole pine – 38.6%, rabbitbrush – 83.2%).

High concentrations of glutamic acid (64.5%) and γ -aminobutyric acid (GABA, 17.4%) were found in hay *Bacillus* bacteria, followed by lysine (5.8%) and alanine (4.5%). *Pedobacter* bacteria also shows high concentrations of glutamic acid (14.8%) and GABA (9.8%) but has higher values of alanine (13.7%). Overall, hay *Bacillus* and *Pedobacter* bacteria have very distinct distributions of amino acids. GABA (45.8%), tryptophan (19.0%), and alanine (11.1%) are the dominant amino acids in western gall rust, and other amino acids (phenylalanine, tryptophan, leucine, isoleucine, valine, proline, alanine, threonine, and glutamic acid) were found in relatively small amounts (< 6%) (see Table A3.4 for exact concentrations and standard deviations). To our knowledge, these are the first available results regarding western gall rust amino acid composition and distribution. Glutamic acid (49.1%) and GABA (39.4%) alone were found to compose 88.5% of the total analyzed amino acids in *Spirulina*. A study by Vendruscolo et al. (2018) found that glutamic acid was the most abundant amino acid in four microalgae species, while Bashir et al. (2016) determined that the major amino acids found in *Spirulina* were glutamic acid followed by leucine, which our data shows only a small amount of. Similarly, Andreeva et al. (2021) showed that *Spirulina*'s main amino acids are glutamic acid, followed by alanine, which is also minimal in our results.

In addition to proline (38.6%), lodgepole pine pollen amino acid analysis shows significant amounts of GABA (11.3%) and arginine (26.9%). Ozler et al. (2009) analyzed pollen of a different pine species (*P. nigra*) and found that the major contributor is also proline and has a less significant contribution of arginine, which agrees with our results. While the amino acid profile of rabbitbrush pollen also shows a high concentration of proline (83.2%), it also contains histidine (8.2%) and hydroxyproline (4.3%). Based on our analysis of amino acids in bioaerosols, glutamic acid may be a suitable atmospheric tracer for hay *Bacillus* bacteria and *Spirulina* alga, while proline may be a better tracer for rabbitbrush and lodgepole pine pollens, as these amino acids are found in the highest concentrations in these bioaerosols. Glycine and serine amino acids were also analyzed but remained below the detection limit.

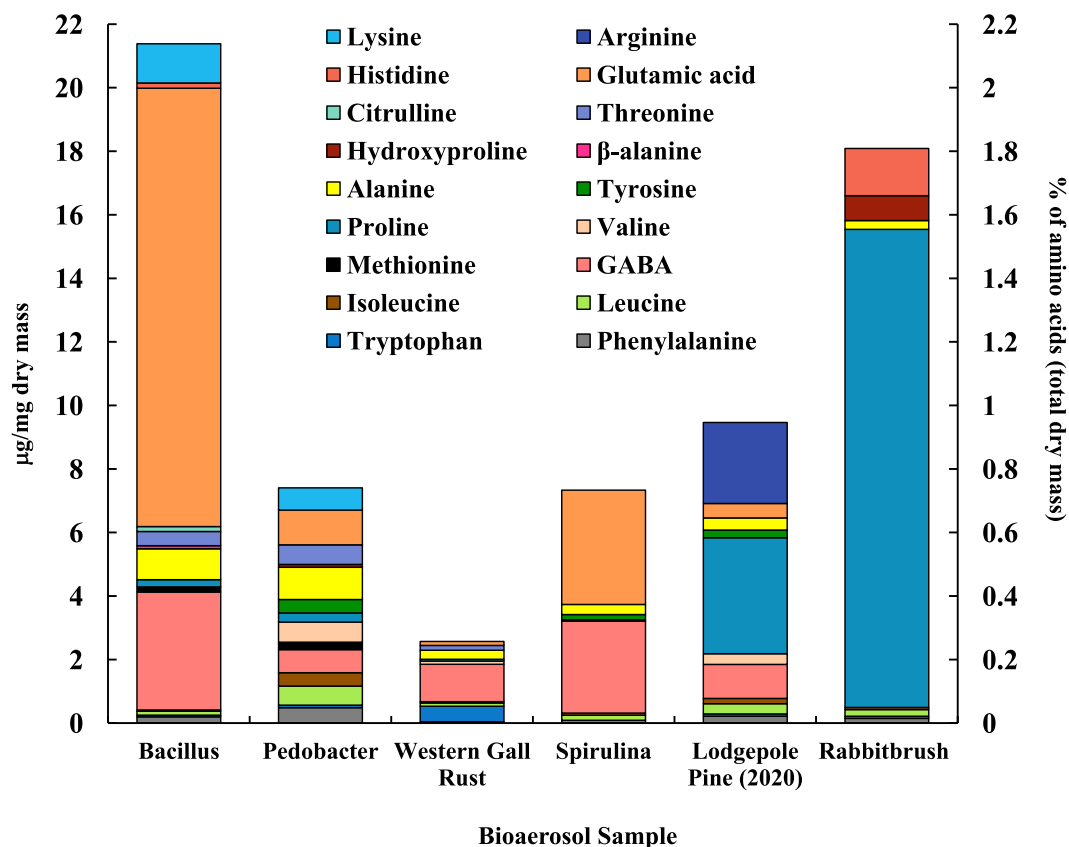


Figure 8. Amino acid concentration (in $\mu\text{g mg}^{-1}$ dry mass) of selected bioaerosols (primary axis). The secondary axis shows the percentage of total amino acids per milligram of dry mass. Standard deviations range from $\pm 0.001 \mu\text{g mg}^{-1}$ in β -alanine (hay Bacillus) to $\pm 1.770 \mu\text{g mg}^{-1}$ in proline (lodgepole pine 2020) (see Table A3.4 for details).

3.4.4. Fatty acid analysis

Figure 9 shows the distribution of ten analyzed fatty acids in selected bioaerosols (analyzed with UPLC-MS). All analyzed bioaerosols, except hay Bacillus (which contained only myristic acid), show a variety of fatty acids. Lodgepole pine pollen ($25.82 \mu\text{g mg}^{-1}$), western gall rust fungus ($10.63 \mu\text{g mg}^{-1}$) and rabbitbrush pollen ($7.72 \mu\text{g mg}^{-1}$) have the highest total concentration of the analyzed fatty acids. Linoleic and palmitic acids were found in the highest concentrations in both pollen species (lodgepole pine and rabbitbrush).

Analysis of hay *Bacillus* bacteria revealed that most fatty acids were below detection limit, except for myristic acid ($0.05 \mu\text{g mg}^{-1}$). The dominant fatty acids in western gall rust are linolenic (26.6% of total analyzed fatty acids) and palmitic (34.0%). Linoleic (15.7%), oleic (11.3%), and stearic (9.5%) acids are also present in lower concentrations. The dominant fatty acid found in *Spirulina* was palmitic acid (42.6%), followed by linolenic (27.7%), linoleic (22.6%), stearic (4.2%), and oleic (2.9%) acids. Our results are comparable to Samburova et al. (2013b) study, where the most abundant fatty acids found between four strains of another algae, *Dunaliella*, were palmitic, linolenic, linoleic, and oleic acids.

Both pollen species (lodgepole pine and rabbitbrush) contain the same variation of fatty acids (except dodecanoic acid) in different concentrations. Major fatty acids found in lodgepole pine pollen are linoleic (28.5%), palmitic (26.9%), and oleic (26.0%) acids, while the main fatty acids in rabbitbrush are palmitic (34.9%), linoleic (33.2%), and linolenic (23.8%) acids. Erdyneeva et al. (2021) found that dominant fatty acids in three *Pinus* species were palmitic and linoleic acids, which were also the major fatty acids present in both of our pollen samples.

According to a review by Kaneda (1977), the most common fatty acids among living organisms are palmitic, oleic, linoleic, linolenic, and stearic acids.¹⁰¹ This combination of fatty acids is seen all analyzed bioaerosols, except for hay *Bacillus* (where most of the fatty acids were below detection limit). Although *Spirulina* and hay *Bacillus* show 73.8 and 50.2% of the aliphatic functional group in their ¹H-NMR proton distribution, these bioaerosol species have the lowest concentrations, according to our fatty acid analysis

via UPLC-MS. This is due to the low mass of hay *Bacillus* and *Spirulina* that was available for quantitative analysis, thus, most fatty acids were below detection limit for hay *Bacillus* samples.

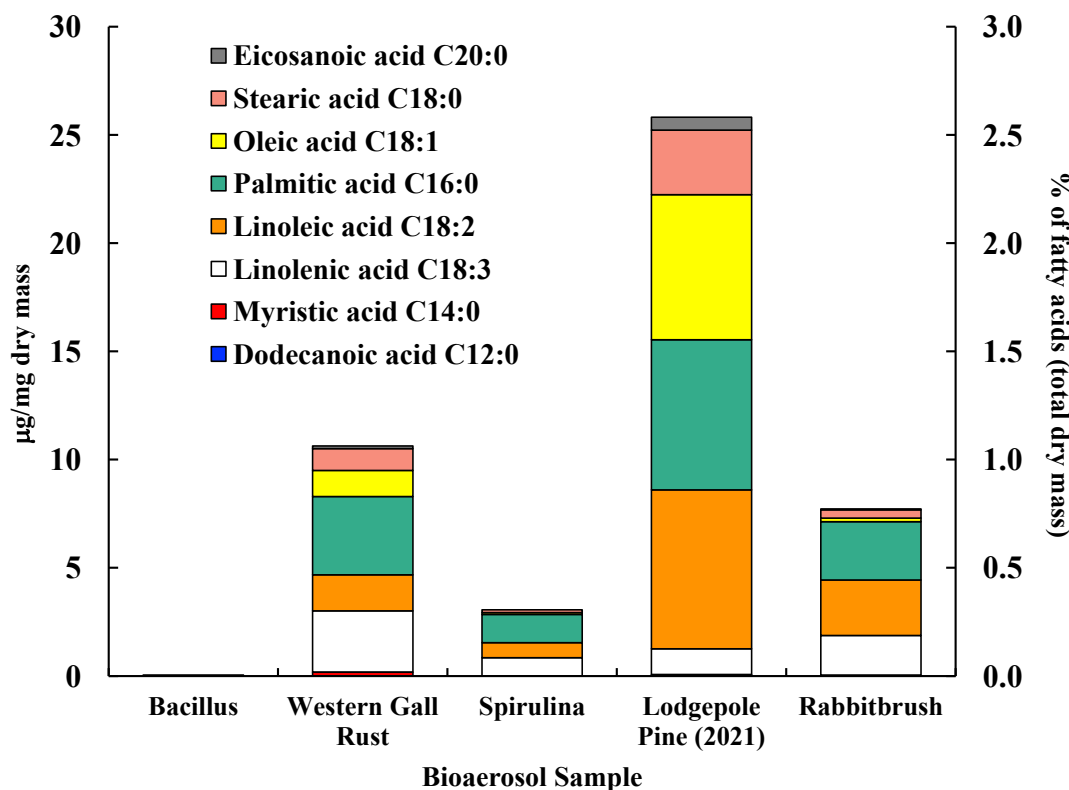


Figure 9. Fatty acid concentration (in $\mu\text{g mg}^{-1}$ dry mass) of selected bioaerosols. The secondary axis shows the percentage of fatty acids per milligram of dry mass. Fatty acids in hay *Bacillus* were below detection limit. Standard deviations range from $0.006 \mu\text{g mg}^{-1}$ in eicosanoic acid (*Spirulina*) to $1.03 \mu\text{g mg}^{-1}$ in palmitic acid (lodgepole pine 2021) (see Table A3.4 for details).

3.4.5. Correlation analysis

To assess if $^1\text{H-NMR}$ analysis of chemically complex bioaerosol extracts can reflect quantitative analysis of organic species, we ran correlations between the aliphatic, saccharide, and amide segments ($^1\text{H-NMR}$ analysis) and quantitative analysis of the organic compounds (GC-MS, UPLC-MS, and UV-Vis-NIR analysis) (Table A3.5). For

this purpose, each segment was normalized by the sum of the three related segments (aliphatic, saccharide, and amide) and correlated with the analyzed organic compounds. The best correlation was for saccharides ($R^2 = 0.608$), where the saccharide segment (segment 3) of $^1\text{H-NMR}$ analysis was correlated with the total saccharide concentration (Figure 7). This relationship indicates that $^1\text{H-NMR}$ can be successfully used for semi-quantitative analysis of saccharide content in bioaerosols. No significant correlation ($R^2 = -0.002$) was detected between amino acids and the amide segment (segment 7), which could be due to weak $^1\text{H-NMR}$ signals of amide groups (Pretsch et al., 2009), a limited number of quantified amino acids, and overlap with signals from other functional groups (i.e., aromatic H in segment 7, Table 3). A negative correlation ($R^2 = -0.442$) was found between individual fatty acid analysis and the aliphatic proton region (segment 1). This can be attributed to other compounds (i.e., peptides) (Mesleh et al., 2007) that contribute to strong aliphatic signals.

3.5. Conclusion

The chemical composition of selected bioaerosols (pollen, fungi, algae, bacteria) was characterized using qualitative ($^1\text{H-NMR}$) and quantitative (GC-MS, UPLC-MS, UV-Vis-NIR) analysis. $^1\text{H-NMR}$ analysis revealed that protons from aliphatic, saccharide, and OH groups had the biggest contributions to the overall proton distribution among all bioaerosols. Hay Bacillus and *Pedobacter* bacteria, western gall rust fungus, *Spirulina* alga, and rabbitbrush pollen had the largest contribution from aliphatic protons (31.3 – 73.8%), while lodgepole pine pollen had the largest contribution from saccharide protons (35.7 – 36.1%). Amide signals were some of the weakest, ranging from 0.3% in western gall rust fungus to 3.4% in *Pedobacter* bacteria.

The chemical composition varies significantly between bioaerosol types and species. The quantitative analysis of selected organics (saccharides, amino acids, and fatty acids) showed that the saccharide glucose, the amino acids proline, leucine, isoleucine, alanine, and phenylalanine, and the fatty acids palmitic, oleic, linoleic, linolenic, and stearic (except in hay *Bacillus* bacteria) are common among analyzed bioaerosol aqueous extracts. The major organic species were found to be saccharides (up to 18.4% of total dry mass), followed by amino acids (up to 2.1% of total dry mass), and fatty acids (up to 2.6% total dry mass). The high saccharide concentrations may be due to the high water solubility of most monosaccharides (Jones and Fleming, 2014). Both pollen species (lodgepole pine and rabbitbrush) were found to have the highest concentrations of saccharides (Figure 7), which can be explained by the tendency of pollen grains to easily rupture in the presence of water (Mampage et al., 2022). Differences in saccharide concentrations of July 2020, June 2021, and May 2022 lodgepole pine samples may be explained by seasonal variations in pollen saccharides (Fu et al., 2012), where the highest sugar concentrations are found earlier in the season (May 2022). This is the first study, to our knowledge, that provided a chemical analysis of western gall rust fungus, which is known to affect pine trees around the world (Old, 1981; Old et al., 1986; Ramsfield et al., 2007). The correlation analysis between qualitative and quantitative results showed a good correlation ($R^2 = 0.608$) between the saccharide $^1\text{H-NMR}$ segment and the total saccharide concentration, which suggests that the $^1\text{H-NMR}$ qualitative data reflects the quantitative analysis of saccharides. For hay *Bacillus* and *Spirulina*, the highest contribution of analyzed organic species came from amino acids, while the major fraction of organics for pollen was saccharides. Based on our chemical analysis of these various bioaerosol species, it can be concluded that

proper tracer analysis of bioaerosols in ambient samples should use fatty acids in addition to amino acids and saccharides, as was suggested by Axelrod et al. (2021).

Several constraints of the study include the limited number of organic species (saccharides, amino acids, fatty acids, etc.) and bioaerosol species analyzed. Future bioaerosol studies may benefit from extracting bioaerosols in solvents of different polarity (i.e., acetone, dichloromethane, hexane) and applying other analytical methods for further functional group characterization. For example, Fourier-transform Infrared Spectroscopy (FTIR) can provide information regarding the polarity of the bioaerosols and higher-resolution NMR (> 500 MHz $^1\text{H-NMR}$) can yield a more detailed analysis of the protons present. An extensive chemical analysis should be conducted and the contribution of other chemical species to the bioaerosols can be explored, such as the contribution of phosphorous-containing compounds in bioaerosols (Violaki et al., 2021). Further, pollen samples may be collected and analyzed at different times over the course of one season to observe a more defined seasonal variation in chemical composition. Subsequent studies should also consider analysis of ambient samples for identification of bioaerosols, using the chemical compositions provided in this study as tracers.

The results of the present study provide valuable insight of bioaerosol contribution to atmospheric chemistry and essential data for future bioaerosol research. It has been highlighted in a recent review (Kumari and Yadav, 2024) that the role bioaerosols play in atmospheric processes have been greatly overlooked and largely understudied mainly due to the complexity of bioaerosols and diversity of their sources. Therefore, as Kumari and Yadav (2024) pointed out, there are large uncertainties in assessing bioaerosol regional and

global climate effects, especially in source apportionment and climate models. As such, our detailed chemical analysis of bioaerosols can help to understand the impact of bioaerosols on atmospheric organic carbon, as well as their role in cloud formation processes such as CCN and INP. Moreover, the chemical constituents can be utilized for better identification and classification of bioaerosols in atmospheric aerosol samples, as suggested in Samburova et al. (2013a). Our fundamental data may be relevant in future research regarding increases in concentrations of pollen and algae due to climate change (Anderegg et al., 2021; May et al., 2018a; Zhang and Steiner, 2022; Zingales et al., 2022). For a broader impact, these results may be relevant for studies in other fields, such as medicine, nutrition, biofuels, toxicology, agriculture, among others (Hashem et al., 2019; Kumar et al., 2014; Tan et al., 2020; Wahlen et al., 2013). For example, all the analyzed bioaerosols are known to have significant effects on human and animal health, as mentioned previously, and understanding their chemical composition in a medical context is significant and necessary. Likewise, the organic and functional group composition of *Spirulina* is relevant from a nutrition and biofuel perspective (Hannon et al., 2010; Sarpal et al., 2016; Vo et al., 2015).

3.6. Acknowledgements

The authors would like to thank Dr. Alison Murray (Desert Research Institute, Reno, NV, USA) for the donation of cultured bacteria species for our bioaerosol study. The authors would also like to thank Dr. Yeongkwon Son (Desert Research Institute, NV, USA) for their analytical expertise in UPLC-MS method development and Dr. Alexander Eletsky (University of Georgia, GA, USA) for their ¹H-NMR expertise.

3.7. Chapter 3 Appendix

Table A3.1. Standard compounds used for ¹H-NMR bioaerosol functional group and chemical shift assignment.

¹ H-NMR Standards	Compounds
1. <u>Saccharides</u> (DMSO- <i>d</i> ₆ and D ₂ O)	D-(+)-Glucose, Fructose, Galactose, Mannose, Sucrose, Starch (potato origin)
2. <u>Sugar Alcohols</u> (DMSO- <i>d</i> ₆ and D ₂ O)	Glycerol, Erythritol, Inositol, Mannitol, Arabitol
3. <u>Fatty Acids</u> (DMSO- <i>d</i> ₆ and D ₂ O)	Palmitic, Stearic, Glutaric, Tridecanoic, Adipic acids
4. <u>Triacylglycerides</u> (DMSO- <i>d</i> ₆ and D ₂ O)	Tri-arachidin, Tri-oleate, Glyceryl tri-heptadecanoate, 1-stearoyl-rac-glycerol, Glyceryl tri-palmitate
5. <u>Amino Acids</u> (DMSO- <i>d</i> ₆ and D ₂ O)	Proline, Leucine, Glutamic Acid, Arginine, Phenylalanine
6. <u>Carboxylic Acids</u> (DMSO- <i>d</i> ₆ only)	Succinic, Malonic acids
7. <u>PAHs</u> (DMSO- <i>d</i> ₆ only)	Phenanthrene, Retene
8. <u>Oxygenated PAHs</u> (DMSO- <i>d</i> ₆ only)	Anthraquinone, Perinaphthenone
9. <u>Aldehydes</u> (DMSO- <i>d</i> ₆ only)	Acetaldehyde
10. <u>Aliphatic Alcohols</u>	Isopropyl (DMSO- <i>d</i> ₆ only), Methanol (DMSO- <i>d</i> ₆ and D ₂ O)
11. <u>Aromatic Alcohols</u> (DMSO- <i>d</i> ₆ only)	Phenol

Table A3.2. Calibration standards for bioaerosol GC-MS saccharide analysis and UPLC-MS amino acid analysis. Internal standard (IS) used for saccharide analysis is glucose-d₇ and nonadecanoic acid (C19:0) for fatty acid analysis.

Saccharide Standards	Amino Acid Standards	Fatty Acid Standards
GC-MS	UPLC-MS	LC/Q-TOF
Sucrose	Phenylalanine	Myristic (C14:0)
Trehalose	Tryptophan	Pentadecanoic (C15:0)
α -D-arabinose	Leucine	Palmitic (C16:0)
β -D-arabinose	Isoleucine	Stearic (C18:0)
α -D-fructose	GABA	Oleic (C18:1)
β -D-fructose	Methionine	Linoleic (C18:2)
d-(+)-galactose	Valine	Linolenic (C18:3)
α -D-glucose	Proline	Nonadecanoic (IS) (C19:0)
β -D-glucose	Tyrosine	
glucose-d ₇ (IS)	Alanine	
α -lactose	β -alanine	
α -L-mannose	Hydroxyproline	
β -L-mannose	Threonine	
α -D-xylose	Glycine	
β -D-xylose	Serine	
	Citrulline	
	Glutamic Acid	
	Histidine	
	Arginine	
	Lysine	

Table A3.3. Chemical shifts of various solvents, determined from solvent spectra and adopted from the “NMR Solvent Data Chart” by Cambridge Isotope Laboratories, Inc. (Cambridge Isotope Laboratories Inc., n.d.). To be consistent with solvent and water peaks present in each spectrum (standard and bioaerosol spectra), these were cut from the calculations as follows: TMS peak was cut from -0.02 to 0.02 ppm, DMSO-d₆ peak was cut from 2.45 to 2.55 ppm, H₂O peak (absorption of water due to DMSO-d₆ solvent use) was cut from 3.23 to 3.43 ppm, and the acetone peak (located at 2.07 ppm and used while preparing samples) was cut from 2.06 to 2.08 ppm.

Solvent	Solvent chemical shift (ppm)
TMS	0.00
DMSO-d ₆	2.50
H ₂ O	3.33
Acetone	2.05 (2.07 in our spectra)
D ₂ O	4.79

Table A3.4. Concentrations and standard deviations (in µg/mg) of individual organic compounds found in bioaerosols. “-” stands for bioaerosols that were not tested for specific compounds. All values presented are above the method detection limit (MDL), which varies for each compound.

		Bioaerosols							
	Compounds	Hay Bacillus	<i>Pedo- bacter</i>	Western gall rust	<i>Spiru- lina</i>	Lodge- pole pine 2020	Lodge- pole pine 2021	Lodge- pole pine 2022	Rabbit- brush
	Saccharides	Starch	0.45 ± 0.05	-	4.30 ± 0.06	0.64 ± 0.05	0.94 ± 0.06	-	-
α-D-arabinose		0	-	0.24 ± 0.04	0	0	0	0	0.61 ± 0.01
β-D-arabinose		0	-	0.17 ± 0.04	0	0.04 ± 0.11	0.19 ± 0.04	0.08 ± 0.02	0.42 ± 0.02
α-D-xylose		0	-	0	0	0	0	0	0
β-D-xylose		0	-	0.29 ± 0.05	0	0	0	0	0
α-L-mannose & α-D-fructose		0	-	1.69 ± 0.28	0	0	0	0	0
β-D-fructose		0	-	5.20 ± 1.03	2.43 ± 0.48	4.84 ± 2.34	11.43 ± 2.27	7.40 ± 1.47	42.25 ± 0.27
D-(+)-galactose		0	-	1.05 ± 0.15	0	1.31 ± 1.42	5.32 ± 0.77	3.41 ± 0.49	0.51 ± 0.004

	D-(+)-glucose	0.12 ± 0.02	-	3.07 ± 0.55	1.62 ± 0.29	12.17 ± 5.65	15.79 ± 2.84	12.29 ± 2.21	43.44 ± 1.22
	β-L-mannose	0	-	1.93 ± 0.31	0	0.33 ± 0.62	0.31 ± 0.05	0.36 ± 0.06	0
	Sucrose	1.45 ± 0.11	-	1.41 ± 0.11	0.17 ± 0.01	75.75 ± 12.92	129.19 ± 10.05	160 ± 12.44	0
	α-lactose	0	-	0	0	0	0	0	0
	Trehalose	0	-	0	0	0	0	0	0
Amino Acids	Phenylalanine	0.20 ± 0.01	0.49 ± 0.03	0.04 ± 0.004	0.09 ± 0.004	0.22 ± 0.06	-	-	0.15 ± 0.008
	Tryptophan	0.06 ± 0.007	0.08 ± 0.004	0.49 ± 0.05	0	0.07 ± 0.01	-	-	0.07 ± 0.003
	Leucine	0.12 ± 0.006	0.60 ± 0.03	0.10 ± 0.001	0.16 ± 0.02	0.32 ± 0.09	-	-	0.21 ± 0.02
	Isoleucine	0.04 ± 0.001	0.42 ± 0.03	0.04 ± 0.004	0.07 ± 0.001	0.17 ± 0.06	-	-	0.07 ± 0.02
	GABA	3.71 ± 0.74	0.73 ± 0.02	1.18 ± 0.11	2.90 ± 0.06	1.07 ± 0.36	-	-	0
	Methionine	0.16 ± 0.009	0.24 ± 0.004	0	0	0	-	-	0
	Valine	0	0.63 ± 0.02	0.10 ± 0.008	0	0.34 ± 0.12	-	-	0
	Proline	0.23 ± 0.005	0.29 ± 0.004	0.06 ± 0.004	0.05 ± 0.001	3.65 ± 1.77	-	-	15.05 ± 0.44
	Tyrosine	0	0.42 ± 0.03	0	0.17 ± 0.04	0.24 ± 0.07	-	-	0
	Alanine	0.97 ± 0.07	1.02 ± 0.04	0.28 ± 0.03	0.32 ± 0.009	0.38 ± 0.13	-	-	0.28 ± 0.01
	β-alanine	0.10 ± 0.0007	0	0	0	0	-	-	0
	Hydroxyproline	0	0.09 ± 0.01	0	0	0	-	-	0.78 ± 0.006
	Threonine	0.45 ± 0.02	0.62 ± 0.01	0.15 ± 0.008	0	0	-	-	0
	Glycine	0	0	0	0	0	-	-	0
	Serine	0	0	0	0	0	-	-	0
Citrulline	0.15 ± 0.01	0	0	0	0	-	-	0	
Glutamic acid	13.80 ± 0.15	1.09 ± 0.05	0.12 ± 0.04	3.60 ± 0.04	0.45 ± 0.22	-	-	0	

	Histidine	0.16 ± 0.01	0	0	0	0	-	-	1.49 ± 0.13
	Arginine	0	0	0	0	2.55 ± 1.20	-	-	0
	Lysine	1.24 ± 0.05	0.70 ± 0.03	0	0	0	-	-	0
	Dodecanoic acid C12:0	0	-	0	0	-	0	-	0.004 ± 0.006
Fatty Acids	Myristic acid C14:0	0.05 ± 0.006	-	0.18 ± 0.02	0	-	0.07 ± 0.009	-	0.03 ± 0.004
	Linolenic acid C18:3	0	-	2.83 ± 0.58	0.85 ± 0.34	-	1.19 ± 0.24	-	1.84 ± 0.38
	Linoleic acid C18:2	0	-	1.67 ± 0.18	0.69 ± 0.32	-	7.35 ± 0.78	-	2.57 ± 0.27
	Palmitic acid C16:0	0	-	3.61 ± 0.53	1.30 ± 0.63	-	6.94 ± 1.03	-	2.69 ± 0.40
	Oleic acid C18:1	0	-	1.20 ± 0.17	0.09 ± 0.07	-	6.70 ± 0.95	-	0.17 ± 0.02
	Stearic acid C18:0	0	-	1.01 ± 0.20	0.13 ± 0.18	-	2.98 ± 0.58	-	0.38 ± 0.07
	Eicosanoic acid C20:0	0	-	0.12 ± 0.02	0	-	0.60 ± 0.11	-	0.04 ± 0.008

Table A3.5. Correlation coefficients of aliphatic, saccharide, and amide $^1\text{H-NMR}$ segments and concentrations of individual organic species (saccharides, amino acids, and fatty acids).

	Aliphatic (Segment 1)	Saccharides (Segment 3)	Amides (Segment 7)
Saccharides	-0.610	0.608	0.441
Amino Acids	-0.130	0.129	-0.002
Fatty Acids	-0.442	0.448	0.090

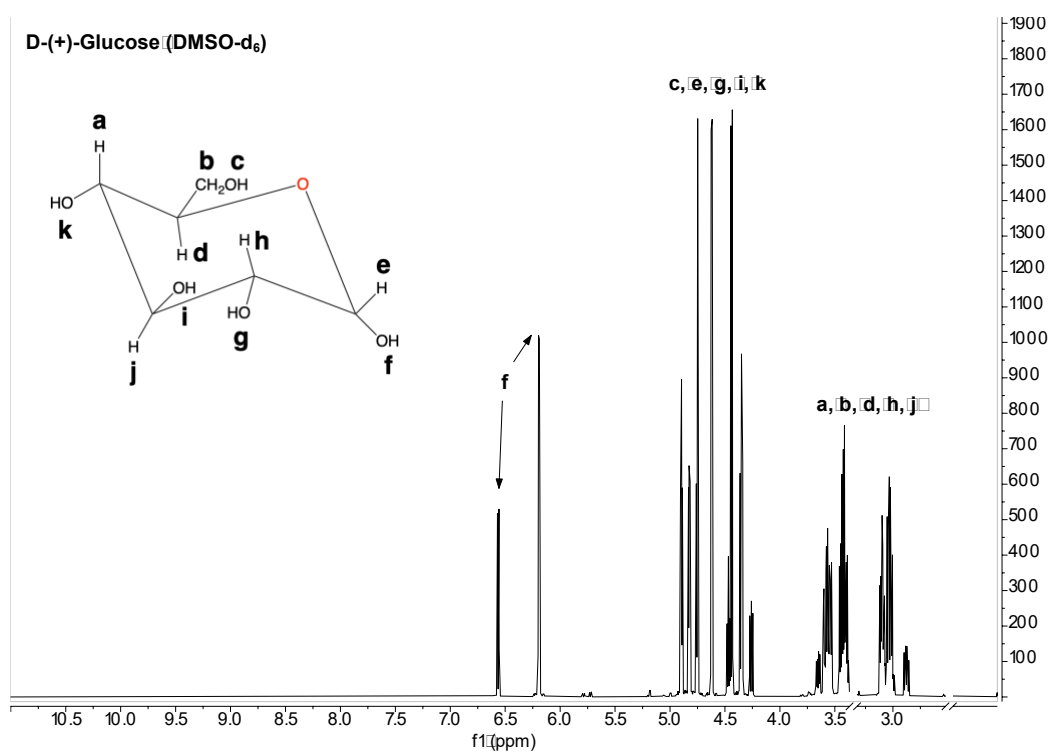


Figure A3.1. $^1\text{H-NMR}$ spectrum (0 – 14 ppm) of D-(+)-Glucose used for assignment of polar (H) and non-polar (OH) regions within the spectrum for bioaerosol analysis.

Chapter 4

Effects of Simulated Atmospheric Aging on Bioaerosol Chemistry

4.1. Abstract

Despite the growing importance of atmospheric aerosols of biological origin (bioaerosols) with the warming climate, little is known about bioaerosol chemical composition and their atmospheric fate (e.g., aging). This study uncovers how various laboratory simulated atmospheric aging processes alter bioaerosol functional groups, and therefore affect their polarity. Lodgepole pine pollen and *Spirulina* alga bioaerosols, which represent typical bioaerosols, were extracted and exposed to (1) simulated solar radiation, ranging from 300 to 800 nm, and (2) OH radicals formed from hydrogen peroxide through photolysis. The bioaerosol extracts were analyzed by proton nuclear magnetic resonance ($^1\text{H-NMR}$) and Fourier-transform infrared (FTIR) spectroscopy before and after aging to determine the chemical transformation that occurred during the two different types of aging. FTIR results indicated an overall increase of polar functional groups' signal in comparison to non-polar functional groups after light aging. The largest increase for both bioaerosols was the OH/CH ratio, with a 30.9% increase in lodgepole pine pollen and a 27.5% increase in *Spirulina*. On the other hand, $^1\text{H-NMR}$ results showed no significant changes in the bioaerosol extracts after light aging. After photooxidative aging with OH radicals, $^1\text{H-NMR}$ analysis shows that the polarity and percent distribution of functional groups of both bioaerosols transformed significantly. The formation of -COOH and -CHO functional groups was observed, with an 11.1% increase in lodgepole pine pollen and a 43.0%

increase in *Spirulina* alga. Additionally, we observed a decrease in aliphatic protons (CH), a decrease in α -carbon protons, and an increase in amide protons, all of which suggest fragmentation of proteins in *Spirulina* upon exposure to OH radicals.

Key words: Laboratory aging; chemical functional groups; pollen; algae; bioaerosols

4.2. Introduction

Bioaerosols have recently become of interest due to their increase in concentration with the warming climate (i.e., pollen season length and concentrations increasing (Anderegg et al., 2021; D'Amato et al., 2020); increase of harmful algal blooms (Carmichael and Boyer, 2016; May et al., 2018a)) and the influence of the COVID-19 pandemic (Erath and Ferro, 2022). Examples of bioaerosols include pollen, fungi, bacteria, and microalgae, which can range in size from a few nanometers to hundreds of microns (Fröhlich-Nowoisky et al., 2016; Pan et al., 2021b). Bioaerosols can influence the climate, weather, and atmospheric processes (such as acting as cloud condensation nuclei (CCN) and ice nucleating particles (INP)) (Burkart et al., 2021; DasSarma and DasSarma, 2018; Schiffer et al., 2018), as well as human health (D'Amato et al., 2020; Mayer et al., 2007; Sénéchal et al., 2015; Taylor et al., 2007). Bioaerosols can be transported intercontinentally (Smith et al., 2011; Tesson et al., 2016; Warren and St. Clair, 2021) and survive extreme atmospheric conditions, even in the stratosphere (DasSarma and DasSarma, 2018). Furthermore, bioaerosols represent a large portion of atmospheric aerosols, and are estimated to be emitted in thousands of tera-grams (Tg) per year (Després et al., 2012; Fröhlich-Nowoisky et al., 2016; Huffman et al., 2013). A study by Hyde et al.

estimated that bioaerosols contribute up to 16.5% of particulate matter smaller than 2.5 micrometers (PM_{2.5}) and 16.3% to PM₁₀ (Hyde and Mahalov, 2020).

Interaction with sunlight, oxidants, and free radicals can change the chemical, physical, and biological properties of bioaerosols (Estillore et al., 2016; Gute et al., 2020; Pan et al., 2014; Sénéchal et al., 2015). According to recent studies, ultra-violet (UV)/solar radiation alone may have the largest impact on pollen florescence (Gute et al., 2020; Kinahan et al., 2019). A study by Kinahan et al., (2019) determined that solar radiation, specifically UV, was a major factor in the aging of aerosolized *E. coli* cells in the atmosphere. Gute et al. (2020) found that the ice nucleation (IN) activity of pollen is changed when exposed to atmospheric processes (solar radiation and OH radicals) and speculated this may be caused by the formation of oxygenated groups at the molecular level, which can lead to an increase in polarity. Bioaerosols can be physically and chemically transformed through interaction with OH radicals, as they are extremely reactive atmospheric oxidants (Liu et al., 2017), modifying organic compounds within the bioaerosols, such as amino acids and phospholipids (Estillore et al., 2016). Liu et al. (2023) investigated the effects of OH radicals (formed by H₂O₂ through photolysis) on live bacteria in simulated cloud-like conditions, and found that even low concentrations (1 x 10⁻¹⁶ M) of OH radicals lysed the live cells and released organic compounds, which were then oxidized and fragmented. Despite these efforts, the aging chemistry of bioaerosols is still poorly understood. An understanding of the changes caused by aging (i.e., oxidation or increase in polarity) is necessary for better assessment of their effects on climate, contribution to atmospheric organic carbon, bioaerosol sampling (i.e., source apportionment), detection, and monitoring.

The lack of research surrounding the topic of atmospheric aging of bioaerosols is the motivation for the present study, which focuses on the characterization of chemical functional groups of fresh and laboratory aged bioaerosols. For this purpose, aqueous extracts of the selected pollen (lodgepole pine) and alga (*Spirulina*) bioaerosols were aged using the Suntest CPS solar simulator and chemical changes in functional groups between fresh and aged extracts were compared. Characterization of functional groups was performed using proton nuclear magnetic resonance ($^1\text{H-NMR}$) and Fourier-transform infrared (FTIR) spectroscopy techniques, which are commonly used for detailed functional group analysis of biological samples.

FTIR is widely used for chemical analysis of various environmental and atmospheric samples, including atmospheric bioaerosols. Research has been conducted on the molecular characterization of a multitude of pollen species via FTIR. For example, Depciuch et al. (2017) studied the effect of pollution on the molecular composition of hazel pollen, and speculated that high concentrations of ozone may have caused oxidation of the pollen. Additionally, Depciuch et al. (2018) used FTIR to distinguish differences in species of birch pollen and found clear chemical variations in their FTIR spectra, even when their morphology is alike. Likewise, Zimmerman et al. conducted multiple studies on the chemical characterization of pollen species and the variations in their chemical composition (Zimmerman et al., 2016; Zimmermann et al., 2017). *Spirulina* alga has also been investigated using FTIR in a previous study (Venkatesan et al., 2012), that determined functional groups that correspond to proteins, carbohydrates, lipids, amino acids, and other organic species in *Spirulina*. Additionally, FTIR has been applied to analysis of atmospheric aerosols in ambient samples (Coury and Dillner, 2009; Maria et al., 2002;

Reggente et al., 2019). These studies suggest that FTIR is a useful analytical tool to determine the chemical composition of bioaerosols, as we have done in this study.

$^1\text{H-NMR}$ has also been previously applied to the analysis of organic and water-soluble atmospheric aerosols (Chalbot and Kavouras, 2019; Duarte and Duarte, 2015; Horník et al., 2020; Suzuki et al., 2001), and some bioaerosols, such as pollen and algae (Chalbot et al., 2013; Kumar et al., 2014; Sarpal et al., 2016). Sarpal et al. (2016) applied $^1\text{H-NMR}$ to determine lipid and fatty acid content in *Spirulina* for biodiesel potential and found strong aliphatic signals, that supports the presence of those compounds. Our previous study's findings agreed with Sarpal et al. (2016), where the majority of the *Spirulina*'s proton contribution came from aliphatic protons (73.8%) (Bahdanovich et al., 2024). While *Spirulina*'s spectrum is dominated by aliphatic protons likely from fatty acids, amino acids, or larger molecules such as lipids, pollen's composition has a heavy contribution from saccharide protons, specifically in water extracts (Bahdanovich et al., 2024; Chalbot et al., 2013). Despite the previous chemical characterization of pollen and algae bioaerosols, neither spectroscopic technique (FTIR or $^1\text{H-NMR}$) has been applied to the analysis of aged atmospheric bioaerosols, as far as we are aware.

The use of these techniques presents a unique perspective on analysis of the changes that bioaerosols undergo in the atmosphere, such as oxidation and changes in polarity. As determined in Chapter 3 (Bahdanovich et al., 2024), pollen and algae differ in their proton and functional group distribution. Thus, the current study focuses on the analysis of these two bioaerosols. Two kinds of aging were performed in our study: (1) simulated solar radiation and (2) oxidation resulting from aqueous formation of OH radicals, which were

formed by photolysis of hydrogen peroxide. The simulated solar radiation covers a broad spectral range (300 – 800 nm) and includes the UV radiation that is necessary for the formation of OH radicals (310 nm). The composition of polar and non-polar functional groups was assessed and compared between fresh and aged bioaerosol extracts.

4.3. Experimental Section

4.3.1. Bioaerosol species

The bioaerosols chosen for this study are *Pinus contorta* pollen (common name: lodgepole pine, collected locally in the Reno-Tahoe area, Nevada, USA) and *Arthrospira platensis* alga (common name: *Spirulina*, Amazon.com, Inc., Seattle, WA, USA). They were chosen for their atmospheric relevance and are representative of typical atmospheric bioaerosols. Lodgepole pine is a species of pine trees, that are widespread across the Northern Hemisphere and are a major producer of pollen in western North America (Chileen et al., 2020; Fall, 1992). *Spirulina* is a type of blue-green microalgae that is present in various environments (Vo et al., 2015) and may be aerosolized by wind due to its small size (Sahu and Tangutur, 2015).

4.3.2. ¹H-NMR analysis

Detailed ¹H-NMR methodology and segment assignment can be found in Chapter 3. Briefly, bioaerosol samples were prepared by adding 10 mg of dry bioaerosol mass to a 2 mL lysing vial (Bertin Instruments Precellys 2 mL Lysing Kit, Rockville, MD, USA) and hydrated with ultra-high purified water ($\geq 18 \text{ M}\Omega \text{ cm}^{-1}$, Elga Veolia PURELAB Chorus 1 water purification system, Woodridge, IL, USA) for a concentration of 10 mg mL⁻¹. The samples were lysed three times at high speed for 20 second intervals (total lysing time =

one minute) and put on ice in between each interval. Lysing was used to fragment the bioaerosol cells and release organic compounds from within the cells. Afterwards, the homogenized samples were centrifuged at 10,000 RPM for two minutes. The supernatant was filtered through 0.45 μm pore sized syringe filters (hydrophilic polytetrafluoroethylene (PTFE) membrane, 25 mm diameter, Thermo Fisher Scientific Inc. (Titan 3), Rockwood, TN, USA). For aging, the samples were placed in a Suntest CPS solar simulator (Atlas Material Testing Solutions, Mount Prospect, IL, USA) for 24 hours. The filtered samples (both fresh and aged) were then completely dried with nitrogen (Airgas Inc., Reno, NV, USA) using the Pierce Reacti-Vap Evaporating Unit (Model 18780, Rockford, IL, USA) and placed in a vacuum oven overnight. The dried samples were resuspended in 0.75 mL of 99.9% deuterated dimethyl sulfoxide (DMSO- d_6) (Cambridge Isotope Laboratories, Inc., Andover, MA, USA) and sonicated for 45 minutes at 30 °C, then transferred to 5 mm high-throughput 8" NMR tubes (Wilmad LabGlass, Vineland, NJ, USA). Bioaerosol samples were prepared in three replicates, all extracted separately, for statistics and preparation consistency. Method blanks (Milli-Q water) were also prepared alongside the samples through the whole process, to determine the presence of any contaminants.

Analysis was conducted using the Agilent Technologies, Inc. 500 MHz PremiumCompact+ NMR (Santa Clara, CA, USA) at 25° C. 256 scans were acquired for each sample and the spectra were processed using VnmrJ software, using a chemical shift range of 0.0 – 14.0 parts per million (ppm). Table 4 shows the functional group and proton placement in ^1H -NMR spectra by spectral segment. The segments were determined using existing literature (Chalbot and Kavouras, 2019; Duarte and Duarte, 2015; Jones and Fleming, 2014; Pretsch et al., 2009) and analysis of a variety of standard compounds, which

is detailed in Chapter 3. Spectra were integrated by each segment (Table 4) using MestReNova software (“MestReNova 14.2,” 2020). Standards (Sigma-Aldrich, Co., St. Louis, MO, USA) were prepared and aged for $^1\text{H-NMR}$ analysis based on our previous findings (Chapter 3) of major contributors of saccharides and amino acids in the analyzed bioaerosols. Sucrose (major contributor in lodgepole pine pollen), glucose (major contributor in *Spirulina*), proline (lodgepole pine pollen), and glutamic acid (*Spirulina*) were aged for 24 hours in the Suntest CPS solar simulator to determine whether oxidation occurred within these compounds, thus providing more insight into the aging chemistry of the bioaerosol samples.

Table 4. Functional group and proton placement in $^1\text{H-NMR}$ spectra.

Segment	Spectral Shift Range (ppm)	Functional groups/proton placement
1	0.5 – 2.0	Aliphatic CH , CH₂ , CH₃
2	2.0 – 2.7	α -carbon O=CH_{1,2} , α -carbon CH-COO: , α to amine H
3	2.7 – 3.7	H in sugar ring, CH-OH in sugar alcohol, C-H in sug- CH₂-OH
4	3.7 – 4.1	Alcohol CH , Alcohol OH , H in saccharide ring, α -carbon CH₂-C-NH₂*
5	4.1 – 5.7	All OH in saccharide ring except - O-CH(OH)- , Glycerol OH , CH=CH₂ , Alcohol OH , OH in TAG
6	6.0 – 6.6	OH in saccharide ring - O-CH(OH)-
7	6.6 – 8.5	Aromatic- H , NH , NH₂
8	9.0 – 14.0	Ar- OH , COOH , CHO

4.3.3. FTIR analysis

For FTIR analysis, bioaerosols were prepared following the same method as for $^1\text{H-NMR}$, except the starting concentration was 50 mg mL^{-1} . After lysing and filtering the samples with $0.45 \text{ }\mu\text{m}$ pore sized PTFE syringe filters, samples were aged for 24 hours in the solar simulator. Then, the samples were dried completely with nitrogen gas and resuspended with $100 \text{ }\mu\text{L}$ acetone, which quickly evaporates when dropped onto potassium bromide powder (KBr, Pike Laboratories, Madison, WI, USA). KBr sample pellets were prepared by adding $100 \text{ }\mu\text{L}$ of resuspended bioaerosol extract onto 200 mg of KBr powder and dried overnight in a glass desiccator lined with sodium hydroxide pellets (NaOH, Ward's Science, Rochester, NY, USA). After the sample was completely dry, a hydraulic press was used to apply 10 tons of pressure for 5 minutes (CrushIR Digital Hydraulic Press, Pike Technologies, Madison, WI, USA) to create a pellet of 13 mm in diameter. Samples were prepared in three replicates alongside method blanks. Bioaerosol samples were analyzed using the Nicolet 6700 FTIR spectrometer (Thermo Fisher Scientific). Spectra were recorded in transmission mode for a total of 32 scans in the spectral range of $4,000 - 400 \text{ cm}^{-1}$, with a resolution of 4 cm^{-1} , and data spacing of 1.929 cm^{-1} .

FTIR spectra were processed by applying a baseline correction to the raw spectra using the Envi Classic 5.6.1 software. Spectral ranges for bioaerosol spectrum interpretation were assigned based on multiple sources. Textbooks were used as the main references (Jones and Fleming, 2014; Pretsch et al., 2009), and peer-reviewed articles provided specific details concerning pollen and algae spectra (Bartošová et al., 2015; Depciuch et al., 2017; Heller et al., 2015; Stehfest et al., 2005; Venkatesan et al., 2012; Zimmermann et al., 2017). In addition, the standards of glucose, sucrose, palmitic acid,

and glutamic acid were aged and analyzed with FTIR for reference. These standards were chosen for their relevance to lodgepole pine pollen and *Spirulina* alga bioaerosols, as found in Chapter 3.

Table 5 shows the functional groups present in different wavenumber ranges, many of which correspond to functional groups found in various chemical compounds relevant to bioaerosols, such as saccharides, polysaccharides, amino acids, fatty acids, lipids, proteins, nucleic acids, and phospholipids. Only major peaks were detected and analyzed for the chosen bioaerosols. The absorption band found in the wavelength range of $3650 - 3000 \text{ cm}^{-1}$ is the result of O-H stretching, that can occur in organic compounds such as saccharides, alcohols, amino acids, and water. The aliphatic C-H stretching absorption band can be found in the range of $3000 - 2840 \text{ cm}^{-1}$, and may be caused by saccharides, amino acids, fatty acids, and lipids, as these compounds all contain multiple aliphatic CH groups. The C=O stretching that is typically found in carboxylic acids of fatty acids absorbs wavelengths of $1750 - 1700 \text{ cm}^{-1}$, while the amide I C=O stretching that is representative of proteins is found in the range of $1680 - 1600 \text{ cm}^{-1}$. The amide II absorption band in the range of $1575 - 1480 \text{ cm}^{-1}$ results from N-H bending and C-N stretching that is found in proteins. Bending in CH_2 and CH_3 , in carbonyls and lipids (respectively), is found in the range $1430 - 1370 \text{ cm}^{-1}$, however, this peak is present in the fresh and aged method blanks, which suggests it is a product of contamination. In the range of $1300 - 1200 \text{ cm}^{-1}$, the stretching vibration of P=O is detected in phosphorous-containing compounds, such as nucleic acids and phospholipids. The last absorption band used in this analysis belongs to stretching of C-O-C, that corresponds to bonds found in polysaccharides (glycosidic bond, present in starch). Although these absorptions bands are standard in FTIR spectrum

analysis (Bartošová et al., 2015; Depciuch et al., 2017; Heller et al., 2015; Jones and Fleming, 2014; Pretsch et al., 2009; Stehfest et al., 2005; Venkatesan et al., 2012; Zimmermann et al., 2017), the assignment of organic compounds to each functional group is speculative, as bioaerosol spectra are complex and can have a matrix effect.

Table 5. Wavenumber ranges of common functional groups found in FTIR spectra.

Wavenumber range (cm⁻¹)	Band assignment (functional groups)	References
3650 – 3000	<i>O-H stretching vibration</i> (saccharides, alcohols, water, amino acids)	(Bartošová et al., 2015; Depciuch et al., 2017; Jones and Fleming, 2014; Pretsch et al., 2009)
3000 – 2840	<i>Aliphatic C-H stretching vibration</i> (saccharides, fatty acids, amino acids, lipids)	(Depciuch et al., 2017; Jones and Fleming, 2014; Pretsch et al., 2009; Venkatesan et al., 2012)
1750 – 1700	<i>C=O stretching vibration of ester</i> (fatty acids, lipids)	(Bartošová et al., 2015; Jones and Fleming, 2014; Pretsch et al., 2009; Stehfest et al., 2005; Venkatesan et al., 2012)
1680 – 1600	<i>C=O stretching vibration</i> (amide I, proteins)	(Bartošová et al., 2015; Depciuch et al., 2017; Heller et al., 2015)
1575 – 1480	<i>N-H bending and C-N stretching vibration</i> (amide II, proteins)	(Bartošová et al., 2015; Depciuch et al., 2017)
1430 – 1370	<i>-CH₂ bending vibration (carbonyl)</i> <i>-CH₃ bending vibration (lipids)</i> (d *Large peak found in aged method blank	(Bartošová et al., 2015; Depciuch et al., 2017; Venkatesan et al., 2012)
1300 – 1200	<i>P=O stretching</i> (nucleic acids, phospholipids)	(Bartošová et al., 2015; Pretsch et al., 2009; Stehfest et al., 2005)
1180 – 990	<i>C-O-C stretching vibration</i> (polysaccharides)	(Bartošová et al., 2015; Depciuch et al., 2017; Heller et al., 2015; Jones and Fleming, 2014; Pretsch et al., 2009; Zimmermann et al., 2017)

To determine the changes in bioaerosols due to aging, ratios of signals of polar vs. non-polar peaks were calculated and compared. These ratios were calculated based on the heights of peaks in the FTIR spectrum for specific functional groups (see Table 5). The

background signal of method blanks (Figure A4.1) was subtracted from the spectra of analyzed bioaerosol extracts. After the correction with the method blank, the peaks were assigned as more polar (O-H, C=O, C-O-C) or less polar (C-H, CH₂/CH₃). The ratios of fresh and aged replicates (three separately extracted replicates) were averaged, then the average fresh ratio was divided by the average aged ratio and calculated as a polarity percent change (see Eq. 1). OH/CH was used for overall polarity increase, as this ratio provided the highest increase in polarity in aged bioaerosol samples based on our observations. C=O/CH was used to determine changes in the amide I C=O functional group, belonging to stretching vibrations in proteins. Similarly, C-O-C/CH was used to find effects of aging on the C-O-C functional group. The CH₂/CH₃ band was not used for determination of aging effects on bioaerosols, as it is present in the method blanks (see Figure A4.1), which may be a product of sample preparation, aging, or contamination. This comparison of the polarity change helps us assess the aging/oxidation of bioaerosols in a semi-quantitative way.

$$\text{Eq. 1} \quad \text{Polarity \% change} = \left(1 - \left(\frac{\text{average ratio of fresh replicates}}{\text{average ratio of aged replicates}} \right) \right) * 100$$

4.3.4. Laboratory aging

Samples were placed in 3.5 mL quartz cuvettes (light path of 10 mm, wavelength range 190 – 2500 nm, polytetrafluoroethylene (PTFE) covers, LifeStyle Visions, Amazon Inc.), covered, and sealed with Parafilm (Amcor, Zurich, Switzerland). The Suntest CPS solar simulator wavelength range (300 – 800 nm, peaking at 460 nm in the visible region) overlaps the range of the cuvettes, making them ideal for this study. The solar simulator irradiance closely simulates the Earth's solar radiation, including UVA, UVB, visible, and

infrared radiation (*SUNTEST CPS / CPS+ Operating Manual*, 1999), making this a valuable instrument for simulated atmospheric aging. The solar simulator is equipped with a cooling fan, to cool down the sample chamber as it is heated by the lamp (NXe 1500 B Atlas xenon lamp). The temperature inside the chamber peaks at 30.8° C (Figure A4.2). This method was inspired by a study that determined IN in sub-pollen pollen particles after aging using the Suntest CPS solar simulator (Gute et al., 2020). In fact, this study found that the simulated solar radiation had the largest impact on IN activation temperature of sub-pollen particles (SPP). The IN activation temperature was lowered after the SPP was aged for 24 hours, meaning that ice was formed on the nuclei at lower temperatures. For hydroxyl radical formation through photolysis, hydrogen peroxide (H₂O₂, 30%, 9.8 M, Fisher Scientific, Fair Lawn, NJ, USA) was added to the bioaerosol samples to create a target H₂O₂ concentration of 1 M (in the final solution), then aged under simulated solar radiation for 24 hours. This concentration was chosen based on Gute et al. (2020) study, where the highest changes in IN temperatures of pollen was from 0.5 M. We doubled the concentration based on the higher extract concentrations in our study. Eq. 2 shows the reaction between H₂O₂ and UV radiation (≤ 254 nm, 280 – 320 nm) that forms OH radicals (Legrini et al., 1993; Li et al., 2021). Two sets of samples were prepared for each bioaerosol; fresh and aged, which were prepared in three separately extracted replicates. Aged samples included a control sample of each bioaerosol, wrapped in aluminum foil, exposed to the same conditions except for light (Figure A4.3). Both sets of samples also included method blanks, which were prepared with ultra-purified water, following the same sample preparation methodology as bioaerosol samples. Table 6 shows a list of samples that were extracted and analyzed for the present study.

Eq. 2



Table 6. Samples that were extracted and analyzed for this study. Bioaerosol samples were not analyzed by FTIR after aging with OH and simulated solar radiation. Saccharides analyzed were glucose and sucrose; amino acids analyzed were proline and glutamic acid.

	¹ H-NMR			FTIR		
	Not aged (fresh)	Aged by simulated solar radiation	Aged by OH + simulated solar radiation	Not aged (fresh)	Aged by Simulated solar radiation	Aged by OH + simulated solar radiation
Lodgepole pine pollen	√	√	√	√	√	Not analyzed
<i>Spirulina alga</i>	√	√	√	√	√	Not analyzed
Method Blanks	√	√	√	√	√	√
Standards (saccharides, amino acids)	√	√	√	√	√	√

4.4. Results and Discussion

Lodgepole pine pollen and *Spirulina alga* extracts were aged with (1) simulated solar radiation and (2) OH radicals formed from H₂O₂ by photolysis. Visually, the color of both pollen and alga extracts changed after exposure to 24 hours of simulated solar radiation (Figure A4.3). Lodgepole pine pollen turned from light yellow to clear, and *Spirulina alga* transformed from a dark green to a dull light yellow. As UV radiation is the strongest radiation experienced by the samples when exposed to the range of wavelengths in the Suntest solar simulator, it is likely UV that causes the greatest damage to various organic compounds within bioaerosols (Kinahan et al., 2019; Pan et al., 2021b). Changes

in pigment of algae have been documented, with decreases in pigments in algae and cyanobacteria following exposure to UVB radiation (Sinha et al., 1995; Xue et al., 2005). Likewise, the change in lodgepole pine pollen pigment may be attributed to the degradation of carotenoids upon exposure to UV (Semitsoglou-Tsiapou et al., 2022), however, research on this topic remains limited.

4.4.1. FTIR results

Aged extracts of lodgepole pine pollen and *Spirulina* alga were analyzed using FTIR spectroscopy. The spectra of fresh and aged lodgepole pine pollen extracts are presented in Figure 10. The aged spectrum closely resembles the fresh one, however, the intensities of some peaks decreased after exposure to simulated solar radiation for 24 hours. All identified FTIR peak signals are presented in Table 5. In both spectra, the O-H peak is visible and dominant (at ~ 3377 (fresh) and ~ 3416 (aged) cm^{-1}), while the aliphatic C-H peak is present at 2925 cm^{-1} and decreased after aging. The C=O stretching vibration band from fatty acids is present at 1745 cm^{-1} , though it is more of a notch than a peak. The C=O amide I band is observed (~ 1652 and $\sim 1639 \text{ cm}^{-1}$), signaling a presence of proteins in the pollen. The fresh and aged pollen spectra show the presence of P=O stretching at 1261 cm^{-1} . C-O-C stretching vibration within carbohydrates/polysaccharides (e.g., starch) is present at ~ 1050 and 1053 cm^{-1} . All peaks decrease in intensity (compared to the O-H peak) after aging, indicating an increase in O-H after aging, which overall increases the polarity of the pollen extracts.

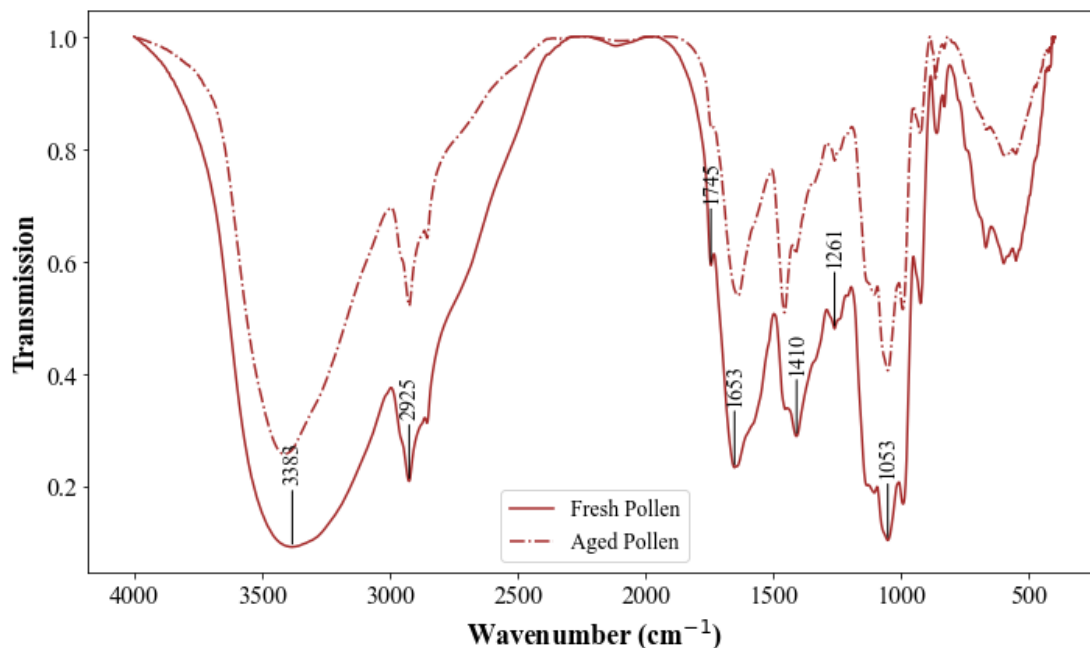


Figure 10. Fresh (solid) and aged (dashed) lodgepole pine pollen extract FTIR spectra. Samples were analyzed using KBr pellets in transmission mode.

Spectra of fresh and aged extracts of *Spirulina* alga analyzed with FTIR are illustrated in Figure 11. The O-H and aliphatic C-H peaks are observed in these spectra, however, there is an absence of the C=O (fatty acid) peak. The amide I peak is more prominent than in pollen spectra (Figure 10) and is greater in intensity than the O-H peak prior to aging. The amide II peak, indicating N-H bending and C-N stretching within proteins is present (1547 and ~ 1542 cm^{-1}). This peak is not observed in the pollen extract; only perhaps as a shoulder on the amide I peak. P=O and C-O-C stretching signals are also present in both alga spectra. Overall, the peaks belonging in the alga spectrum do not change in intensity as much as in case of fresh vs. aged pollen spectra, but the peaks still decrease in comparison to the O-H stretching. Although the CH₂ and CH₃ bending vibrations (1430 – 1370 cm^{-1}) are present in both bioaerosol spectra, they will not be discussed due to background noise (Figure A4.1).

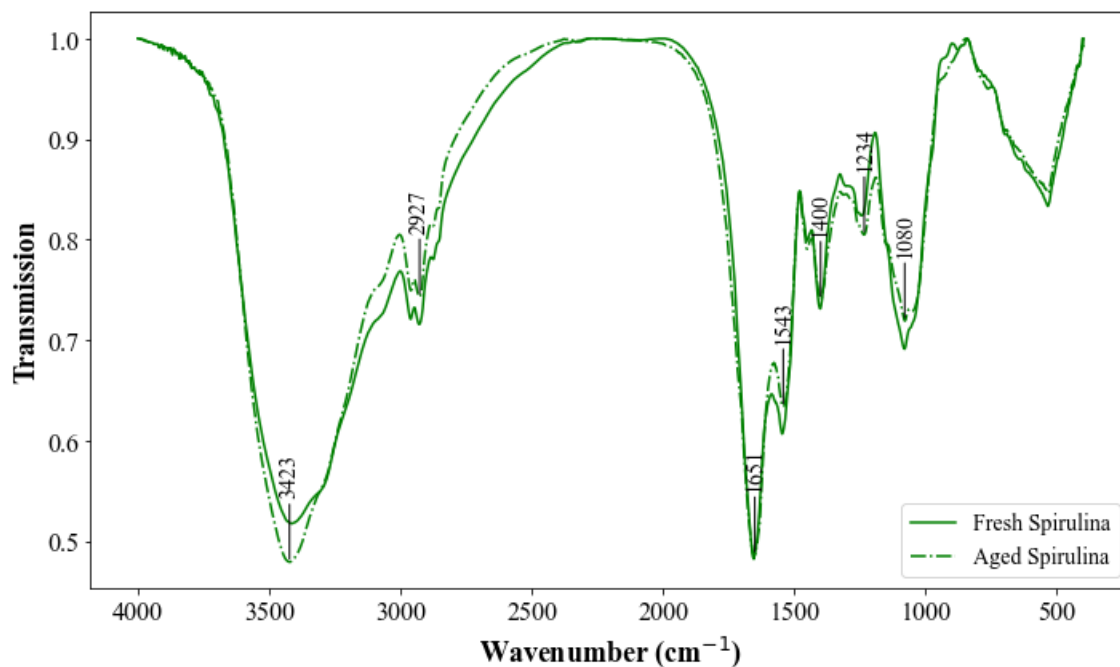


Figure 11. Fresh (solid) and aged (dashed) *Spirulina* alga extract FTIR spectra. Samples were analyzed using KBr pellets in transmission mode.

To assess changes in chemical functional groups after exposure to simulated solar radiation, ratios of the peaks in FTIR spectra were calculated and interpreted. An increase in a polar to non-polar chemical functional groups' ratio may indicate the formation of an oxygen-containing group, such as O-H, C=O, or C-O-C, or the degradation of a C-H bond within a molecule (e.g., hydrogen abstraction). Similarly, a decrease in the ratio may indicate the degradation of a polar group, or a formation of more C-H groups. Since the amide I C=O bond is representative of proteins, the decrease in the ratio in pollen may be caused by broken C=O bonds in the carboxylic acids in the amino acids found in proteins (Jones and Fleming, 2014).

Table 7 shows the percent change of ratios of polar to non-polar groups (polarity) in lodgepole pine pollen and *Spirulina* after aging due to simulated solar radiation. O-H/C-

H increased in both pollen and alga after aging, signifying an increase in polarity for both bioaerosols. C=O/C-H ratio decreased after aging in pollen. C=O can be found in carboxyl groups of amino acids and fatty acids (-COOH), as well as in larger molecules such as lipids and proteins (Jones and Fleming, 2014). C-O-C/C-H decreased after aging in *Spirulina* but increased in pollen. The decrease of C-O-C in *Spirulina* may be attributed to the degradation of glycosidic bonds in starch molecules or di-saccharides (i.e., sucrose), which can be caused by UV radiation (Nowak et al., 2023). Both bioaerosols contain polysaccharides like sucrose and starch, as determined in our previous studies (Bahdanovich et al., 2024, 2022). After analysis of standards (saccharides-glucose and sucrose; amino acids-proline and glutamic acid) aged with OH radicals (Figures A4.4 and A4.5), we found that the O-H signal from the oxidation agent overlaps with O-H signal of the analyzed compounds in bioaerosol extracts and oversaturates the spectra (Table A4.1). Therefore, bioaerosols were not analyzed for aging with OH radicals using the FTIR technique.

Table 7. Polar/non-polar functional group ratios of light-aged bioaerosols. Calculations of ratios explained in Section 4.3.3.

$\frac{\text{Polar}}{\text{Non - polar}}$	Lodgepole pine pollen % change	<i>Spirulina</i> alga % change
$\frac{OH}{CH}$	+30.9	+27.5
$\frac{C = O}{CH}$	-7.8	+15.6
$\frac{C - O - C}{CH}$	+12.9	-19.1
$\frac{OH + C = O}{CH}$	+15.2	+20.8
$\frac{OH + C = O + C - O - C}{CH}$	+12.9	+12.5

4.4.2. ^1H -NMR results

Figure 12 shows the percent distribution of functional groups' protons analyzed with ^1H -NMR before and after aging for lodgepole pine pollen and *Spirulina* alga extracts. The bioaerosol extracts were aged by exposure to (1) simulated solar radiation for 24 hours and (2) OH radicals formed by photolysis of H_2O_2 . The largest proton contributions in fresh lodgepole pine pollen came from saccharides (segment 3; $40.2 \pm 2.6\%$), OH (segment 5; $26.9 \pm 1.3\%$), and aliphatic CH (segment 1; $21.1 \pm 1.5\%$). For *Spirulina*, the major contributions come from aliphatic CH ($56.9 \pm 5.5\%$) and α -carbon (segment 2; $22.7 \pm 6.8\%$).

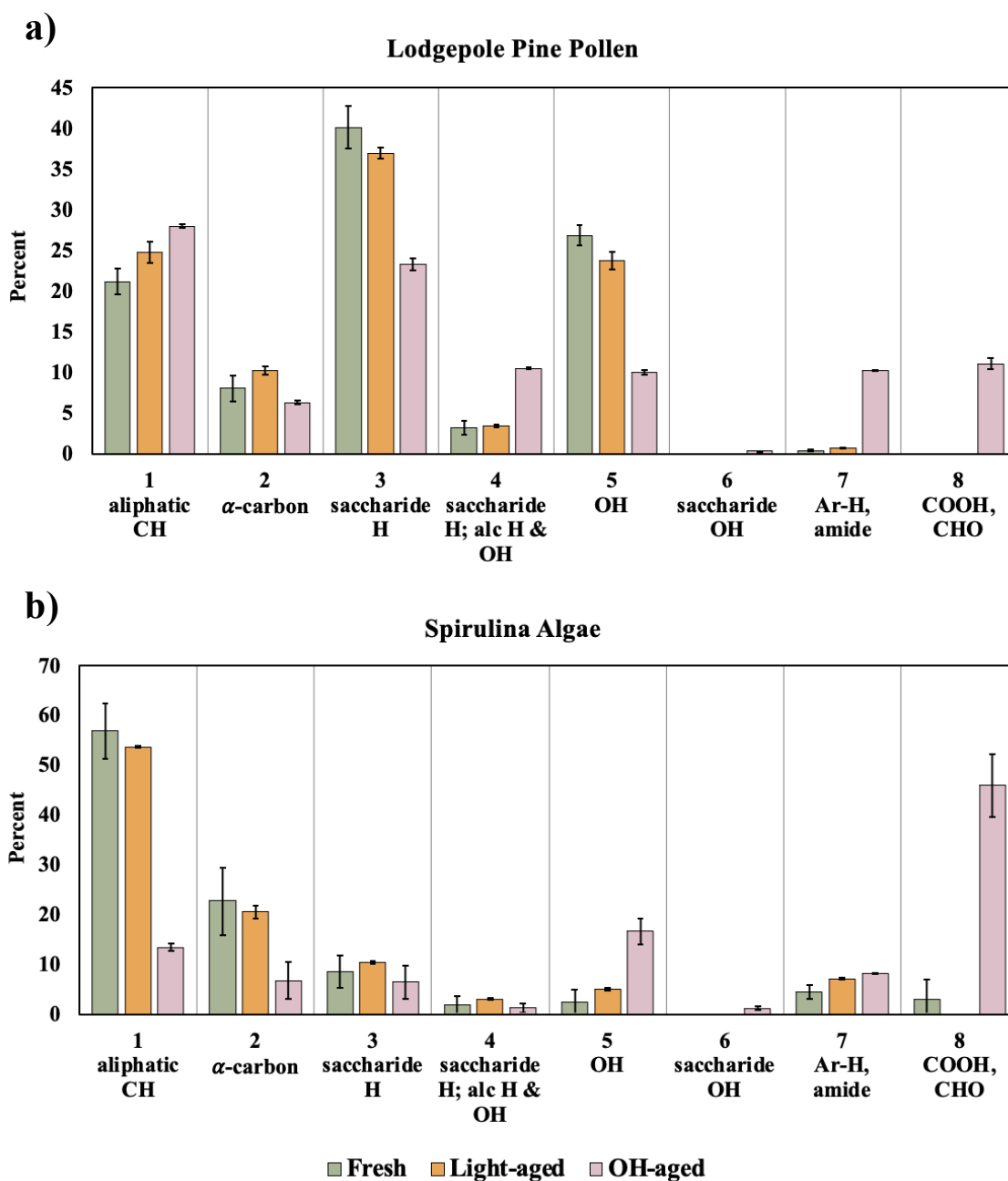


Figure 12. Functional group percent distribution of a) lodgepole pine pollen and b) *Spirulina* alga extracts after exposure to (1) simulated solar radiation and (2) OH radicals formed under simulated solar radiation. Extracts were resuspended with DMSO- d_6 and analyzed with 500 MHz 1H -NMR. Ar-H stands for aromatic H; alc H stands for alcohol H. Detailed segment information can be found in Table 4. Error bars represent the standard deviations determined from three separately extracted replicates.

The functional group percent difference after aging of the selected bioaerosols is presented in Figure 13. Overall, both bioaerosols experienced transformation of their functional group distribution, with a greater change occurring after OH radical aging (represented by green bars). While there is a minor change after light aging, based on an unpaired (independent) t-test of percent distribution of fresh and light-aged bioaerosols, for most functional groups, the changes were not statistically significant ($p < 0.05$). As such, only OH radical aging results will be discussed. Results show a major aliphatic CH (+43.4%) and α -carbon (+16.0%) proton signal decrease in *Spirulina* after OH radical aging. An increase in segment 8 was observed for both bioaerosols (pollen: +11.1%, alga: +43.0%), which suggests the formation of carboxylic acids or aldehydes, and thus, an increase in polar functional groups. Both bioaerosol extracts also saw an increase of segment 7 signal (pollen: +9.8%, alga: +3.7%), which belongs to aromatic H and amide protons. The segment 5 proton signal increased in *Spirulina* (+14.2%), but decreased in pollen (-16.8%), which corresponds to all OH in saccharide ring (except -O-CH(OH)-), glycerol OH, alcohol OH, and OH in triglycerides (Table 4).

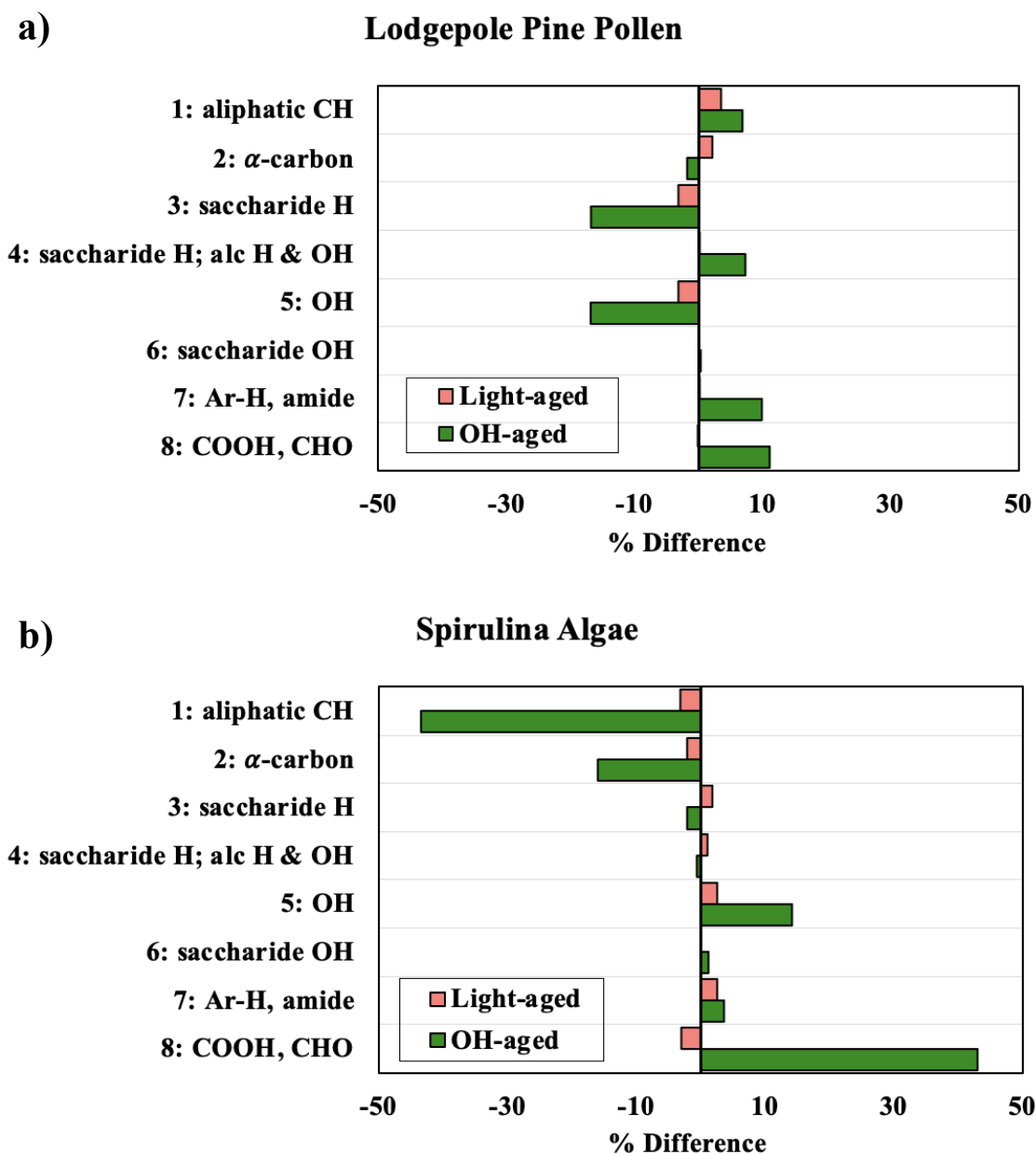


Figure 13. Functional group percent difference of a) lodgepole pine pollen and b) *Spirulina* alga extracts after exposure to (1) simulated solar radiation and (2) OH radicals formed under simulated solar radiation. Ar-H stands for aromatic H; alc H stands for alcohol H. Detailed segment information can be found in Table 4.

To determine which compounds and their functional groups may play a role in the aging of the selected bioaerosols, percent differences in functional groups of saccharides (glucose and sucrose) and amino acids (proline and glutamic acid) were determined through $^1\text{H-NMR}$ analysis (Figure 14). These compounds were chosen based on their presence in the analyzed bioaerosols in Chapter 3. Briefly, sucrose was a major saccharide found in lodgepole pine pollen (16% of total analyzed saccharides), followed by glucose (1.23%). *Spirulina* had drastically lower concentrations of saccharides, however, sucrose (0.017%) and glucose (0.16%) were still quantified. The amino acids proline and glutamic acid were present in both bioaerosols, though in low amounts ($< 0.36\%$). Thus, these compounds were aged and analyzed, following the same method as the bioaerosols, to hypothesize the chemistry occurring in pollen and alga. The percent difference patterns in saccharides and amino acids are similar to the patterns in the analyzed pollen and alga, respectively. This may be due to the high percentage of saccharides found in lodgepole pine pollen (18.4% of total dry pollen weight) (Bahdanovich et al., 2024). There is little connection between the similarity of *Spirulina* and amino acid percent differences, as we found that the analyzed amino acids contributed to only 0.73% of total *Spirulina* dry weight (Bahdanovich et al., 2024). However, amino acids share functional groups such as carboxylic acids, α -carbon, and aliphatic CH with other organic compounds like fatty acids, proteins, and lipids (Jones and Fleming, 2014).

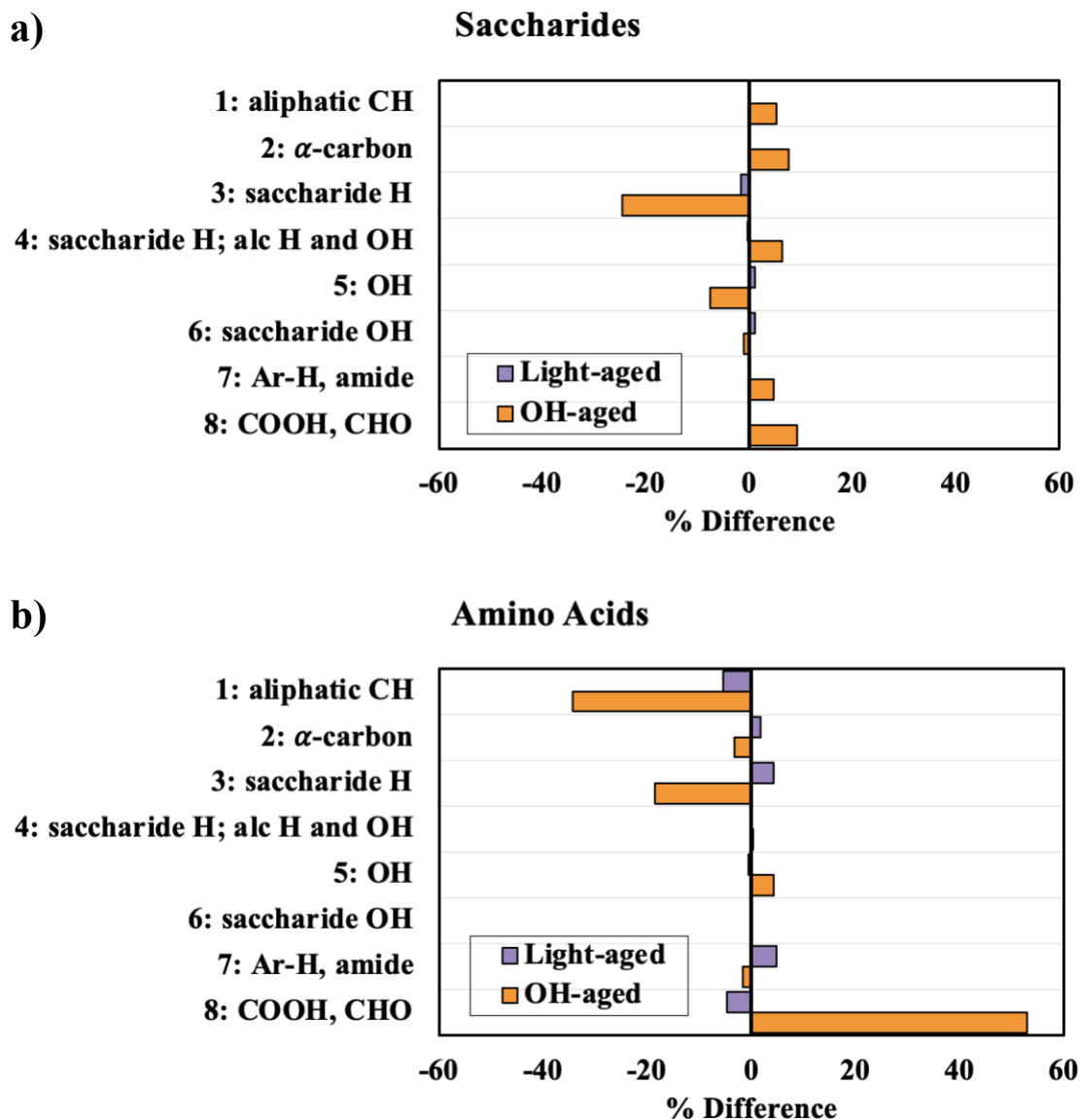


Figure 14. Functional group percent difference of a) saccharide (glucose and sucrose) and b) amino acid (proline and glutamic acid) after exposure to (1) simulated solar radiation and (2) OH radicals formed under simulated solar radiation. Ar-H stands for aromatic H; alc H stands for alcohol H. Detailed segment information can be found in Table 4.

Studies show that OH radical reactions with amino acids and proteins cause a hydrogen abstraction (removal) from C-H bonds, which can occur at an amino acid side

chain or a protein backbone (Estillore et al., 2016; Liu et al., 2017). The 34.3% decrease in the aliphatic CH in amino acids (Figure 14b) may be due to the hydrogen abstraction in the side chains of the analyzed amino acids (proline and glutamic acid). In addition to the decrease in segment 1 (aliphatic CH), we also observed a 53.0% increase in segment 8 (COOH and CHO), which can be explained by the addition of an OH group to the carbon where the hydrogen abstraction occurred. Using proline (aged and analyzed) as a simple example, the side chain can undergo hydrogen abstraction, therefore reducing the amount and intensity of the aliphatic CH signal in the $^1\text{H-NMR}$ spectrum. The abstraction creates a carbon-centered radical in the side chain, creating an opportunity for another OH radical to attach itself (Figure 15) and form a more polar group, such as an aldehyde (CHO). If further oxidation occurs, a carboxylic acid (COOH) may form, of which an increase was observed after OH aging (Mujika et al., 2013; Signorelli et al., 2014). This hypothesis originates from a study by Signorelli et al. (2014) where the reaction pathways between OH radicals and proline were explored.

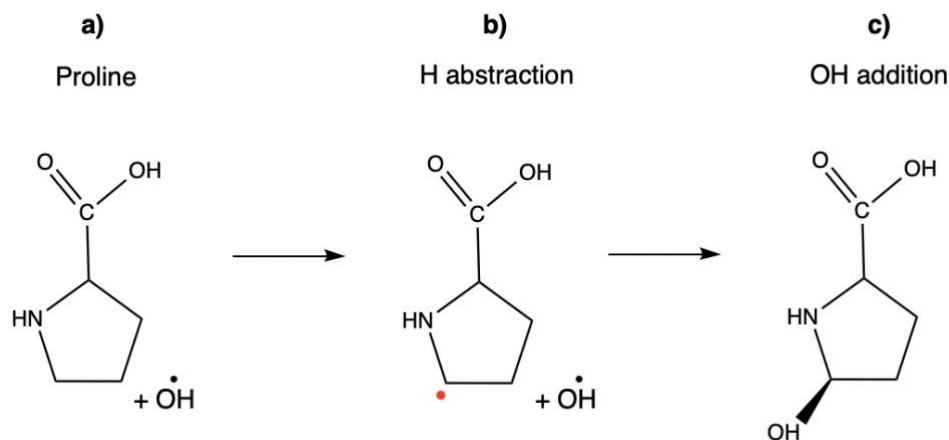


Figure 15. Possible oxidation pathway for OH radical reaction with the amino acid proline: a) proline is exposed to OH radical, b) hydrogen abstraction occurs and leaves a carbon-centered radical (red), c) another OH radical is present and attaches itself to the carbon-centered radical. Mechanism based on a study by Signorelli et al. (2014). Figure created in ChemDraw 20.1.

In a similar process, the backbone of a peptide or protein can be cleaved (broken) upon exposure to OH radicals, with hydrogen abstraction at the α -carbon, creating smaller amide and carbonyl fragments (Liu et al., 2017). Figure 16 shows part of a peptide backbone containing leucine and tyrosine amino acids, which were both found in lodgepole pine pollen and *Spirulina* alga in our previous studies (Axelrod et al., 2021; Bahdanovich et al., 2024). This figure is a visual representation of where the peptide can be cleaved (dashed lines) at the α -carbon hydrogen, fragmenting the peptide. *Spirulina* alga contains an estimated 60% of protein (Grosshagauer et al., 2020), while pine pollen contains roughly 10% (Cheng et al., 2023). Reactions of OH radicals with proteins may be the cause for a decrease in aliphatic CH, decrease in protons from α -carbon, increase in amide protons, and an increase in COOH and CHO in the analyzed bioaerosols (Figure 13).

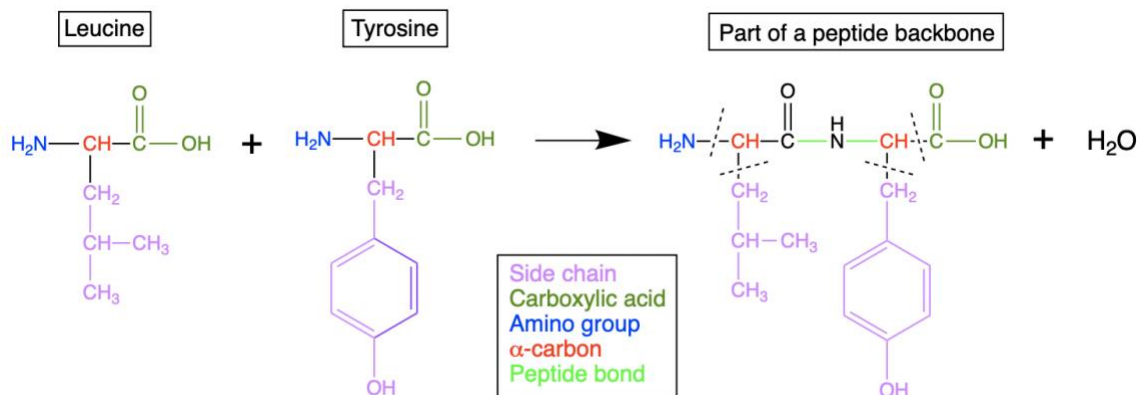


Figure 16. Diagram of a part of a peptide backbone containing leucine and tyrosine amino acids. Dashed lines represent possible cleaving due to abstraction of the α-carbon hydrogen in the peptide, creating smaller fragments of carbonyls and amines after exposure to OH radicals. Amino acids and peptide backbone modeled after Alberts B et al. (2002). Figure created in ChemDraw 20.1.

OH radicals also affect lipids such as triglycerides by creating a carbon-centered radical (lipid radical) near or between double bonds in unsaturated fatty acids, through hydrogen abstraction (Figure 17) (Ayala et al., 2014). Oxygen (O₂) is then added to the lipid radical, creating a peroxy radical, which then continues to propagate through the fatty acid chain, oxidizing the triglyceride. The propagated oxidation can result in the formation of compounds such as alkanes (CH), aldehydes (CHO), and ketones (containing C=O) (Hadidi et al., 2022). Lipid peroxidation may be another process that plays a role in the oxidation of bioaerosols (Abd El-Baky et al., 2007; Wu et al., 2024), and may be a mechanism that causes the increase of aliphatic CH signal (+6.8%), from formation of alkanes, in pollen. In addition to amino acids, proteins, and lipids, OH radicals can also abstract hydrogen atoms from polysaccharides. In particular, this process can occur at the glycosidic bond, fragmenting the polysaccharide (Chen et al., 2021; Peshev et al., 2013). Further, hydrogen abstraction can occur in the saccharide ring that can lead to the formation

of other functional groups such as aldehydes and ketones (Xie et al., 2025), which we observed in both bioaerosol extracts after OH aging.

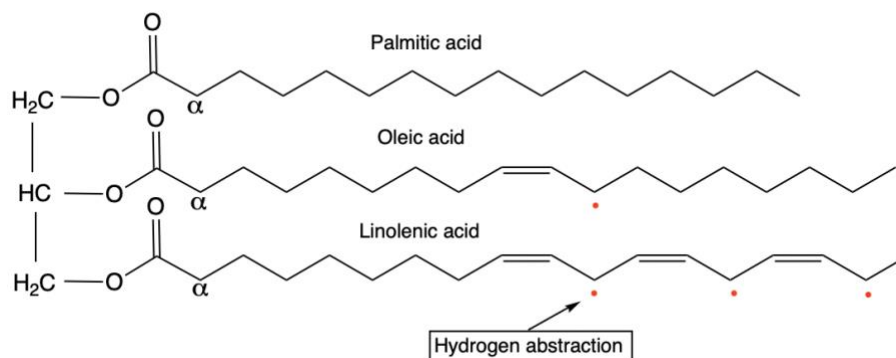


Figure 17. Example of a triglyceride, containing three fatty acids (from top to bottom: palmitic, oleic, linolenic acids). The start of lipid peroxidation, hydrogen abstraction (red), is represented by the carbon-centered radicals in the fatty acid chains, after exposure to OH radicals. Mechanism based on (Ayala et al., 2014). Figure created in ChemDraw 20.1.

4.5. Conclusion

This study investigated the changes in chemical functional groups of lodgepole pine pollen and *Spirulina* bioaerosols' water extracts after exposure to (1) simulated solar radiation and (2) OH radicals formed by photolysis. FTIR results indicate that the polarity of the bioaerosol extracts increase after aging with simulated solar radiation. The largest increases came from the OH/CH ratio, with an increase of 30.9% for lodgepole pine pollen and 27.5% for *Spirulina* alga. An increase in the OH/CH ratio suggests an increase in polarity, however, it is difficult to speculate which chemical processes occurred for which chemical compounds using FTIR. Thus, we analyzed the bioaerosols with ¹H-NMR after exposing the extracts to simulated solar radiation and the ¹H-NMR spectra showed no substantial changes in the functional group protons' signals. Exposing the pollen and alga

bioaerosols to OH radicals (formed by H₂O₂ through photolysis) produced interesting results, specifically the increase in -COOH and -CHO functional groups in both bioaerosol ¹H-NMR spectra (pollen: +11.1%, alga: 43.0%). Along with the decrease of the aliphatic CH (-43.4%) and α-carbon (-16.0%) proton signals in *Spirulina*, we hypothesize that these changes may be due to oxidation of amino acids, proteins, or triglycerides/lipids. While these processes may have also affected pollen, we observed an increase in aliphatic CH protons (+6.8%) (may be due to the formation of alkanes from lipid peroxidation) and a decrease in OH protons (-16.8%), suggesting a different mechanism involved.

Only two types of bioaerosol species were analyzed; other types and species should be analyzed prior to and after aging in the future. It is important to assess how individual organic compounds change after aging (i.e., saccharides, amino acids, fatty acids), since it is challenging to see specific compound transformations using FTIR and NMR, especially considering the matrix of the bioaerosol extracts. Quantitative analysis via mass spectrometry techniques, such as GC-MS and UPLC-MS can provide more insight into these changes. Future studies may look at IN ability of these aged particles to see if an increase in polarity influences IN ability. The solvent used in this study was water, due to its atmospheric relevance and likely interaction with bioaerosols. Since pollen readily ruptures in the presence of water, due to osmotic rupturing (Hughes et al., 2020; Mampage et al., 2022), more compounds may have been extracted compared to alga; which can exist in aqueous environments and does not readily rupture in the presence of water. Thus, different solvents should be used in future studies to determine the complete composition of both bioaerosols, even if the solvents are not atmospherically relevant. Finally, the conditions of atmospheric bioaerosol aging should be optimized in future studies for

atmospheric relevance. Based on Liu et al. (2023) study of photooxidation of live bacteria with OH radicals, lower concentrations of H_2O_2 and whole pollen/algae cells can be used, as they are expected to lyse on their own in the presence of hydrogen peroxide and OH radicals.

4.6. Chapter 4 Appendix

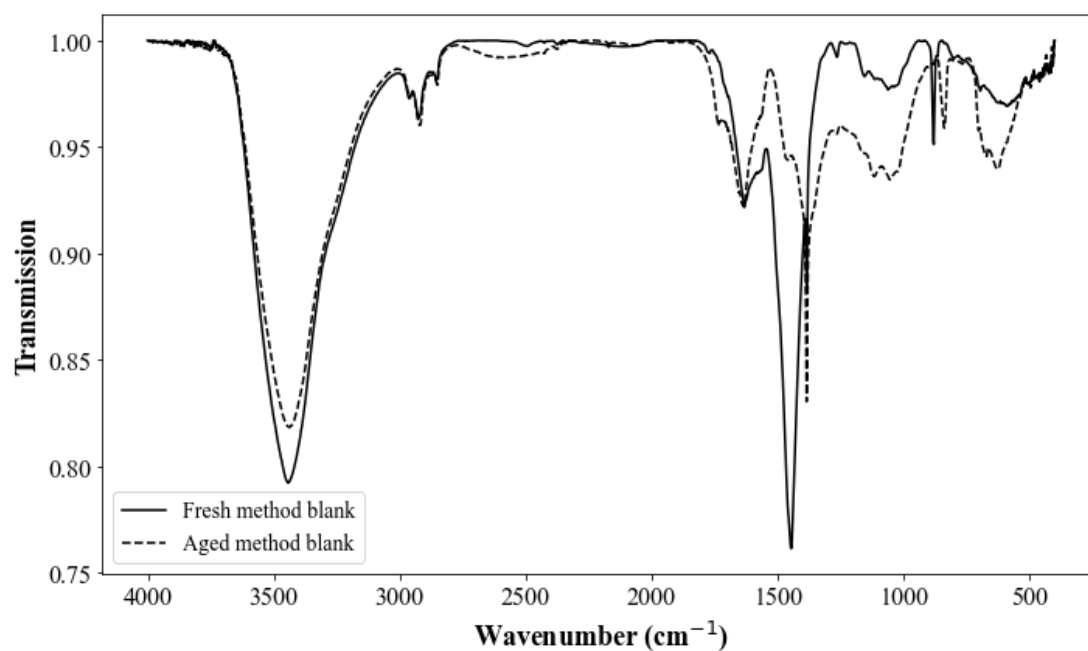


Figure A4.1. FTIR spectra of fresh and light-aged method blanks.

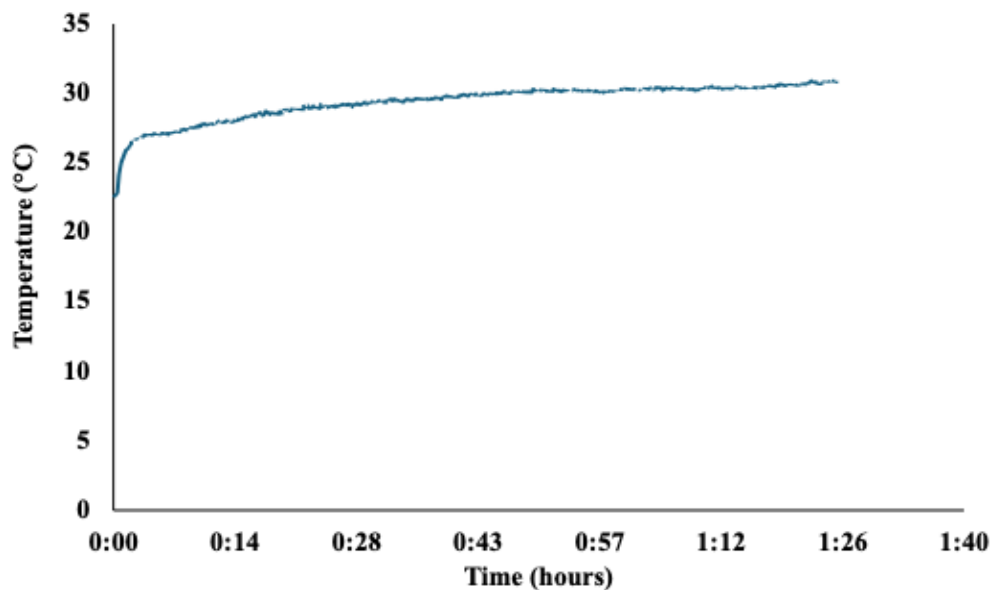


Figure A4.2. Temperature inside Suntest CPS solar simulator chamber.

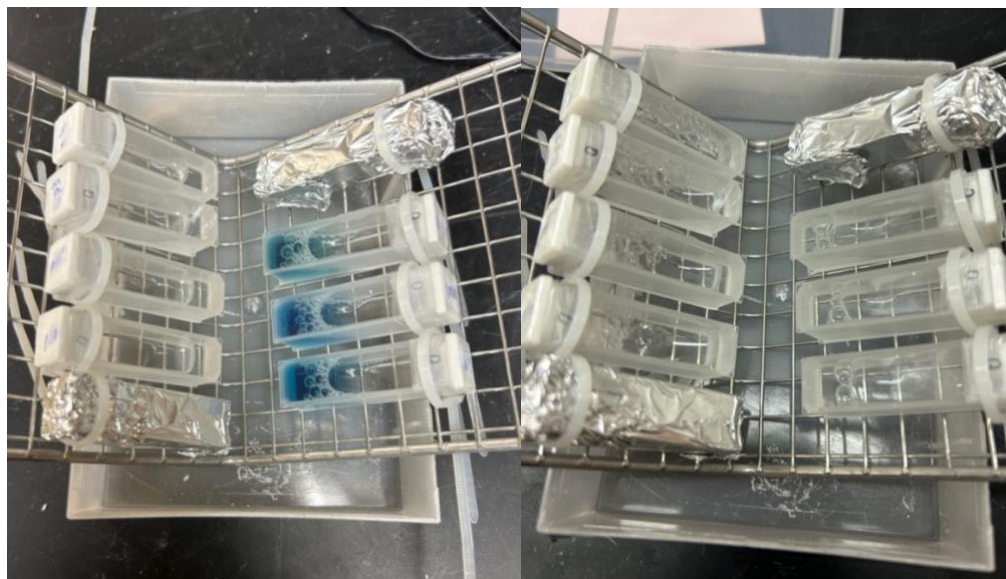


Figure A4.3. Samples before (left) and after (right) aging in the Suntest CPS. Three replicates of lodgepole pine pollen extract are on the left side of the sampling set-up, while the replicates of *Spirulina* extract are on the right. Additionally, control samples in foil for each bioaerosol and a method blank were aged.

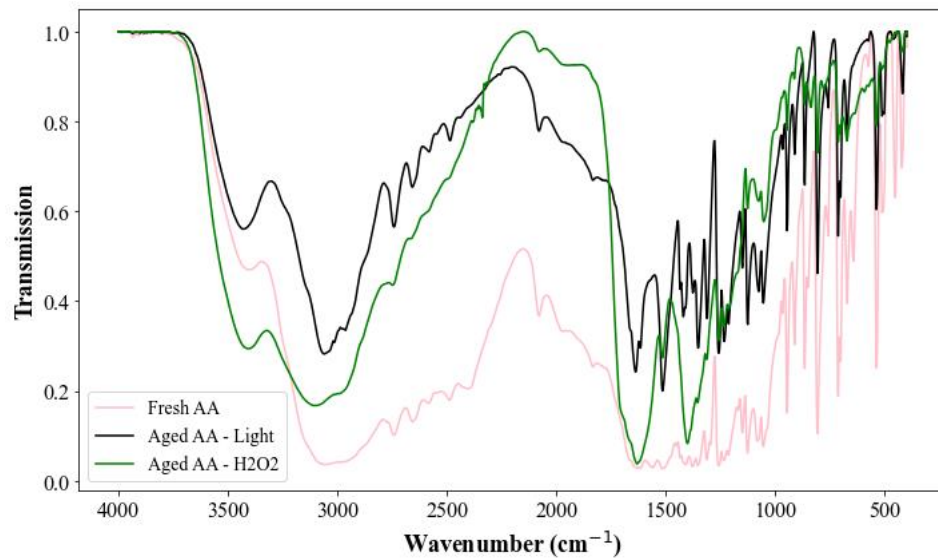


Figure A4.4. FTIR spectra of amino acids (glutamic acid and proline) fresh, aged with the Suntest solar simulator, and aged with OH radicals produced by photolysis.

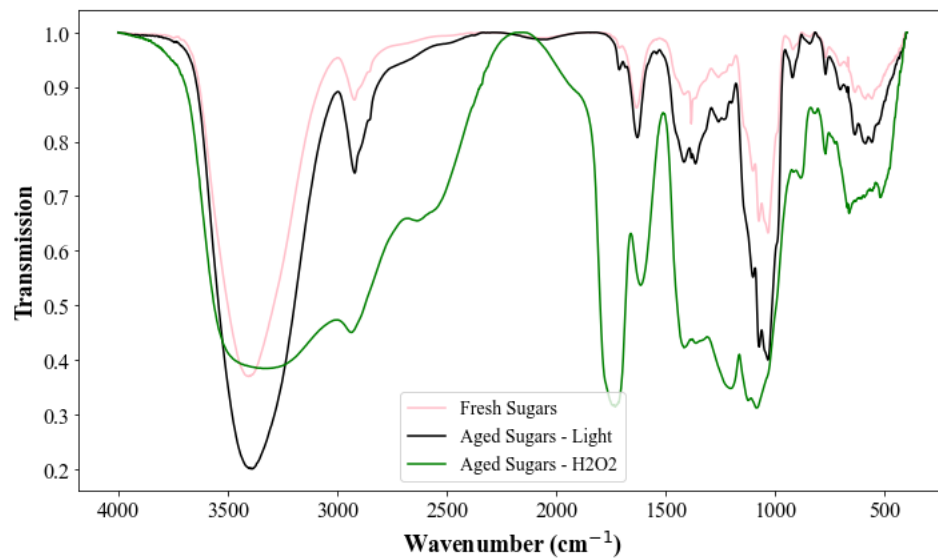


Figure A4.5. FTIR spectra of saccharides (glucose and sucrose) fresh, aged with the Suntest solar simulator, and aged with OH radicals produced by photolysis.

Table A4.1. Polar/non-polar functional group ratios of light-aged and OH-aged standards analyzed with FTIR. Calculations of ratios explained in Section 4.3.3.

	Light-aged		OH-aged	
$\frac{\text{Polar}}{\text{Non-polar}}$	Saccharide % change	Amino acid % change	Saccharide % change	Amino acid % change
$\frac{OH}{CH}$	-70.5	+30.7	-679.7	+3.0
$\frac{C=O}{CH}$	-39.8	+36.9	+12.5	+23.6
$\frac{C-O-C}{CH}$	-37.0	+24.9	-141.0	-41.0
$\frac{OH + C=O}{CH}$	-65.1	+34.2	-259.4	+15.2
$\frac{OH + C=O + C-O-C}{CH}$	-53.3	+31.3	-203.4	+1.8

Chapter 5

Summary, Conclusions, and Future Recommendations

The goal of this research was to characterize major organic species and functional groups in typical bioaerosols and determine effects of aging on their chemical composition. In the first chapter, we determined four research questions that were going to be answered in this dissertation:

1. What is the organic chemical composition of bioaerosols?
2. What are the major chemical functional groups of the most common bioaerosols (e.g., algae, pollen, fungi, bacteria)?
3. How do bioaerosols change chemically upon exposure to atmospheric oxidants and photolysis (i.e., exposure to OH radicals, ultra-violet radiation, and simulated solar radiation)?
4. How do the polarity and functional groups of bioaerosols change after aging, which can be important for ice nucleating (IN) activity and their role as cloud condensation nuclei (CCN)?

For this purpose, we used water-soluble extracts of lodgepole pine and rabbitbrush pollen, Western gall rust fungi, *Pedobacter* and hay *Bacillus* bacteria, and *Spirulina* alga bioaerosols. Chapter 2 was focused on determining starch content in the bioaerosols using UV-Vis-NIR spectrophotometry. This study optimized an existing spectrophotometry method to be used on low-concentration starch samples, such as bioaerosols. The optimized

experimental conditions were found to be bioaerosol extracts at pH 6, and the iodine reagent concentration at 0.2%. The starch content in bioaerosols ranged from 0.45 ± 0.05 (in bacteria) to 4.3 ± 0.06 g/mg (in fungi). Quantifying the starch content was necessary for quantitative analysis of organic compounds in bioaerosols and for differentiating between poly-saccharides (starch) and mono-saccharides (simple sugars) present in bioaerosols.

In Chapter 3, organic species (saccharides, amino acids, and fatty acids) using chromatography (GC-MS and UPLC-MS) and functional groups using $^1\text{H-NMR}$ were determined. This study provided valuable insight into the chemical composition of common bioaerosols and their contribution to atmospheric chemistry. The results revealed that the major contribution of protons came from aliphatic proton signals in all of the analyzed bioaerosols (rabbitbrush pollen, western gall rust fungi, hay *Bacillus* and *Pedobacter* bacteria, and *Spirulina* alga), except for lodgepole pine pollen, where the major contribution came from protons belonging to saccharides. The saccharide glucose was common among all analyzed bioaerosols, as well as a few amino acids (proline, leucine, isoleucine, alanine, and phenylalanine) and fatty acids (palmitic, oleic, linoleic, linolenic, and stearic acids). These results can be used as tracers for these bioaerosols in ambient filter samples.

In Chapter 4, we exposed water-soluble extracts of lodgepole pine pollen and *Spirulina* alga to simulated solar radiation and OH radicals (formed through photolysis by hydrogen peroxide and solar radiation) and analyzed the functional group changes using FTIR and $^1\text{H-NMR}$. The effects of aging on functional groups can be used to explain

polarity changes of bioaerosols and their organic compounds, which can affect IN activity. After simulated solar radiation, FTIR results showed an overall increase in polar functional groups compared to the non-polar functional groups, with an OH/CH ratio increase of 30.9% in lodgepole pine pollen and a 27.5% increase in *Spirulina* alga. While ¹H-NMR results did not show any significant changes after exposure to simulated solar radiation, we did see an increase in polar functional groups after OH aging. Specifically, the formation of -COOH and -CHO functional groups was observed in both bioaerosols.

Although this dissertation provided a thorough chemical characterization of a few common bioaerosols, there are additional studies and experiments that may be carried out in the future. For example, additional species and types of bioaerosols can be analyzed, especially with other solvents, for a more comprehensive chemical analysis. Chemical analysis of other organic compounds can be conducted, such as the contribution of lipids, phosphorous-containing compounds, and proteins, in bioaerosols. Based on the chemical profiles of the bioaerosols analyzed in this dissertation, ambient filter analysis can be conducted, and the chemical profiles can be used as tracers. Other kinds of aging, such as exposure to ozone, can be done and changes in functional groups and polarity can be explored. Aged bioaerosols should be quantitatively analyzed using GC-MS, UPLC-MS, or other chromatographic techniques, to determine the transformation, formation, or destruction of compounds in the bioaerosols. Additionally, it would be worthwhile to age the bioaerosols in a laboratory setting and analyze their IN activity alongside changes in functional groups/polarity so that IN activity can be correlated to specific chemical changes in bioaerosols. The aging methodology can be optimized to determine at which point in the

24-hour aging window the bioaerosols are fully oxidized and the lowest concentration of hydrogen peroxide that can be used to oxidize the bioaerosols.

In conclusion, all four research questions were addressed and the chemistry and atmospheric fate of bioaerosols was explored through laboratory aging. This research provides valuable data and insight into the chemical composition of bioaerosols, which helps close the knowledge gap in this field. The results of this work can be used for modeling of bioaerosol chemical behavior in the atmosphere. Future bioaerosol studies will benefit from our findings and the fundamental data is relevant for future studies involving climate change related increases in bioaerosol concentrations. Furthermore, we provided an important analysis of chemical transformation and polarity change after bioaerosol aging, which will be useful for future IN and CCN studies. Due to the interdisciplinary nature of bioaerosol research, our results can also be applied to studies in other fields, such as nutrition, biofuel, toxicology, agriculture, and medicine.

Products

Peer-reviewed Publications

- Bahdanovich, P.**, Axelrod, K., Khlystov, A. Y., Samburova, V. (2025). Effects of simulated atmospheric aging on bioaerosol chemistry, in progress.
- Axelrod, K., **Bahdanovich, P.**, Samburova, V., Khlystov, A. Y. (2025). Photooxidative aging of water-soluble pollen extracts and their primary constituents in an oxidation flow reactor. *Environmental Chemistry*, under review.
- Bahdanovich, P.**, Axelrod, K., Khlystov, A. Y., Samburova, V. (2024). Characterization of organic species and functional groups in pollen, fungi, algae, and bacteria bioaerosols. *Environmental Science: Atmospheres*, 4 (9), 1091-1104.
- Axelrod, K.; Bhattarai, C.; **Bahdanovich, P.**; Samburova, V.; Khlystov, A. (2023). The volatility of pollen extracts and their main constituents in aerosolized form via the integrated volume method (IVM) and the volatility basis set (VBS), *Aerosol Science and Technology*, 57 (12), 1236-1250.
- Samburova, V.; Schneider, E.; Rüger, C.P.; Inouye, S.; Sion, B.; Axelrod, K.; **Bahdanovich, P.**; Friederici, L.; Raeofy, Y.; Berli, M.; Lutz, A.; Zimmermann, R.; Moosmüller, H. (2023). Modification of Soil Hydroscopic and Chemical Properties Caused by Four Recent California, USA Megafires, *Fire*, 6 (5), 186.
- Bahdanovich, P.**, Axelrod, K., Khlystov, A. Y., Samburova, V. (2022). Optimized Spectrophotometry Method for Starch Quantification, *Analytica*, 3 (4), 394-405.

Proposals

- Graduate Dean Merit's Scholarship, 2024-2025 (funded)
- Nevada Doctoral Research in Innovation, Vision, and Excellence (DRIVE) 2-year Scholarship, 2023-2025 (funded)
- Desert Research Institute Graduate Student Fellowship, 2021 (funded)
- National Science Foundation Graduate Research Fellowship Program, 2021 (declined)

Presentations/Conference Proceedings

- Bahdanovich P.**, Axelrod K., Khlystov A.Y., Samburova V. (2024) Chemical Characterization of Atmospheric Bioaerosols, Dust Aerosols and Bioaerosols Session, European Geosciences Union 2024 General Assembly: Vienna, Austria, April 17, 2024
- Bahdanovich P.**, Axelrod K., Khlystov A.Y., Samburova V. (2023) Chemical Characterization of Atmospheric Bioaerosols, Graduate Poster Symposium, University of Nevada, Reno: Reno, Nevada, USA, November 1, 2023
- Bahdanovich P.**, Axelrod K., Khlystov A.Y., Samburova V. (2023) Chemical Characterization of Atmospheric Bioaerosols, Desert Research Institute Science Talk: Reno, Nevada, USA, October 24, 2023
- Bahdanovich P.**, Axelrod K., Khlystov A.Y., Samburova V. (2023) Characterization of Bioaerosol Components and Functional Groups, Bioaerosols Session, 13th International Conference on Carbonaceous Particles in the Atmosphere: Berkeley, CA, USA, July 11, 2023
- Axelrod K., **Bahdanovich P.**, Bhattarai, C., Samburova V., Khlystov A.Y. (2023) Quantitative Chemical Analysis and Volatility of Pollen, Bioaerosols Session, 13th International Conference on Carbonaceous Particles in the Atmosphere: Berkeley, CA, USA, July 11, 2023
- Bahdanovich P.**, Axelrod K., Khlystov A.Y., Samburova V. (2023) Qualitative Analysis of Bioaerosol Chemical Composition and Shift Using ¹H-NMR Spectroscopy, Desert Research Institute Graduate Student Poster Competition: Reno, NV, USA, April 7, 2023 (2nd place)
- Axelrod K., **Bahdanovich P.**, Samburova V., Khlystov A.Y. (2023) Quantitative Chemical Analysis and Volatility of Pollen, Desert Research Institute Graduate Student Poster Competition: Reno, NV, USA, April 7, 2023
- Bahdanovich P.**, Axelrod K., Khlystov A.Y., Samburova V. (2023) Qualitative Analysis of Bioaerosol Chemical Composition and Shift Using ¹H-NMR Spectroscopy, Atmospheric Chemistry, Aerosols, and Air Quality Session, 103rd American Meteorological Society Annual Meeting: Denver, CO, USA, January 8, 2023
- Samburova V., Sion B., **Bahdanovich P.**, Axelrod K., Raeofi Y., Berli M., Moosmüller H. (2022) Physical and Chemical Characterization of Post-Fire Soil Samples (2021-2022 mega-fires), Desert Research Institute Science Talk: Reno, Nevada, USA, December 9, 2022

- Samburova, V., Moosmüller, H., **Bahdanovich, P.**, Axelrod, K., Sion, B., Berli, M. (2022). Seeking answers from the wild-fire ashes, University of Rostock: Germany, October 17, 2022, Invited speaker
- Chang, C., Atkinson, C., Axelrod, K., **Bahdanovich, P.**, Ross, S., Xia, S., Hosseinpour, F. E. (2022) Aerosol-Cloud Interactions over the Tropical Atlantic Ocean, Atmospheric Chemistry, Aerosols, and Air Quality Session, 102nd American Meteorological Society Annual Meeting: Houston, TX, January 23, 2022
- Bahdanovich P.**, Axelrod K., Khlystov A.Y., Samburova. V. (2021) Analysis of Chemical Compounds Found in Common Bioaerosols Using ¹H-NMR Spectroscopy, Desert Research Institute Science Talk: Las Vegas, Nevada, USA, December 10, 2021
- Bahdanovich P.**, Axelrod K., Khlystov A.Y., Samburova. V. (2021) Analysis of Chemical Compounds Found in Common Bioaerosols Using ¹H-NMR Spectroscopy, Desert Research Institute Science Talk: Reno, Nevada, USA, November 30, 2021

References

- Abd El-Baky, H.H., El Baz, F.K., El-Baroty, G.S., 2007. Enhancement of Antioxidant Production in *Spirulina Plantensis* Under Oxidative Stress. *J. Sci. Res.* 2, 170–179.
- Alberts, B., Johnson, A., Lewis, J., 2002. *The Shape and Structure of Proteins*, in: *Molecular Biology of the Cell*. Garland Science, New York.
- Anderegg, W.R.L., Abatzoglou, J.T., Anderegg, L.D.L., Bielory, L., Kinney, P.L., Ziska, L., 2021. Anthropogenic climate change is worsening North American pollen seasons. *Proc. Natl. Acad. Sci.* 118. <https://doi.org/10.1073/pnas.2013284118>
- Andreeva, A., Budenkova, E., Babich, O., Sukhikh, S., Ulrikh, E., Ivanova, S., Prosekov, A., Dolganyuk, V., 2021. Production, purification, and study of the amino acid composition of microalgae proteins. *Molecules* 26, 2767. <https://doi.org/10.3390/molecules26092767>
- Ariano, R., Canonica, G.W., Passalacqua, G., 2010. Possible role of climate changes in variations in pollen seasons and allergic sensitizations during 27 years. *Ann. Allergy Asthma Immunol.* 104, 215–222. <https://doi.org/10.1016/j.anai.2009.12.005>
- Axelrod, K., Samburova, V., Khlystov, A.Y., 2021. Relative abundance of saccharides, free amino acids, and other compounds in specific pollen species for source profiling of atmospheric aerosol. *Sci. Total Environ.* 799. <https://doi.org/10.1016/j.scitotenv.2021.149254>
- Ayala, A., Muñoz, M.F., Argüelles, S., 2014. Lipid peroxidation: Production, metabolism, and signaling mechanisms of malondialdehyde and 4-hydroxy-2-nonenal. *Oxid. Med. Cell. Longev.* 2014. <https://doi.org/10.1155/2014/360438>
- Bahdanovich, P., Axelrod, K., Khlystov, A.Y., Samburova, V., 2024. Characterization of organic species and functional groups in pollen, fungi, algae, and bacteria bioaerosols. *Environ. Sci. Atmospheres.* <https://doi.org/10.1039/d4ea00083h>
- Bahdanovich, P., Axelrod, K., Khlystov, A.Y., Samburova, V., 2022. Optimized Spectrophotometry Method for Starch Quantification. *Analytica* 3, 394–405. <https://doi.org/10.3390/analytica3040027>
- Baldwin, R.R., Bear, R.S., Rundle, R.E., 1944. The Relation of Starch-Iodine Absorption Spectra to the Structure of Starch and Starch Components. *J. Am. Chem. Soc.* 66, 111–115. <https://doi.org/10.1021/ja01229a032>
- Bartošová, A., Blinová, L., Bartošová, I.A., Blinová, I.L., Gerulová, I.K., 2015. CHARACTERISATION OF POLYSACCHARIDES AND LIPIDS FROM SELECTED GREEN ALGAE SPECIES BY FTIR-ATR SPECTROSCOPY.

- Bashir, K., Aggarwal, M., 2019. Physicochemical, structural and functional properties of native and irradiated starch: a review. *J. Food Sci. Technol.* 56, 513–523. <https://doi.org/10.1007/s13197-018-3530-2>
- Bashir, S., Sharif, M.K., Butt, M.S., Shahid, M., 2016. Functional Properties and Amino acid Profile of *Spirulina platensis* Protein Isolates. *Pak. J. Sci. Ind. Res., Ser. B* 59, 12–19. <https://doi.org/10.52763/PJSIR.BIOL.SCI.59.1.2016.12.19>
- Bates, L.F., French, D., Rundle, R.E., 1943. Amylose and Amylopectin Content of Starches Determined by their Iodine Complex Formation. *J. Am. Chem. Soc.* 65, 142–148. <https://doi.org/10.1021/ja01242a003>
- Bauer, H., Giebl, H., Hitzenberger, R., Kasper-Giebl, A., Reischl, G., Zibuschka, F., Puxbaum, H., 2003. Airborne bacteria as cloud condensation nuclei. *J. Geophys. Res.: Atmos.* 108. <https://doi.org/10.1029/2003jd003545>
- Bauer, H., Kasper-Giebl, A., Löflund, M., Giebl, H., Hitzenberger, R., Zibuschka, F., Puxbaum, H., 2002. The contribution of bacteria and fungal spores to the organic carbon content of cloud water, precipitation and aerosols. *Atmos. Res.* 64, 109–119. [https://doi.org/10.1016/S0169-8095\(02\)00084-4](https://doi.org/10.1016/S0169-8095(02)00084-4)
- Beltrani, T., Chiavarini, S., Cicero, D.O., Grimaldi, M., Ruggeri, C., Tamburini, E., Cremisini, C., 2015. Chemical characterization and surface properties of a new bioemulsifier produced by *Pedobacter* sp. strain MCC-Z. *Int. J. Biol. Macromol.* 72, 1090–1096. <https://doi.org/10.1016/j.ijbiomac.2014.10.025>
- Bjerketorp, J., Levenfors, J.J., Nord, C., Guss, B., Öberg, B., Broberg, A., 2021. Selective Isolation of Multidrug-Resistant *Pedobacter* spp., Producers of Novel Antibacterial Peptides. *Front. Microbiol.* 12. <https://doi.org/10.3389/fmicb.2021.642829>
- Boonpo, S., Kungwankunakorn, S., 2017. Study on Amylose Iodine Complex from Cassava Starch by Colorimetric Method. *J. Adv. Agric. Technol.* 4, 345–349. <https://doi.org/10.18178/joaat.4.4.345-349>
- Boucher, O., Randall, D., Artaxo, P., Bretherton, C., Feingold, G., Forster, P., Kerminen, V.M., Kondo, Y., Liao, H., Lohmann, U., Rasch, P., Satheesh, S.K., Sherwood, S., Stevens, B., Zhang, X.Y., 2013. Clouds and Aerosols, in: Stocker, T.F., Qin, D., Plattner, G.K., Tignor, M., Allen, S.K., Boschung, J., Nauels, A., Xia, Y., Bex, V., Midgley, P.M. (Eds.), *Climate Change 2013: The Physical Science Basis. Contribution of Working Group I to the Fifth Assessment Report of the Intergovernmental Panel on Climate Change*. Cambridge University Press, Cambridge, United Kingdom and New York, NY, USA.
- Bowers, R.M., Sullivan, A.P., Costello, E.K., Collett, J.L., Knight, R., Fierer, N., 2011. Sources of Bacteria in Outdoor Air across Cities in the Midwestern United States. *Appl. Environ. Microbiol.* 77, 6350–6356. <https://doi.org/10.1128/AEM.05498-11>

- Brown, M.R., 1991. The amino-acid and sugar composition of 16 species of microalgae used in mariculture. *J. Exp. Mar. Biol. Ecol.* 145, 79–99. [https://doi.org/10.1016/0022-0981\(91\)90007-J](https://doi.org/10.1016/0022-0981(91)90007-J)
- Brust, H., Orzechowski, S., Fettke, J., 2020. Starch and Glycogen Analyses: Methods and Techniques. *Biomolecules* 10. <https://doi.org/10.3390/biom10071020>
- Buléon, A., Colonna, P., Planchot, V., Ball, S., 1998. Mini review Starch granules: structure and biosynthesis. *Int. J. Biol. Macromol.* 23, 85–112. [https://doi.org/10.1016/S0141-8130\(98\)00040-3](https://doi.org/10.1016/S0141-8130(98)00040-3)
- Burg, W.R., Shotwell, O.L., Saltzman, B.E., 1981. Measurements of airborne aflatoxins during the handling of contaminated corn. *Am. Ind. Hyg. Assoc. J.* 42, 1–11. <https://doi.org/10.1080/15298668191419271>
- Burja, A.M., Armenta, R.E., Radianingtyas, H., Barrow, C.J., 2007. Evaluation of fatty acid extraction methods for *Thraustochytrium* sp. ONC-T18. *J. Agric. Food Chem.* 55, 4795–4801. <https://doi.org/10.1021/jf070412s>
- Burkart, J., Gratzl, J., Seifried, T.M., Bieber, P., Grothe, H., 2021. Isolation of subpollen particles (SPPs) of birch: SPPs are potential carriers of ice nucleating macromolecules. *Biogeosciences* 18, 5751–5765. <https://doi.org/10.5194/bg-18-5751-2021>
- Cambridge Isotope Laboratories Inc., n.d. NMR Solvent Data Chart.
- Carmichael, W.W., Boyer, G.L., 2016. Health impacts from cyanobacteria harmful algae blooms: Implications for the North American Great Lakes. *Harmful Algae.* <https://doi.org/10.1016/j.hal.2016.02.002>
- Center for Health Statistics, N., 2018. Table A-2. Selected respiratory diseases among adults aged 18 and over, by selected characteristics: United States, 2018.
- Chaiklahan, R., Chirasuwan, N., Triratana, P., Loha, V., Tia, S., Bunnag, B., 2013. Polysaccharide extraction from *Spirulina* sp. and its antioxidant capacity. *Int. J. Biol. Macromol.* 58, 73–78. <https://doi.org/10.1016/j.ijbiomac.2013.03.046>
- Chalbot, Marie Cecile G., Gamboa da Costa, G., Kavouras, I.G., 2013. NMR Analysis of the Water-Soluble Fraction of Airborne Pollen Particles. *Appl. Magn. Reson.* 44, 1347–1358. <https://doi.org/10.1007/s00723-013-0492-4>
- Chalbot, M.C.G., Kavouras, I.G., 2019. Nuclear magnetic resonance characterization of water soluble organic carbon of atmospheric aerosol types. *Nat. Prod. Commun.* 14. <https://doi.org/10.1177/1934578X19849972>
- Chen, X., Sun-Waterhouse, D., Yao, W., Li, X., Zhao, M., You, L., 2021. Free radical-mediated degradation of polysaccharides: Mechanism of free radical formation and degradation, influence factors and product properties. *Food Chem.* <https://doi.org/10.1016/j.foodchem.2021.130524>

- Cheng, Y., Wang, Zhenyu, Quan, W., Xue, C., Qu, T., Wang, T., Chen, Q., Wang, Zhaojun, Zeng, M., Qin, F., Chen, J., He, Z., 2023. Pine pollen: A review of its chemical composition, health effects, processing, and food applications. *Trends Food Sci. Technol.* <https://doi.org/10.1016/j.tifs.2023.07.004>
- Chileen, B. V., McLauchlan, K.K., Higuera, P.E., Parish, M., Shuman, B.N., 2020. Vegetation response to wildfire and climate forcing in a Rocky Mountain lodgepole pine forest over the past 2500 years. *Holocene* 30, 1493–1503. <https://doi.org/10.1177/0959683620941068>
- Cornwell, G.C., McCluskey, C.S., J Hill, T.C., Levin, E.T., Rothfuss, N.E., Tai, S.-L., Petters, M.D., DeMott, P.J., Kreidenweis, S., Prather, K.A., Burrows, S.M., 2023. Bioaerosols are the dominant source of warm-temperature immersion-mode INPs and drive uncertainties in INP predictability. *Sci. Adv.* 9, eadg3715. <https://doi.org/10.1126/sciadv.adg3715>
- Coury, C., Dillner, A.M., 2009. ATR-FTIR characterization of organic functional groups and inorganic ions in ambient aerosols at a rural site. *Atmos. Environ.* 43, 940–948. <https://doi.org/10.1016/j.atmosenv.2008.10.056>
- D'Amato, G., Baena-Cagnani, C.E., Cecchi, L., Annesi-Maesano, I., Nunes, C., Ansotegui, I., D'Amato, M., Liccardi, G., Sofia, M., Canonica, W.G., 2013. Climate change, air pollution and extreme events leading to increasing prevalence of allergic respiratory diseases. *Multidiscip. Respir. Med.* 8. <https://doi.org/10.1186/2049-6958-8-12>
- D'Amato, G., Chong-Neto, H.J., Monge Ortega, O.P., Vitale, C., Ansotegui, I., Rosario, N., Haahtela, T., Cecchi, L., Bergmann, C., Ridolo, E., Ramon, G., Gonzalez Diaz, S., D'Amato, M., Annesi-Maesano, I., 2020. The effects of climate change on respiratory allergy and asthma induced by pollen and mold allergens. *Eur. J. Allergy Clin. Immunol.* 75, 2219–2228. <https://doi.org/10.1111/all.14476>
- DasSarma, P., DasSarma, S., 2018. Survival of microbes in Earth's stratosphere. *Curr. Opin. Microbiol.* 43, 24–30. <https://doi.org/10.1016/J.MIB.2017.11.002>
- Delort, A.M., Vařtilingom, M., Amato, P., Sancelme, M., Parazols, M., Mailhot, G., Laj, P., Deguillaume, L., 2010. A short overview of the microbial population in clouds: Potential roles in atmospheric chemistry and nucleation processes. *Atmos. Res.* 98, 249–260. <https://doi.org/10.1016/j.atmosres.2010.07.004>
- De-Melo, A.A.M., de Almeida-Muradian, L.B., 2017. Chemical composition of bee pollen, in: *Bee Products - Chemical and Biological Properties*. Springer International Publishing, pp. 221–259. https://doi.org/10.1007/978-3-319-59689-1_11
- Depciuch, J., Kasprzyk, I., Drzymała, E., Parlinska-Wojtan, M., 2018. Identification of birch pollen species using FTIR spectroscopy. *Aerobiologia (Bologna)* 34, 525–538. <https://doi.org/10.1007/s10453-018-9528-4>

- Depciuch, J., Kasprzyk, I., Sadik, O., Parlińska-Wojtan, M., 2017. FTIR analysis of molecular composition changes in hazel pollen from unpolluted and urbanized areas. *Aerobiologia (Bologna)* 33, 1–12. <https://doi.org/10.1007/s10453-016-9445-3>
- Desai, B.S., Modi, Z.S., Amit, K.J., Parmar, S.C., Shaikh, A.I., Aparnathi, K.D., 2018. Development of spectroscopic method for quantification of starch in milk. *Int. J. Chem. Stud.* 6, 53–57.
- Després, V.R., Huffman, J.A., Burrows, S.M., Hoose, C., Safatov, A.S., Buryak, G., Fröhlich-Nowoisky, J., Elbert, W., Andreae, M.O., Pöschl, U., Jaenicke, R., 2012. Primary biological aerosol particles in the atmosphere: a review. *Tellus B: Chem. Phys. Meteorol.* 64, 15598. <https://doi.org/10.3402/tellusb.v64i0.15598>
- Duarte, R.M.B.O., Duarte, A.C., 2015. Unraveling the structural features of organic aerosols by NMR spectroscopy: A review. *Magn. Reson. Chem.* 53, 658–666. <https://doi.org/10.1002/mrc.4227>
- Egharevba, H.O., 2019. Chemical Properties of Starch and Its Application in the Food Industry, IntechOpen. <https://doi.org/10.5772/intechopen.87777>
- Elbert, W., Taylor, P.E., Andreae, M.O., Pöschl, U., 2007. Contribution of fungi to primary biogenic aerosols in the atmosphere: wet and dry discharged spores, carbohydrates, and inorganic ions. *Atmos. Chem. Phys.* 7, 4569–4588. <https://doi.org/10.5194/acp-7-4569-2007>
- Erath, B.D., Ferro, A.R., 2022. Infectious disease transmission from bioaerosols. *J. Expo. Sci. Environ. Epidemiol.* <https://doi.org/10.1038/s41370-022-00476-z>
- Erdyneeva, S.A., Shiretorova, V.G., Tykheev, Z.A., Radnaeva, L.D., 2021. Fatty-Acid Composition of Pollen from *Pinus sylvestris*, *P. sibirica*, and *P. pumila*. *Chem. Nat. Compd.* 57, 741–742. <https://doi.org/10.1007/s10600-021-03462-3>
- Estillore, A.D., Trueblood, J. V, Grassian, V.H., 2016. Atmospheric chemistry of bioaerosols: Heterogeneous and multiphase reactions with atmospheric oxidants and other trace gases. *Chem. Sci.* 7, 6604–6616. <https://doi.org/https://doi.org/10.1039/C6SC02353C>
- Fall, P.L., 1992. Spatial patterns of atmospheric pollen dispersal in the Colorado Rocky Mountains, USA. *Review of Paleobotany and Palymology.* 74, 293-313.
- Faske, T.M., Agneray, A.C., Jahner, J.P., Sheta, L.M., Leger, E.A., Parchman, T.L., 2021. Genomic and common garden approaches yield complementary results for quantifying environmental drivers of local adaptation in rubber rabbitbrush, a foundational Great Basin shrub. *Evol. Appl.* 14, 2881–2900. <https://doi.org/10.1111/eva.13323>
- Fidai, Y.A., Dash, J., Tompkins, E.L., Tonon, T., 2020. A systematic review of floating and beach landing records of sargassum beyond the sargasso sea. *Environ. Res. Commun.* 2. <https://doi.org/10.1088/2515-7620/abd109>

- Fröhlich-Nowoisky, J., Kampf, C.J., Weber, B., Huffman, J.A., Pöhlker, C., Andreae, M.O., Lang-Yona, N., Burrows, S.M., Gunthe, S.S., Elbert, W., Su, H., Hoor, P., Thines, E., Hoffmann, T., Després, V.R., Pöschl, U., 2016. Bioaerosols in the Earth system: Climate, health, and ecosystem interactions. *Atmos. Res.* 182, 346–376. <https://doi.org/10.1016/j.atmosres.2016.07.018>
- Fu, P., Kawamura, K., Kobayashi, M., Simoneit, B.R.T., 2012. Seasonal variations of sugars in atmospheric particulate matter from Gosan, Jeju Island: Significant contributions of airborne pollen and Asian dust in spring. *Atmos. Environ.* 55, 234–239. <https://doi.org/10.1016/j.atmosenv.2012.02.061>
- Gou, M., Wu, H., Saleh, A.S.M., Jing, L., Liu, Y., Zhao, K., Su, C., Zhang, B., Jiang, H., Li, W., 2019. Effects of repeated and continuous dry heat treatments on properties of sweet potato starch. *Int. J. Biol. Macromol.* 129, 869–877. <https://doi.org/10.1016/j.ijbiomac.2019.01.225>
- Grosshagauer, S., Kraemer, K., Somoza, V., 2020. The True Value of Spirulina. *J Agric Food Chem.* <https://doi.org/10.1021/acs.jafc.9b08251>
- Gute, E., David, R.O., Kanji, Z.A., Abbatt, J.P.D., 2020. Ice Nucleation Ability of Tree Pollen Altered by Atmospheric Processing. *ACS Earth Space Chem.* 4, 2312–2319. <https://doi.org/10.1021/acsearthspacechem.0c00218>
- Gartner, G., Stoyneva-Gartner, M., Uzunov, B., 2021. Algal Toxic Compounds and Their Aeroterrestrial, Airborne and other Extremophilic Producers with Attention to Soil and Plant Contamination: A Review. *Toxins (Basel)* 13. <https://doi.org/10.3390/toxins13050322>
- Hadidi, M., Orellana-Palacios, J.C., Aghababaei, F., Gonzalez-Serrano, D.J., Moreno, A., Lorenzo, J.M., 2022. Plant by-product antioxidants: Control of protein-lipid oxidation in meat and meat products. *LWT* 169. <https://doi.org/10.1016/j.lwt.2022.114003>
- Haga, D.I., Burrows, S.M., Iannone, R., Wheeler, M.J., Mason, R.H., Chen, J., Polishchuk, E.A., Pöschl, U., Bertram, A.K., 2014. Ice nucleation by fungal spores from the classes agaricomycetes, ustilaginomycetes, and eurotiomycetes, and the effect on the atmospheric transport of these spores. *Atmos. Chem. Phys.* 14, 8611–8630. <https://doi.org/10.5194/acp-14-8611-2014>
- Han, J.A., BeMiller, J.N., 2007. Preparation and physical characteristics of slowly digesting modified food starches. *Carbohydr. Polym.* 67, 366–374. <https://doi.org/10.1016/j.carbpol.2006.06.011>
- Hannon, M., Gimpel, J., Tran, M., Rasala, B., Mayfield, S., 2010. Biofuels from algae: challenges and potential. *Biofuels* 1, 763–784. <https://doi.org/10.4155/bfs.10.44>
- Hashem, A., Tabassum, B., Abd-Allah, E.F., 2019. *Bacillus subtilis*: A plant-growth promoting rhizobacterium that also impacts biotic stress. *Saudi J. Biol. Sci.* 26, 1291–1297. <https://doi.org/10.1016/j.sjbs.2019.05.004>

- Heller, C., Ellerbrock, R.H., Roßkopf, N., Klungenfuß, C., Zeitz, J., 2015. Soil organic matter characterization of temperate peatland soil with FTIR-spectroscopy: Effects of mire type and drainage intensity. *Eur. J. Soil Sci.* 66, 847–858. <https://doi.org/10.1111/ejss.12279>
- Hermansson, A.-M., Svegmark, K., 1996. Developments in the understanding of starch functionality. *Trends Food Sci. Technol.* 7, 345–353. [https://doi.org/doi.org/10.1016/S0924-2244\(96\)10036-4](https://doi.org/doi.org/10.1016/S0924-2244(96)10036-4)
- Hlersa, F.A., Lam, J., Wiermanna, R., 1999. Structural Elements of Sporopollenin from the Pollen of *Torreya californica* Torr. (Gymnospermae): Using the 1H-NMR Technique, *Z. Naturforsch* 54c, 492-495.
- Hoffman, J., Hagle, S., 2011. Western Gall Rust Management.
- Horník, Š., Sýkora, J., Schwarz, J., Ždímal, V., 2020. Nuclear magnetic resonance aerosolomics: A tool for analysis of polar compounds in atmospheric aerosols. *ACS Omega* 5, 22750–22758. <https://doi.org/10.1021/acsomega.0c01634>
- Huffman, J.A., Prenni, A.J., Demott, P.J., Pöhlker, C., Mason, R.H., Robinson, N.H., Fröhlich-Nowoisky, J., Tobo, Y., Després, V.R., Garcia, E., Gochis, D.J., Harris, E., Müller-Germann, I., Ruzene, C., Schmer, B., Sinha, B., Day, D.A., Andreae, M.O., Jimenez, J.L., Gallagher, M., Kreidenweis, S.M., Bertram, A.K., Pöschl, U., 2013. High concentrations of biological aerosol particles and ice nuclei during and after rain. *Atmos. Chem. Phys.* 13, 6151–6164. <https://doi.org/10.5194/acp-13-6151-2013>
- Hughes, D.D., Mampage, C.B.A., Jones, L.M., Liu, Z., Stone, E.A., 2020. Characterization of Atmospheric Pollen Fragments during Springtime Thunderstorms. *Environ. Sci. Technol. Lett.* 7, 409–414. <https://doi.org/10.1021/acs.estlett.0c00213>
- Hughes, K.M., Price, D., Torriero, A.A.J., Symonds, M.R.E., Suphioglu, C., 2022. Impact of Fungal Spores on Asthma Prevalence and Hospitalization. *Int. J. Mol. Sci.* 23. <https://doi.org/10.3390/ijms23084313>
- Hyde, P., Mahalov, A., 2020. Contribution of bioaerosols to airborne particulate matter. *J. Air Waste Manage. Assoc.* 70, 71–77. <https://doi.org/10.1080/10962247.2019.1629360>
- IPCC Sixth Assessment Report, 2023. URL <https://www.ipcc.ch/assessment-report/ar6/> (accessed 4.4.23).
- Jaenicke, R., 2005. Abundance of cellular material and proteins in the atmosphere. *Science* 308, 73. <https://doi.org/10.1126/science.1106335>
- Jędrzycka, M., Żuraw, B., Zagórski, P., Rodzik, J., Mędrek, K., Pidek, I.A., Haratym, W., Kaczmarek, J., Sadyś, M., 2023. The origin of pine pollen grains captured from air at Calypsobyen, Svalbard. *Pol. Polar Res.* 44, 313–338. <https://doi.org/10.24425/ppr.2022.143312>

- Jia, G., Shevliakova, E., Artaxo, P., De Noblet-Ducoudré, N., Houghton, R., House, J., Kitajima, K., Lennard, C., Popp, A., Sirin, A., Sukumar, R., Verchot, L., 2019. Land–climate interactions, in: Shukla, P.R., Skea, J., Calvo Buendia, E., Masson-Delmotte, V., Portner, H.O., Roberts, D.C., Zhai, P., Slade, R., Connors, S., Van Diemen, R., Ferrat, M., Haughey, E., Luz, S., Neogi, S., Pathak, M., Petzold, J., Portugal Pereira, J., Vyas, P., Huntley, E., Kissick, K., Belkacemi, M., Malley, J. (Eds.), *Climate Change and Land: An IPCC Special Report on Climate Change, Desertification, Land Degradation, Sustainable Land Management, Food Security, and Greenhouse Gas Fluxes in Terrestrial Ecosystems*. In Press, pp. 131–247.
- Jones, M.Jr., Fleming, S.A., 2014. *Organic Chemistry (Fifth Edition)*, in: Fahlgren, E., Talmadge, C.L., Cotton, R. (Eds.), *Organic Chemistry*. W.W. Norton & Company, Inc., New York, NY 10110.
- Kampa, M., Castanas, E., 2008. Human health effects of air pollution. *Environ. Pollut.* 151, 362–367. <https://doi.org/10.1016/j.envpol.2007.06.012>
- Kaneda, T., 1977. Fatty Acids of the Genus *Bacillus*: an Example of Branched-Chain Preference. *Bacteriol. Rev.* 41, 391–418. <https://doi.org/10.1128/br.41.2.391-418.1977>
- Kavisri, M., Marykutty Abraham, Gopal Prabakaran, Manickam Elangovan, Meivelu Moovendhan, 2021. Phytochemistry, bioactive potential and chemical characterization of metabolites from marine microalgae (*Spirulina platensis*) biomass. *Biomass Convers. Biorefin.* 13, 10147–10154. <https://doi.org/10.1007/s13399-021-01689-2>
- Kim, K.H., Kabir, E., Jahan, S.A., 2018. Airborne bioaerosols and their impact on human health. *J. Environ. Sci.* 67, 23–35. <https://doi.org/10.1016/j.jes.2017.08.027>
- Kinahan, S.M., Tezak, M.S., Siegrist, C.M., Lucero, G., Servantes, B.L., Santarpia, J.L., Kalume, A., Zhang, J., Felton, M., Williamson, C.C., Pan, Y. Le, 2019. Changes of fluorescence spectra and viability from aging aerosolized *E. coli* cells under various laboratory-controlled conditions in an advanced rotating drum. *Aerosol Sci. Tech.* 53, 1261–1276. <https://doi.org/10.1080/02786826.2019.1653446>
- Komosinska-Vassev, K., Olczyk, P., Kaźmierczak, J., Mencner, L., Olczyk, K., 2015. Bee pollen: Chemical composition and therapeutic application. *Evid. Based Complement. Alternat. Med.* 2015. <https://doi.org/10.1155/2015/297425>
- Krajang, M., Malairuang, K., Sukna, J., Rattanapradit, K., Chamsart, S., 2021. Single-step ethanol production from raw cassava starch using a combination of raw starch hydrolysis and fermentation, scale-up from 5-L laboratory and 200-L pilot plant to 3000-L industrial fermenters. *Biotechnol. Biofuels* 14, 1–15. <https://doi.org/10.1186/s13068-021-01903-3>
- Kumar, R., Bansal, V., Patel, M.B., Sarpal, A.S., 2014. Compositional Analysis of Algal Biomass in a Nuclear Magnetic Resonance (NMR) Tube. *J. Algal Biomass Util.* 5, 36–45.

- Kumari, K., Yadav, S., 2024. Unveiling the Role of Bioaerosols in Climate Processes: A Mini Review. *Int. J. Environ. Res.* 18. <https://doi.org/10.1007/s41742-024-00633-2>
- Kunert, A.T., Pöhlker, M.L., Tang, K., Krevert, C.S., Wieder, C., Speth, K.R., Hanson, L.E., Morris, C.E., Schmale, D.G., Pöschl, U., Fröhlich-Nowoisky, J., 2019. Macromolecular fungal ice nuclei in *Fusarium*: Effects of physical and chemical processing. *Biogeosciences* 16, 4647–4659. <https://doi.org/10.5194/bg-16-4647-2019>
- Kuznetsova, M., Lee, C., Aller, J., 2005. Characterization of the proteinaceous matter in marine aerosols. *Mar. Chem.* 96, 359–377. <https://doi.org/10.1016/j.marchem.2005.03.007>
- Lafont-Mendoza, J.J., Severiche-Sierra, C.A., Jaimes-Morales, J., 2018. Evaluation of the Starch Quantification Methods of *Musa paradisiaca*, *Manihot esculenta*, and *Dioscorea trifida* Using Factorial Experiments. *Int. J. Food Sci.* 2018, 1–7. <https://doi.org/10.1155/2018/5901930>
- Lazaridis, M., 2019. Bacteria as cloud condensation nuclei (CCN) in the atmosphere. *Atmosphere (Basel)* 10. <https://doi.org/10.3390/atmos10120786>
- Legrini, O., Oliveros, E., Braun, A.M., 1993. Photochemical Processes for Water Treatment. *Chem. Rev* 93, 671–698.
- Li, J., Zhang, Q., Chen, B., Wang, L., Zhu, R., Yang, J., 2021. Hydrogen peroxide formation in water during the VUV/UV irradiation process: Impacts and mechanisms of selected anions. *Environ. Res.* 195. <https://doi.org/10.1016/j.envres.2021.110751>
- Lindsley, W.G., Green, B.J., Blachere, F.M., Martin, S.B., Law, B.F., Jensen, P.A., Schafer, M.P., 2017. NIOSH Manual of Analytical Methods (NMAM), 5th Edition Sampling and characterization of bioaerosols.
- Liu, F., Lai, S., Tong, H., Lakey, P.S.J., Shiraiwa, M., Weller, M.G., Pöschl, U., Kampf, C.J., 2017. Release of free amino acids upon oxidation of peptides and proteins by hydroxyl radicals. *Anal. Bioanal. Chem.* 409, 2411–2420. <https://doi.org/10.1007/s00216-017-0188-y>
- Liu, K.-S., 1994. Preparation of Fatty Acid Methyl Esters for Gas-Chromatographic Analysis of Lipids in Biological Materials. *J. Am. Oil Chem. Soc.* 71, 1179–1187. <https://doi.org/10.1007/BF02540534>
- Liu, Y., Lee, P.K.H., Nah, T., 2023. Emerging investigator series: aqueous photooxidation of live bacteria with hydroxyl radicals under cloud-like conditions: insights into the production and transformation of biological and organic matter originating from bioaerosols. *Environ. Sci. Process Impacts* 25, 1150–1168. <https://doi.org/10.1039/d3em00090g>
- Madhavi, K., Venkataraman, S.L. V, Salimath, P. V, 1987. CARBOHYDRATE COMPOSITION AND CHARACTERIZATION OF TWO UNUSUAL SUGARS FROM THE BLUE GREEN ALGA, *SPZRUlina PLATENSIS*. *Phytochem.* 26, 2267–2269.

- Magnussen, A., Parsi, M.A., 2013. Aflatoxins, hepatocellular carcinoma and public health. *World J Gastroenterol* 19, 1508–1512. <https://doi.org/10.3748/wjg.v19.i10.1508>
- Mainelis, G., 2020. Bioaerosol sampling: Classical approaches, advances, and perspectives. *Aerosol Sci. Technol.* 54, 496–519. <https://doi.org/10.1080/02786826.2019.1671950>
- Maltsev, Y., Maltseva, K., 2021. Fatty acids of microalgae: diversity and applications. *Rev. Environ. Sci. Biotechnol.* 20, 515–547. <https://doi.org/10.1007/s11157-021-09571-3>
- Mampage, C.B.A., Hughes, D.D., Jones, L.M., Metwali, N., Thorne, P.S., Stone, E.A., 2022. Characterization of sub-pollen particles in size-resolved atmospheric aerosol using chemical tracers. *Atmos. Environ.* X 15. <https://doi.org/10.1016/j.aeoa.2022.100177>
- Manning, R., 2001. Fatty acids in pollen: a review of their importance for honey bees. *Bee World* 82, 60–75. <https://doi.org/10.1080/0005772X.2001.11099504>
- Margaoan, R., Marghitas, L., Dezmirean, D., Mihai, X., Bobis, O., 2010. Bee Collected Pollen - General Aspects and Chemical Composition. *Anim. Sci. Biotechnol.* 67.
- Maria, S.F., Russell, L.M., Turpin, B.J., Porcja, R.J., 2002. FTIR measurements of functional groups and organic mass in aerosol samples over the Caribbean. *Atmos. Environ.* 36, 5185–5196. [https://doi.org/10.1016/S1352-2310\(02\)00654-4](https://doi.org/10.1016/S1352-2310(02)00654-4)
- May, N.W., Olson, N.E., Panas, M., Axson, J.L., Tirella, P.S., Kirpes, R.M., Craig, R.L., Gunsch, M.J., China, S., Laskin, A., Ault, A.P., Pratt, K.A., 2018a. Aerosol Emissions from Great Lakes Harmful Algal Blooms. *Environ. Sci. Technol.* 52, 397–405. <https://doi.org/10.1021/acs.est.7b03609>
- Mayer, S., Curtui, V., Usleber, E., Gareis, M., 2007. Airborne mycotoxins in dust from grain elevators. *Mycotoxin Res.* 23, 94–100. <https://doi.org/10.1007/BF02946033>
- McCready, R.M., Hassid, W.Z., 1943. The Separation and Quantitative Estimation of Amylose and Amylopectin in Potato Starch. *J. Am. Chem. Soc.* 65, 1154–1157. <https://doi.org/10.1021/ja01246a038>
- McGrance, S.J., Cornell, H.J., Rix, C.J., 1998. A Simple and Rapid Colorimetric Method for the Determination of Amylose in Starch Products. *Starch/Staerke* 50, 158–163. [https://doi.org/10.1002/\(SICI\)1521-379X\(199804\)50:4<158::AID-STAR158>3.0.CO;2-7](https://doi.org/10.1002/(SICI)1521-379X(199804)50:4<158::AID-STAR158>3.0.CO;2-7)
- Merrill, L., Dunbar, J., Richardson, J., Kuske, C.R., 2006. Composition of Bacillus Species in Aerosols from 11 U.S. Cities. *J. Forensic Sci.* 51, 559–565. <https://doi.org/10.1111/j.1556-4029.2006.00132.x>
- Mesleh, M.F., Shirley, W.A., Heise, C.E., Ling, N., Maki, R.A., Laura, R.P., 2007. NMR structural characterization of a minimal peptide antagonist bound to the extracellular domain of the corticotropin-releasing factor receptor. *J. Biol. Chem.* 282, 6338–6346. <https://doi.org/10.1074/jbc.M609816200>

MestReNova 14.2, 2020.

- Mohapatra, S., Sarkar, B., Samantaray, D.P., Daware, A., Maity, S., Pattnaik, S., Bhattacharjee, S., 2017. Bioconversion of fish solid waste into PHB using *Bacillus subtilis* based submerged fermentation process. *Environ. Tech.* 38, 3201–3208. <https://doi.org/10.1080/09593330.2017.1291759>
- Möhler, O., Demott, P.J., Vali, G., Levin, Z., 2007. Microbiology and atmospheric processes: the role of biological particles in cloud physics. *Biogeosciences* 4, 1059–1071.
- Mujika, J.I., Uranga, J., Matxain, J.M., 2013. Computational study on the attack of ·OH radicals on aromatic amino acids. *Chemistry - A European Journal* 19, 6862–6873. <https://doi.org/10.1002/chem.201203862>
- Muth, F., Breslow, P.R., Masek, P., Leonard, A.S., 2018. A pollen fatty acid enhances learning and survival in bumblebees. *Behav. Ecol.* 29, 1371–1379. <https://doi.org/10.1093/beheco/ary111>
- Nakayoshi, Y., Nakamura, S., Kameo, Y., Shiiba, D., Katsuragi, Y., Ohtsubo, K., 2015. Measurement of resistant starch content in cooked rice and analysis of gelatinization and retrogradation characteristics. *Biosci., Biotechnol., Biochem.* 79, 1860–1866. <https://doi.org/10.1080/09168451.2015.1044934>
- Noranizan, M.A., Dzulkifly, M.H., Russly, A.R., 2010. Effect of heat treatment on the physico-chemical properties of starch from different botanical sources. *Int. Food Res. J.* 17, 127–135.
- Nowak, E., Wisła-Świder, A., Leszczyńska, T., Koronowicz, A., 2023. Physicochemical and Molecular Properties of Spelt and Wheat Starches Illuminated with UV Light. *Appl. Sci.* 13. <https://doi.org/10.3390/app13042360>
- Old, K.M., 1981. Western gall rust, a serious disease of *Pinus radiata* in California. *Aust. For.* 44, 178–184. <https://doi.org/10.1080/00049158.1981.10674311>
- Old, K.M., Libby, W.J., Russell, J.H., 1986. Genetic Variability in susceptibility of *Pinus radiata* to Western Gall Rust. *Silvae Genet.* 35, 145–149.
- Otify, A.M., El-Sayed, A.M., Michel, C.G., Farag, M.A., 2019. Metabolites profiling of date palm (*Phoenix dactylifera* L.) commercial by-products (pits and pollen) in relation to its antioxidant effect: a multiplex approach of MS and NMR metabolomics. *Metabolomics* 15. <https://doi.org/10.1007/s11306-019-1581-7>
- Ozler, H., Pehlivan, S., Bayrak, F., 2009. Analysis of Free Amino Acid and Total Protein Content in Pollen of Some Allergenic Taxa. *Asian J. Plant Sci.* 8. <https://doi.org/10.3923/ajps.2009.308.312>
- Pacini, E., Guarnieri, M., Nepi, M., 2006. Pollen carbohydrates and water content during development, presentation, and dispersal: A short review. *Protoplasma* 228, 73–77. <https://doi.org/10.1007/s00709-006-0169-z>

- Pan, Y. Le, Kalume, A., Wang, C., Santarpia, J., 2021b. Atmospheric aging processes of bioaerosols under laboratory-controlled conditions: A review. *J. Aerosol Sci.* <https://doi.org/10.1016/j.jaerosci.2021.105767>
- Pan, Y. Le, Santarpia, J.L., Ratnesar-Shumate, S., Corson, E., Eshbaugh, J., Hill, S.C., Williamson, C.C., Coleman, M., Bare, C., Kinahan, S., 2014. Effects of ozone and relative humidity on fluorescence spectra of octapeptide bioaerosol particles. *J Quant Spectrosc. Radiat. Transf.* 133, 538–550. <https://doi.org/10.1016/j.jqsrt.2013.09.017>
- Pemmaraju, S.C., Sharma, D., Singh, N., Panwar, R., Cameotra, S.S., Pruthi, V., 2012. Production of microbial surfactants from oily sludge-contaminated soil by bacillus subtilis DSVP23. *Appl. Biochem. Biotechnol.* 167, 1119–1131. <https://doi.org/10.1007/s12010-012-9613-z>
- Peshev, D., Vergauwen, R., Moglia, A., Hideg, É., Van Den Ende, W., 2013. Towards understanding vacuolar antioxidant mechanisms: A role for fructans? *J. Exp. Bot.* 64, 1025–1038. <https://doi.org/10.1093/jxb/ers377>
- Pokhrel, S., 2015. A review on introduction and applications of starch and its biodegradable polymers. *Int. J. Environ.* 4, 114–125. <https://doi.org/10.3126/ije.v4i4.14108>
- Pope, F.D., 2010. Pollen grains are efficient cloud condensation nuclei. *Environ. Res. Lett.* 5, 044015. <https://doi.org/10.1088/1748-9326/5/4/044015>
- Powell, J.M., Hiratsuka, Y., 1973. Serious Damage Caused by Stalactiform Blister Rust and Western Gall Rust to a Lodgepole Pine Plantation in Central Alberta. *Can. Plant Dis. Surv.* 53, 67–71.
- Pretsch, E., Bühlmann, P., Badertscher, M., 2009. Structure determination of organic compounds: Tables of spectral data, 4th ed, Structure Determination of Organic Compounds: Tables of Spectral Data. Springer, Berlin, Germany. <https://doi.org/10.1007/978-3-540-93810-1>
- Qin, Y., Zhang, H., Dai, Y., Hou, H., Dong, H., 2019. Effect of Alkali Treatment on Structure and Properties of High Amylose Corn Starch Film. *Materials* 12. <https://doi.org/10.3390/ma12101705>
- R. Ellson, R. Stearns, M. Mutz, C. Brown, B. Browning, D. Harris, S. Qureshi, J. Shieh, D. Wold, 2005. In situ DMSO Hydration Measurements of HTS Compound Libraries. *Comb. Chem. High Throughput Screening* 8, 489–498. <https://doi.org/10.2174/1386207054867382>
- Rajasekar, P., Palanisamy, S., Anjali, R., Vinosha, M., Elakkiya, M., Marudhupandi, T., Tabarsa, M., You, S.G., Prabhu, N.M., 2019. Isolation and structural characterization of sulfated polysaccharide from *Spirulina platensis* and its bioactive potential: In vitro antioxidant, antibacterial activity and Zebrafish growth and reproductive performance. *Int. J. Biol. Macromol.* 141, 809–821. <https://doi.org/10.1016/J.IJBIOMAC.2019.09.024>

- Ramsfield, T.D., Kriticos, D.J., Vogler, D.R., Geils, B.W., 2007. Western gall rust - A threat to *Pinus radiata* in New Zealand. *N. Z. J. For. Sci.* 37, 143–152.
- Reggente, M., Dillner, A.M., Takahama, S., 2019. Analysis of functional groups in atmospheric aerosols by infrared spectroscopy: systematic intercomparison of calibration methods for US measurement network samples. *Atmos. Meas. Tech.* 12, 2287–2312. <https://doi.org/10.5194/amt-12-2287-2019>
- Reichhardt, C., Cegelski, L., 2014. Solid-state NMR for bacterial biofilms. *Mol. Phys.* 112, 887–894. <https://doi.org/10.1080/00268976.2013.837983>
- Ripp, J., 1996. Analytical Detection Limit Guidance & Laboratory Guide for Determining Method Detection Limits. Madison, WI, USA.
- Roberts, S.A., Cameron, R.E., 2022. The effects of concentration and sodium hydroxide on the rheological properties of potato starch gelatinisation. *Carbohydr. Polym.* 50, 133–143. [https://doi.org/10.1016/S0144-8617\(02\)00007-3](https://doi.org/10.1016/S0144-8617(02)00007-3)
- Romaniuk, J.A.H., Cegelski, L., 2015. Bacterial cell wall composition and the influence of antibiotics by cell-wall and whole-cell NMR. *Philos. Trans. R. Soc., B* 370. <https://doi.org/10.1098/rstb.2015.0024>
- Romano, S., 2023. Bioaerosols: Composition, Meteorological Impact, and Transport. *Atmosphere (Basel)* 14, 590. <https://doi.org/10.3390/atmos14030590>
- Ross, A., Willson, V.L., 2017. Independent Samples T-Test, in: *Basic and Advanced Statistical Tests*. Sense Publishers, Rotterdam, Zuid-Holland, The Netherlands, pp. 13–16. https://doi.org/doi.org/10.1007/978-94-6351-086-8_3
- Sahu, N., Tangutur, A.D., 2015. Airborne algae: overview of the current status and its implications on the environment. *Aerobiologia (Bologna)* 31, 89–97. <https://doi.org/10.1007/s10453-014-9349-z>
- Saleh Al-Rubaye, T., Hashim Risan, M., Al-Rubaye, D., Radi, R.O., Talib Saleh Al-Rubaye, C., 2018. Characterization of marine *Streptomyces* spp. bacterial isolates from Tigris river sediments in Baghdad city with Lc-ms and 1 HNMNR. *J. Pharmacogn. Phytochem.* 7, 2053–2060.
- Salimon, J., Abdullah, B.M., Salih, N., 2011. Hydrolysis optimization and characterization study of preparing fatty acids from *Jatropha curcas* seed oil. *Chem. Cent. J.* 5. <https://doi.org/10.1186/1752-153X-5-67>
- Samburova, V., Gannet Hallar, A., Mazzoleni, L.R., Saranjampour, P., Lowenthal, D., Kohl, S.D., Zielinska, B., 2013a. Composition of water-soluble organic carbon in non-urban atmospheric aerosol collected at the Storm Peak Laboratory. *Environ. Chem.* 10, 370–380. <https://doi.org/10.1071/EN13079>
- Samburova, V., Lemos, M.S., Hiibel, S., Kent Hoekman, S., Cushman, J.C., Zielinska, B., 2013b. Analysis of triacylglycerols and free fatty acids in algae using ultra-

- performance liquid chromatography mass spectrometry. *J. Am. Oil Chem. Soc.* 90, 53–64. <https://doi.org/10.1007/s11746-012-2138-3>
- Sarpal, A.S., K. Sharma, B., Scott, J., kumar, R., Sugmaran, V., Chopra, A., Bansal, V., Rajagopalan, N.K., 2016. Comparison of oil extraction methods for algae by NMR and Chromatographic techniques. *J. Anal. Bioanal. Tech.* 1, 17–41. <https://doi.org/10.15436/2476-1869.16.1166>
- Schiffer, J.M., Mael, L.E., Prather, K.A., Amaro, R.E., Grassian, V.H., 2018. Sea Spray Aerosol: Where Marine Biology Meets Atmospheric Chemistry. *ACS Cent. Sci.* 4, 1617–1623. <https://doi.org/10.1021/acscentsci.8b00674>
- Schumacher, C.J., Pöhlker, C., Aalto, P., Hiltunen, V., Petäjä, T., Kulmala, M., Pöschl, U., Huffman, J.A., 2013. Seasonal cycles of fluorescent biological aerosol particles in boreal and semi-arid forests of Finland and Colorado. *Atmos. Chem. Phys.* 13, 11987–12001. <https://doi.org/10.5194/acp-13-11987-2013>
- Schummer, C., Delhomme, O., Appenzeller, B.M.R., Wennig, R., Millet, M., 2009. Comparison of MTBSTFA and BSTFA in derivatization reactions of polar compounds prior to GC/MS analysis. *Talanta* 77, 1473–1482. <https://doi.org/10.1016/j.talanta.2008.09.043>
- Semitsoglou-Tsiapou, S., Meador, T.B., Peng, B., Aluwihare, L., 2022. Photochemical (UV–vis/H₂O₂) degradation of carotenoids: Kinetics and molecular end products. *Chemosphere* 286, 131697. <https://doi.org/10.1016/j.chemosphere.2021.131697>
- Sénéchal, H., Visez, N., Charpin, D., Shahali, Y., Peltre, G., Biolley, J.P., Lhuissier, F., Couderc, R., Yamada, O., Malrat-Domenge, A., Pham-Thi, N., Poncet, P., Sutra, J.P., 2015. A review of the effects of major atmospheric pollutants on pollen grains, pollen content, and allergenicity. *Sci. World J.* 2015. <https://doi.org/10.1155/2015/940243>
- Siahbalaie, R., Kavooosi, G., Noroozi, M., 2021. Protein nutritional quality, amino acid profile, anti-amylase and anti-glucosidase properties of microalgae: Inhibition and mechanisms of action through in vitro and in silico studies. *LWT* 150. <https://doi.org/10.1016/j.lwt.2021.112023>
- Signorelli, S., Coitiño, E.L., Borsani, O., Monza, J., 2014. Molecular mechanisms for the reaction between •OH radicals and proline: Insights on the role as reactive oxygen species scavenger in plant stress. *J. Phys. Chem. B* 118, 37–47. <https://doi.org/10.1021/jp407773u>
- Sinha, R.P., Kumar, H.D., Kumar, A., Hader, D.-P., 1995. Effects of UV-B Irradiation on Growth, Survival, Pigmentation and Nitrogen Metabolism Enzymes in Cyanobacteria, *Acta Protozoologica* 34, 187-192.
- Smith, D.J., Griffin, D.W., McPeters, R.D., Ward, P.D., Schuerger, A.C., 2011. Microbial survival in the stratosphere and implications for global dispersal. *Aerobiologia (Bologna)* 27, 319–332. <https://doi.org/10.1007/s10453-011-9203-5>

- Starkey, L.S., n.d. 1H NMR Chemical Shifts. California State Polytechnic University, Pomona.
- Stehfest, K., Toepel, J., Wilhelm, C., 2005. The application of micro-FTIR spectroscopy to analyze nutrient stress-related changes in biomass composition of phytoplankton algae. *Plant Physiol. Biochem.* 43, 717–726. <https://doi.org/10.1016/j.plaphy.2005.07.001>
- Subroto, E., Jeanette, G., Meiyanasari, Y., Luwinsky, I., Baraddiaz, S., 2020. Review on the Analysis Methods of Starch, Amylose, Amylopectinin Food and Agricultural Products. *Int. J. Emerg. Trends Eng. Res.* 8, 3519–3524. <https://doi.org/10.30534/ijeter/2020/103872020>
- Sulistiyarti, H., Atikah, A., Fardiyah, Q., Febriyanti, S., Asdauna, A., 2015. A Simple and Safe Spectrophotometric Method for Iodide Determination. *Makara J. Sci.* 19, 43–48. <https://doi.org/10.7454/mss.v19i2.4736>
- Sun, J., Ariya, P.A., 2006. Atmospheric organic and bio-aerosols as cloud condensation nuclei (CCN): A review. *Atmos. Environ.* 40, 795–820. <https://doi.org/10.1016/j.atmosenv.2005.05.052>
- Sun, Q., Gong, M., Li, Y., Xiong, L., 2014. Effect of dry heat treatment on the physicochemical properties and structure of proso millet flour and starch. *Carbohydr. Polym.* 110, 128–134. <https://doi.org/10.1016/j.carbpol.2014.03.090>
- SUNTEST CPS / CPS+ Operating Manual, 1999.
- Suzuki, Y., Kawakami, M., Akasaka, K., 2001. 1H NMR application for characterizing water-soluble organic compounds in urban atmospheric particles. *Environ. Sci. Technol.* 35, 2656–2664. <https://doi.org/10.1021/es001861a>
- Takeda, C., Takeda, Y., Hizukuri, S., 1989. Structure of Amylomaize Amylose. *Cereal Chem.* 66, 22–25.
- Tan, W., Wang, J., Bai, W., Qi, J., Chen, W., 2020. Soil bacterial diversity correlates with precipitation and soil pH in long-term maize cropping systems. *Sci. Rep.* 10, 6012. <https://doi.org/10.1038/s41598-020-62919-7>
- Taylor, P.E., Jacobson, K.W., House, J.M., Glovsky, M.M., 2007. Links between pollen, atopy and the asthma epidemic. *Int. Arch. Allergy Immunol.* 144, 162–170. <https://doi.org/10.1159/000103230>
- Tesson, S.V.M., Skjøth, C.A., Šantl-Temkiv, T., Löndahl, J., 2016. Airborne microalgae: Insights, opportunities, and challenges. *Appl. Environ. Microbiol.* 82, 1978–1991. <https://doi.org/10.1128/AEM.03333-15>
- Tiers, G.V.D., 1958. Reliable proton nuclear resonance shielding values by “internal referencing” with tetramethylsilane. *J. Phys. Chem.* 62, 1151–1152. <https://doi.org/10.1021/j150567a041>

- Vendruscolo, R.G., Facchi, M.M.X., Maroneze, M.M., Fagundes, M.B., Cichoski, A.J., Zepka, L.Q., Barin, J.S., Jacob-Lopes, E., Wagner, R., 2018. Polar and non-polar intracellular compounds from microalgae: Methods of simultaneous extraction, gas chromatography determination and comparative analysis. *Food Res. Int.* 109, 204–212. <https://doi.org/10.1016/j.foodres.2018.04.017>
- Venkatesan, S., Pugazhendy, K., Sangeetha, D., Vasantharaja, C., Prabakaran, S., Meenambal, M., 2012. Fourier Transform Infrared (FT-IR) Spectroscopic Analysis of Spirulina. *Int. J. Pharm. Biol. Arch.* 3, 969–972.
- Violaki, K., Nenes, A., Tsagkaraki, M., Paglione, M., Jacquet, S., Sempéré, R., Panagiotopoulos, C., 2021. Bioaerosols and dust are the dominant sources of organic P in atmospheric particles. *npj Clim. Atmos. Sci.* 4. <https://doi.org/10.1038/s41612-021-00215-5>
- VnmrJ 4.0 (Revision A), 2013.
- Vo, T.S., Ngo, D.H., Kim, S.K., 2015. Nutritional and Pharmaceutical Properties of Microalgal Spirulina, in: *Handbook of Marine Microalgae: Biotechnology Advances*. Academic Press, pp. 299–308. <https://doi.org/10.1016/B978-0-12-800776-1.00019-4>
- Wahlen, B.D., Morgan, M.R., McCurdy, A.T., Willis, R.M., Morgan, M.D., Dye, D.J., Bugbee, B., Wood, B.D., Seefeldt, L.C., 2013. Biodiesel from microalgae, yeast, and bacteria: Engine performance and exhaust emissions. *Energy and Fuels* 27, 220–228. <https://doi.org/10.1021/ef3012382>
- Warren, S.D., St. Clair, L.L., 2021. Atmospheric transport and mixing of biological soil crust microorganisms. *AIMS Environ. Sci.* 8, 498–516. <https://doi.org/10.3934/environsci.2021032>
- Wu, H., Lu, Y., Wang, R., Lai, A.C.K., 2024. Synergistic Disinfection by 222 nm Far-UVC and Negative Air Ions of Airborne Bacteria and the Induced Oxidative Stress Responses: A Bioaerosol Chamber Study. *ACS ES&T Air* 1, 1629–1636. <https://doi.org/10.1021/acsestair.4c00162>
- Xie, W., Li, Y., Bai, W., Hou, J., Ma, T., Zeng, X., Zhang, L., An, T., 2021. The source and transport of bioaerosols in the air: A review. *Front. Environ. Sci. Eng.* 15. <https://doi.org/10.1007/s11783-020-1336-8>
- Xie, Y., Ding, K., Zhang, S., Xu, S., Xu, H., Li, H., Wang, R., Shan, Y., Ding, S., 2025. Fenton reaction-driven oxidative modification of natural polysaccharides: Insights and innovations on properties. *Trends Food Sci. Technol.* <https://doi.org/10.1016/j.tifs.2025.104866>
- Xue, L., Zhang, Y., Zhang, T., An, L., Wang, X., 2005. Effects of Enhanced Ultraviolet-B Radiation on Algae and Cyanobacteria. *Crit. Rev. Microbiol.* 31, 79–89. <https://doi.org/10.1080/10408410590921727>

- Yong, T.C., Chiu, C.S., Chen, C.N.N., 2019. Optimization of a simple, accurate and low cost method for starch quantification in green microalgae. *Bot. Stud.* 60, 1–6. <https://doi.org/10.1186/S40529-019-0273-Y>
- Zhang, Y., Steiner, A.L., 2022. Projected climate-driven changes in pollen emission season length and magnitude over the continental United States. *Nat. Commun.* 13, 1–10. <https://doi.org/10.1038/s41467-022-28764-0>
- Zimmerman, B., Tafintseva, V., Bağcıoğlu, M., Høegh Berdahl, M., Kohler, A., 2016. Analysis of Allergenic Pollen by FTIR Microspectroscopy. *Anal. Chem.* 88, 803–811. <https://doi.org/10.1021/acs.analchem.5b03208>
- Zimmermann, B., Bağcıoğlu, M., Tafinstseva, V., Kohler, A., Ohlson, M., Fjellheim, S., 2017. A high-throughput FTIR spectroscopy approach to assess adaptive variation in the chemical composition of pollen. *Ecol. Evol.* 7, 10839–10849. <https://doi.org/10.1002/ece3.3619>
- Zingales, V., Taroncher, M., Martino, P.A., Ruiz, M.J., Caloni, F., 2022. Climate Change and Effects on Molds and Mycotoxins. *Toxins (Basel)* 14. <https://doi.org/10.3390/toxins14070445>